Mechanism of air−vegetated surface exchange of gaseous and particulate reactive nitrogen by flux measurements in a forest and an agricultural field

2023.3

Symbiotic Science of Environment and Natural Resources
United Graduate School of Agricultural Science
Tokyo University of Agriculture and Technology

Mao XU

Table of contents

Chapter 1: Background

1.1 Deposition of reactive nitrogen

- Nitrogen cycle

Nitrogen is one of the essential elements for all life (Gruber and Galloway, 2008). Simple substance of nitrogen exists as a diatomic molecule (N_2) and dominates about 80% of the atmosphere of earth. Despite the abundance, N_2 is stable and has little reactivity, limiting its use by most organisms. In the natural environment, N_2 is converted to bioavailable forms through nitrogen fixation by some microorganisms and natural discharge such as lightning. Nitrogen fixation is a process of converting stable N_2 to reactive nitrogen (Nr), which is all form of nitrogen compound with high reactivity except N_2 (Galloway and Cowling, 2002). This small amount of produced Nr is cyclically utilized in the ecosystem and finally return to the atmosphere as N_2 (denitrification). This series of processes in which N_2 is fixed as Nr and eventually returned to the atmosphere as N_2 is called "nitrogen cycle". Nitrogen cycle is originally well-balanced in natural ecosystems (Galloway, 1998).

- Disruption of nitrogen cycle due to human activities

However, with the economic development accompanying the industrial revolution that began in the 18th century and the Haber-Bosch process that was realized in the early 20th century, humans began to release excessive amounts of Nr into the environment (Galloway et al. 2013). The amount of Nr released into the environment mainly through human activity like combustion of fuel, production of chemical fertilizers, cultivation of crops, is now said to be about the same as the amount of nitrogen compound fixed by terrestrial natural ecosystems (Fowler et al., 2013). This amount is expected to increase further in the future against the backdrop of increasing demand for food and energy production due to global population growth. Changes in nitrogen supply not only disturb the nitrogen cycle, but also severely affect ecosystem productivity and biodiversity (Erisman et al., 2013).

- Main processes of major reactive nitrogen and their effects on terrestrial ecosystem

Major Nr emitted from the surface of earth into the atmosphere due to human activities include NO_x as oxidized nitrogen and ammonia (NH_3) as reduced nitrogen. NO_x is a general term for nitrogen monoxide (NO) and nitrogen dioxide (NO_2), and is mainly from combustion of fossil fuels. NH_3 is mainly from agricultural activities and is emitted to the atmosphere through application of chemical fertilizer and livestock. In addition, a certain amount of NH_3 is also emitted from the human body and automobiles. NO_x emitted into the atmosphere transforms through chemical reactions while advection and diffusion, and is finally oxidized to nitric acid gas (HNO_3) and nitrate (NO_3^-). NH_3 also transforms into ammonium (NH_4^+) through chemical reactions. These Nr not only cause air pollution, but also transport in the atmosphere while changing their forms, and eventually deposit on the surface (Galloway et al, 2003). As shown in Fig. 1-1, excess deposition of nitrogen can cause acidification, eutrophication, and biodiversity loss (Sutton et al, 2011).

- Nitrogen deposition in East Asia

From simulations using global scale chemical transport models, Vet et al. (2014) clarified that nitrogen deposition is particularly extensive in the eastern United States, central Europe, and large parts of East Asia including Japan. Bleeker et al. (2011) also used a model-based approach to assess the impact of nitrogen deposition on protected

areas around the world, and revealed that nitrogen deposition is a significant and growing problem for biodiversity in Asia, where forest and grassland ecosystems are particularly at risk. Focusing on recent research, Yamaga et al. (2021) evaluated the trends of sulfur and nitrogen deposition in remote areas of Japan and reported that the ratio of nitrogen deposition to sulfur deposition significantly increased between 2003 and 2017, and most of these sites had nitrogen deposition exceeding 10 kg N ha^{-1} $year^{-1}$. This value is a tentative threshold for nitrogen deposition effects based on empirical critical load studies in Europe (Bleeker et al., 2011). From these backgrounds, a more detailed evaluation for nitrogen deposition is still required in East Asia.

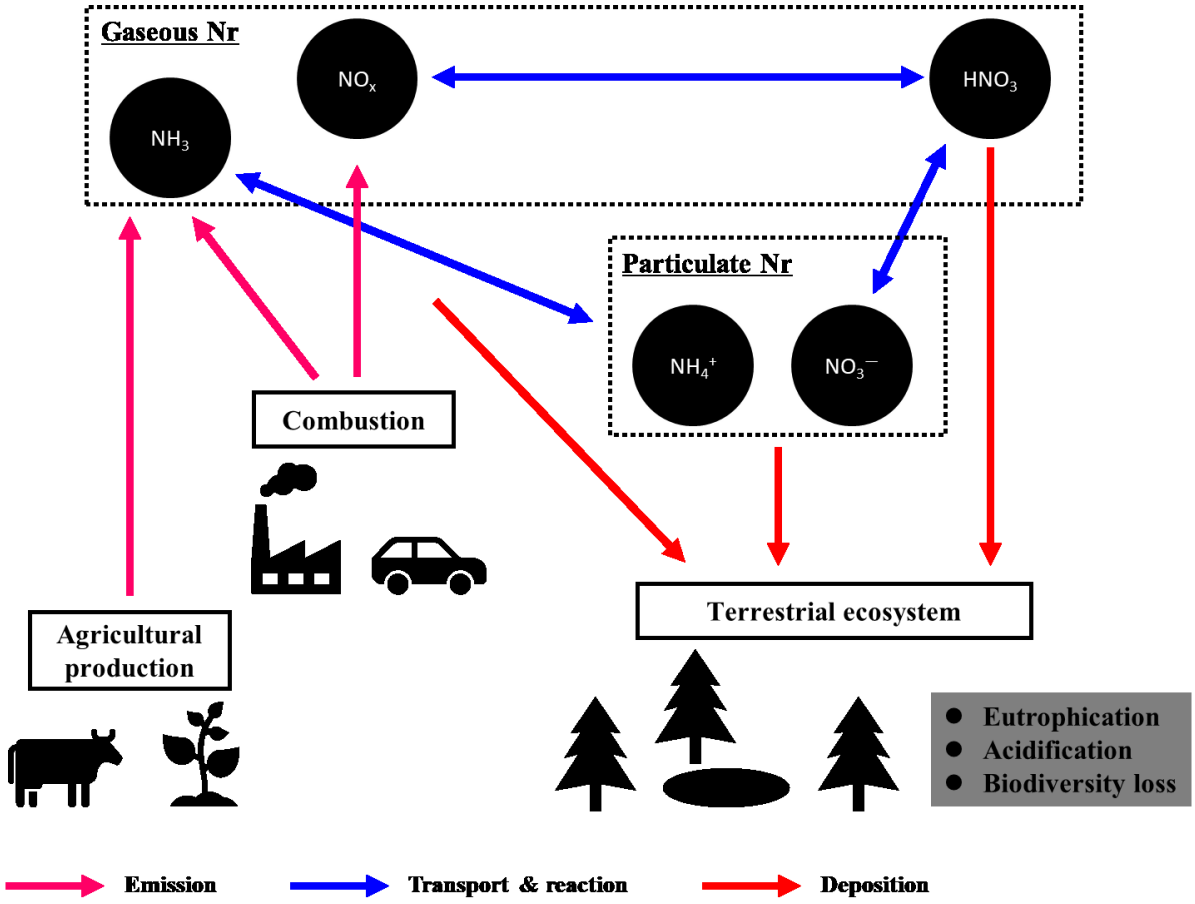

Fig. 1-1. Main processes of reactive nitrogen and their effects on terrestrial ecosystem.

➢ Estimates of Nr deposition

Nr is deposited on the surface from atmosphere by wet or dry deposition (Erisman and Draaijers, 1995). Wet deposition is a process in which gaseous or particulate Nr is scavenged by cloud, rain, or snow, and then deposited on the surface. On the other hand, dry deposition is a process in which gaseous or particulate Nr is directly deposited on the surface from the atmosphere by turbulent diffusion or gravitational sedimentation without precipitation (Wesely and Hicks, 2000). In general, the major Nr that dominates wet deposition is NO_3^- and NH_4^+, and that dominates dry deposition are gaseous HNO_3 and NH_3 and particulate NO_3^- and NH_4^+ (Wright et al. 2018). The amounts of wet deposition can be directly determined by collecting precipitation and multiplying the concentration

of each component in the precipitation by the amount of precipitation. For this reason, extensive monitoring of wet deposition has been carried out around the world. The amounts of dry deposition can be determined from direct and indirect measurement methods, however, it is more difficult to quantify than wet deposition (Hayashi et al. 2007). Direct measurement methods include the eddy covariance (EC), relaxed eddy accumulation (REA), and aerodynamic gradient method (AGM) etc., and can measure the vertical dry deposition flux, which is the amount of net vertical mass transfer of target substance per unit area and unit time (Seinfeld and Pandis, 2006). Although direct measurement methods can measure flux and determine dry deposition more accurately than indirect measurement methods, they are not applied to wide-area and long-term monitoring network because they require specialized equipment, and the measurable targets and locations are limited (Walker et al. 2020). On the other hand, inferential method is widely used as an indirect measurement method, which has been adopted by North American monitoring network: the Clean Air Status and Trend Network (CASTNET) and the Canadian Air and Precipitation Network (CAPMoN) (Schwede et al. 2011), and regional scale monitoring network in East Asia: the Acid Deposition Monitoring Network in East Asia (EANET) (Endo et al., 2011; Ban et al., 2016). In the inferential method, the concentrations of gaseous substance and particulate matter are measured, and the dry deposition amount is estimated from the product of the measured concentration and the inferred deposition velocity (V_d) (Hicks et al. 1987). The V_d is an index that expresses the easiness of deposition of a substance, and can be estimated from available input data such as meteorological elements and land-use information using the resistance model (explained in Section 3.2.3). Thus, the inferential method can be routinely applied to wide-area and long-term monitoring and is useful method for estimating dry deposition (Erisman et al. 1994). However, the resistance model still leaves many uncertainties.

- Uncertainties in estimates of Nr dry deposition

For particulate matter, it is generally known that the V_d mainly depends on the particle size, and the resistance model estimates the V_d for particles based on this theory (Gallagher et al, 1997). However, there are still uncertainties about this common theory (Pryor et al, 2008). Although deposition of particles has been studied worldwide over the 40 years, large discrepancies in V_d remain between the results of measurements and model predictions, especially for submicron particles (0.1−1 μm). According to Saylor et al. (2019), observed values for V_d of submicron particles tend to be larger than theoretical values in forest sites. Flechard et al. (2011) investigated the differences in V_d for inorganic gaseous and particulate Nr at four vegetation types (forest, semi-natural short vegetation, grassland, and cropland) using four resistance model that are commonly implemented in chemical transport models at national or continental scales in Europe and North America. They found that the differences in V_d between these models are particularly large for NO_3^- and NH_4^+ over forest site, and NH_3 for all vegetation types. In Japan, model studies using chemical transport models tended to overestimate the concentration of NO_3^- in particulate matter with diameters of less than 2.5 μm ($PM_{2.5}$), suggesting that the simulated NO_3^- concentration was highly dependent on the uncertainty in the dry deposition process of NH_3 and HNO_3 (Shimadera et al., 2014). As described in next Section 1.2, there are still many unexplained processes in the dry deposition of these Nr, which leads to the uncertainty in the resistance model and estimation of dry deposition.

1.2 Air−vegetated surface exchange of reactive nitrogen

Ammonium nitrate (NH_4NO_3) particle, one of the main components of $PM_{2.5}$, is formed by the chemical reaction of NH_3 and HNO_3 as follows:

$$NH_3(g) + HNO_3(g) \rightleftarrows NH_4NO_3(s) \quad (1\text{-}1)$$

where g and s indicate gas and solid phase (Seinfeld and Pandis, 2006), respectively. Chemical reaction shown in Eq. (1-1) is reversible, and semi-volatile NH_4NO_3 can shift to the gas phase at higher temperature and/or low concentration of NH_3 and HNO_3 conditions. The process of converting HNO_3 into particulate matter that has a low V_d and can be long-range transported is thought to be important for evaluation of Nr deposition (Erisman and Draaijers, 1995).

Ammonium sulfate ($(NH_4)_2SO_4$) particle is also one of the main components of $PM_{2.5}$ but non-volatile. Current theories estimating the V_d for particulate matter assume that the V_d depends on aerodynamics and its size. In this case, the V_d values for NH_4NO_3 and $(NH_4)_2SO_4$ in $PM_{2.5}$ must be similar because they are in almost same size. However, some measurement-based studies indicate large differences in the V_d for these components (Nemitz, 2015). It is also reported that the volatilization of NH_4NO_3 to NH_3 and HNO_3 during dry deposition process possibly enhance the deposition of NO_3^-, resulting in larger V_d than those of sulfate (SO_4^{2-}) (Fowler et al., 2009). Moreover, Nemitz (2015) reported that HNO_3, which is theoretically and empirically known to have a large V_d among Nr, is not only rapidly removed from the atmosphere, but also is possibly emitted from surface in association with the volatilization of NH_4NO_3 particles.

NH_3 is more complicated compared to NO_3^- and HNO_3, and has a bi-directional exchange process of emission into the atmosphere via plant stomata and soil in addition to deposition. Although this process was already modeled in the 1990s and various bi-directional exchange models to infer NH_3 exchange flux have been developed so far, many uncertainties still remain due to the complex behavior (Flechard et al., 2013). Under the current situation where sulfur dioxide and nitrogen oxide emissions are clearly decreasing and NH_3 emissions are increasing worldwide (Fowler et al., 2020), it is necessary to clarify the bi-directional exchange process of NH_3 as a particularly important Nr.

As shown in Table 1-1, various measurement-based studies have been conducted in Europe, the United States, and other regions focusing on the air−vegetated surface exchange process of NH_4NO_3, NH_3, and HNO_3, which is intricately intertwined with each other. From Table 1-1, we can see the following three characteristics on these studies.

- There are only a limited number of studies in East Asia, where the effects of Nr deposition on ecosystem are of particular concern.
- The gradient methods, such as the modified Bowen ratio method (MBR), the aerodynamic gradient method (AGM) and the vertical profile measurement (VPM), are mostly used.
- Gaseous substances are more often observed than particulate matters.

Table 1-1(a). Measurement-based studies on air−vegetated surface exchange of NH_4NO_3, NH_3, and HNO_3.

Reference	Region	Vegetation	Method	Component			
				NH_4^+	NO_3^-	NH_3	HNO_3
Huebert and Robert (1985)	United States	Grassland	MBR		✓		✓
Huebert et al. (1988)	United States	Grassland (crested wheatgrass)	MBR		✓		✓
Harrison et al. (1989)	England	Grassland	AGM	✓	✓	✓	✓
		Cropland					
Andersen et al. (1993)	Denmark	Forest (spruce)	AGM			✓	
Erisman and Wyers (1993)	Netherlands	Heathland	AGM			✓	
Müller et al. (1993)	United Kingdom	Grassland	MBR				✓
	Germany	Cropland (wheat)	AGM				
Duyzer (1994)	Netherlands	Heathland	AGM	✓		✓	
Sievering et al. (1994)	Germany	Forest (spruce)	VPM	✓	✓	✓	✓
Neftel et al. (1996)	Switzerland	Grassland	AGM				✓
Yamulki et al. (1996)	England	Cropland (wheat)	AGM			✓	
Wyers and Duyzer (1997)	Netherlands	Forest (conifer)	AGM		✓		
Flechard and Fowler (1998)	Scotland	Moorland	EC			✓	
			AGM				
Wyers and Erismana (1998)	Netherlands	Forest (conifer)	AGM			✓	
Andersen et al. (1999)	Denmark	Forest (spruce)	AGM			✓	
Nemitz et al. (2000)	Scotland	Cropland (oilseed rape)	AGM	✓		✓	
Sutton et al. (2000)	Scotland	Cropland (oilseed rape)	AGM			✓	

Method: MBR, AGM, VPM, EC, and REA indicates, the modified Bowen ratio method, the aerodynamic gradient method, the vertical profile measurement, and the eddy covariance method, and the relaxed eddy accumulation method, respectively.

Table 1-1(b). Measurement-based studies on air−vegetated surface exchange of NH_4NO_3, NH_3, and HNO_3.

Reference	Region	Vegetation	Method	Component			
				NH_4^+	NO_3^-	NH_3	HNO_3
Milford et al. (2001a)	Scotland	Heathland	AGM			✓	
Milford et al. (2001b)	Scotland	Grassland	AGM			✓	
Rattray and Sievering (2001)	United States	Grassland (tundra)	AGM	✓	✓	✓	✓
Sievering et al. (2001)	United States	Forest (spruce)	AGM				✓
Spindler et al. (2001)	Germany	Grassland	AGM			✓	
Pryor et al. (2002)	United States	Forest (deciduous)	AGM				✓
			REA				
Nemitz et al. (2004a)	Netherlands	Heathland	AGM			✓	✓
Nemitz et al. (2004b)	Netherlands	Heathland	AGM	✓	✓		
Phillips et al. (2004)	United States	Grassland	AGM			✓	
Pryor and Klemm (2004)	Germany	Forest (conifer)	REA				✓
Takahashi and Wakamatsu (2004)	Japan	Forest (red pine)	AGM	✓	✓		
Horváth et al. (2005)	Hungary	Grassland	AGM			✓	
Neirynck et al. (2005)	Belgium	Forest (coniferous/deciduous)	AGM			✓	
Farmer et al. (2006)	United States	Forest (ponderosa pine)	EC				✓
Kruit et al. (2006)	Netherlands	Grassland	AGM			✓	
Meyers et al. (2006)	United States	Cropland (maize)	REA			✓	
Walker et al. (2006)	United States	Cropland (soybean)	MBR			✓	
Myles et al. (2007)	United States	Grassland	REA			✓	✓

Method: MBR, AGM, VPM, EC, and REA indicates, the modified Bowen ratio method, the aerodynamic gradient method, the vertical profile measurement, and the eddy covariance method, and the relaxed eddy accumulation method, respectively.

Table 1-1(c). Measurement-based studies on air−vegetated surface exchange of NH_4NO_3, NH_3, and HNO_3.

Reference	Region	Vegetation	Method	Component			
				NH_4^+	NO_3^-	NH_3	HNO_3
Hole et al. (2008)	Norway	Grassland	AGM			✓	✓
Wolff et al. (2010a)	Germany	Forest (spruce)	AGM	✓	✓	✓	✓
Myles et al. (2011)	United States	Cropland (soybean)	AGM			✓	✓
Sintermann et al. (2011)	Switzerland	Cropland (wheat)	EC			✓	
		Grassland					
Twigg et al. (2011)	Scotland	Grassland (perennial ryegrass)	AGM	✓	✓		✓
			EC			✓	
Hayashi et al. (2012)	Japan	Cropland (paddy rice)	AGM	✓	✓	✓	✓
Khoomsab and Khummongkol (2013)	Thailand	Forest (deciduous)	REA		✓		
Walker et al. (2013)	United States	Cropland (corn)	MBR			✓	
Hansen et al. (2015)	United States	Forest (deciduous)	REA			✓	✓
Personne et al. (2015)	France	Cropland (wheat)	AGM			✓	
Yamazaki et al. (2015)	Japan	Forest (deciduous)	VPM		✓		
Honjo et al. (2016)	Japan	Forest (deciduous)	REA		✓		
Sakamoto et al. (2018)	Japan	Forest (deciduous)	REA		✓		✓
Nakahara et al. (2019)	Japan	Forest (hybrid larch)	VPM		✓		✓
Nelson et al. (2019)	United States	Cropland (corn)	REA			✓	
			AGM				

Method: MBR, AGM, VPM, EC, and REA indicates, the modified Bowen ratio method, the aerodynamic gradient method, the vertical profile measurement, and the eddy covariance method, and the relaxed eddy accumulation method, respectively.

1.3 Research objectives

To better understand the mechanism of the air−vegetated surface exchange of Nr and contribute to the more accurate assessment of the impact of Nr deposition on ecosystems in the East Asian region, I conducted observations mainly focusing on NH_4NO_3, NH_3, and HNO_3 in forest and agricultural field in Japan. I developed various observation and model studies particularly focusing on the following two goals.

- Understand the mechanism of the dry deposition of NH_4NO_3 (NO_3^-) and HNO_3 associated with the NH_4NO_3−NH_3−HNO_3 interactions.
- Investigate the NH_3 bi-directional exchange and verify the applicability of the bi-directional exchange model based on field measurements in Japan with the aim of expanding to East Asia.

In **Chapter 2**, I report the results of vertical profile measurements for NO_3^- and NH_3 in a forest in the suburbs of Tokyo, Japan. The observations were conducted intensively in summer (Jul. 2015), winter (Feb. 2016), and autumn (Sep.-Oct. 2016) focusing on diurnal and seasonal variations in dry deposition process.

In **Chapter 3**, I report the results of long-term flux measurements for NO_3^- and HNO_3 over a forest in the suburbs of Tokyo. In this observation, REA method combined with denuder/filter-pack method was used to enable more accurate flux measurements. The observation was performed from 2016 to 2018 in order to evaluate the long-term variations in the V_d for NO_3^- and HNO_3.

In **Chapter 4**, I report the results of flux measurements for NH_3 using the REA over an agricultural field in west of central Tokyo. The observations were carried out during soybean-growing (Jul.-Aug. 2020) and fallow (March 2021) periods, with the aim of clarifying the bi-directional exchange process of NH_3. In addition, foliage and soil analysis associated with NH_3 emission was performed. The applicability of the NH_3 bi-directional exchange model for the agricultural field was also evaluated.

In **Chapter 5**, I introduce attempts to update the NH_3 bi-directional exchange model for application in forest surface based on the results of **Chapter 2**.

In **Chapter 6**, I present conclusions of this study and propose future issues towards the better understanding of Nr deposition in East Asia.

Chapter 2 Seasonal vertical profiles of nitrate and ammonia in a deciduous forest

2.1 Introduction

As mentioned in **Chapter 1**, there are large uncertainties in the resistance models to estimate the V_d for NO_3^- in $PM_{2.5}$ and NH_3, particularly on forest surfaces (Flechard et al., 2011). Large uncertainties also exist in the bi-directional exchange models to infer NH_3 flux. However, the dry deposition process of NO_3^- and bi-directional exchange process of NH_3 has rarely been studied in East Asia, where the effects of excessive Nr deposition are concerned. Therefore, a better understanding of these process in this region will contribute to improve the model accuracy for estimation of nitrogen deposition.

Lagging behind Europe and the United States, several measurement-based studies to determine the V_d of NO_3^- in $PM_{2.5}$ using AGM or REA have been performed over forests in Japan since 2000s (Takahashi and Wakamatsu, 2004; Honjo et al., 2016; Sakamoto et al., 2018). These experiments suggest that the volatilization of NH_4NO_3 during dry deposition likely enhances the deposition of NO_3^-, as indicated by previous studies in other regions (Huebert et al., 1988; Sievering et al., 1994; Wyers and Duyzer, 1997; Nemitz et al., 2004b; Wolff et al. 2010a). Vertical profile measurement is also a useful method to understand dry deposition or exchange processes in forests (Nakahara et al., 2019). Using this approach, Yamazaki et al. (2015) found a significant difference in concentration gradients for NO_3^- and SO_4^{2-} in $PM_{2.5}$ in a forest in Tokyo over the course of a year. This result was also likely due to the enhancement of deposition of NO_3^- associated with the volatilization of NH_4NO_3.

However, these studies conducted in Japan did not intensively examine the diurnal and seasonal variations in dry deposition process. Regarding NH_3, there are no examples of study in forests in Japan. Therefore, I conducted intensive field observations in a forest in suburban Tokyo to understand the enhancement process of dry deposition of NO_3^- and the bi-directional exchange of NH_3. I obtained the vertical profiles of the $PM_{2.5}$ components, NH_3, and sulfur dioxide (SO_2). SO_2 is a stereotypical gas and the deposition processes have been well generalized (Nemitz, 2015). I particularly focused on the daytime and nighttime processes in a forest during leafy and leafless periods.

2.2 Methods

2.2.1 Site description

I conducted the observations at the Field Museum Tamakyuryo (FM Tama) site of the Tokyo University of Agriculture and Technology (about 12 ha). FM Tama is located in a western suburb of Tokyo, Japan (35° 38' N, 139° 23' E) and is on hilly terrain (Fig. 2-1). The north and south sides of the site are residential areas, and small-scale agricultural fields are located in the southeast side. A 30 m walk-up tower (Fig. 2-2) is installed in the forest at the site (168 m above sea level). The top of the tower was the highest point in the surrounding area (Fig. 2-3). An area within a radius of 200 m from the tower was dominated by the forest. Deciduous trees (*Quercus*) were the dominant tree species around the tower in addition to some Japanese cedar (*Crytomeria*). The canopy height around the tower was approximately 20 m. The deciduous trees were generally leafy from April and leafless from December.

Fig. 2-1. Surrounding environment of FM tama and location of observation tower. The aerial photograph is taken by Geospatial Information Authority of Japan (2019).

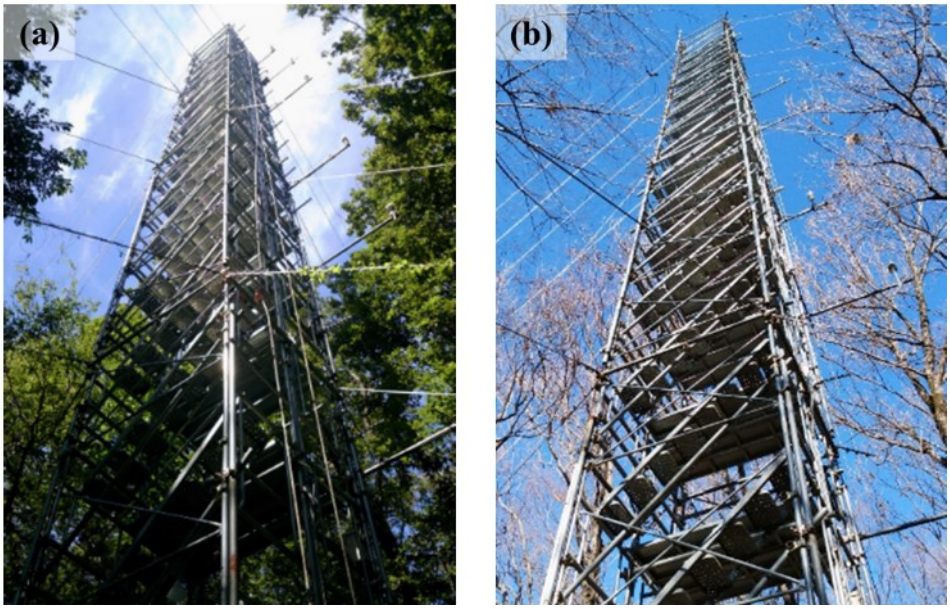

Fig. 2-2. Observation tower in (a) leafy and (b) leafless periods. The leaf layer was distributed in a range between 10 and 20 m in leafy period.

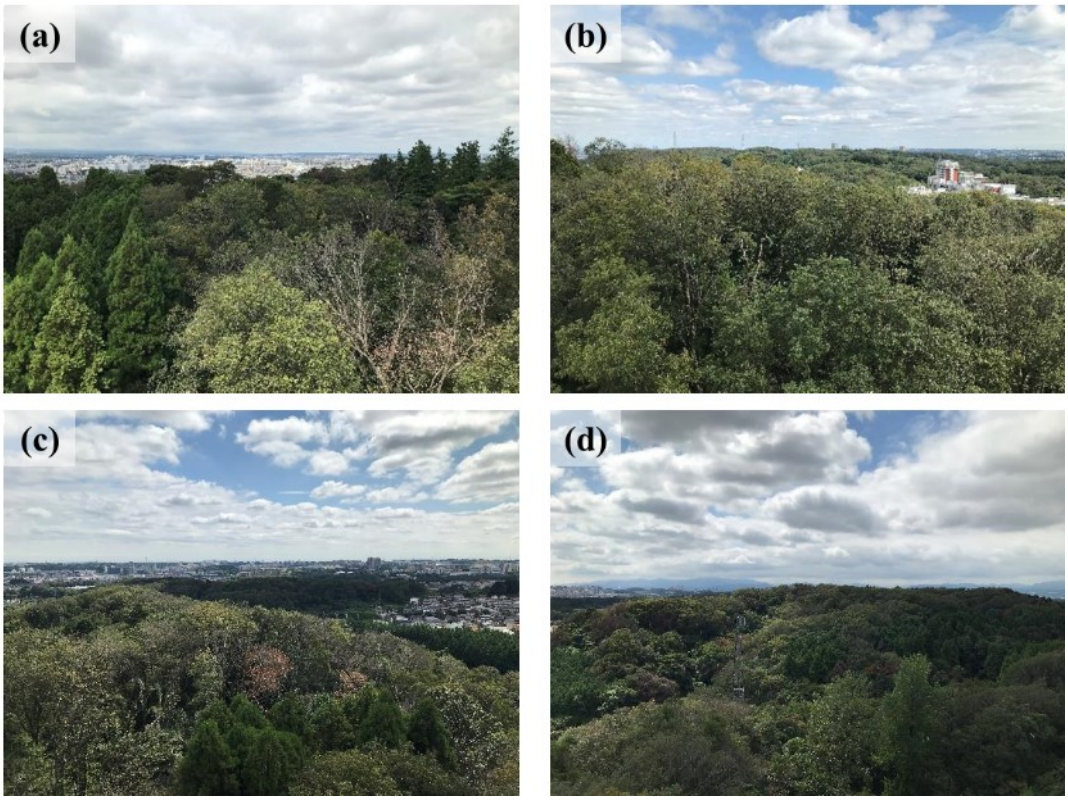

Fig. 2-3. View from the top of the tower to (a) north, (b) east, (c) south, and (d) west side.

2.2.2 Sampling system for vertical profile measurements

Observation periods and strategies of vertical profile measurements are given in Table 2-1, and schematic diagrams of the sampling system for vertical profile measurements are shown in Fig. 2-4. I performed two observations during leafy periods (15-summer: Jul. 21 to Aug. 1, 2015, and 16-autumn: Sep. 27 to Oct. 11, 2016) and one during a leafless period (16-winter: Feb. 23 to Feb. 29, 2016).

I sampled $PM_{2.5}$, NH_3, and SO_2 simultaneously using a filter-pack holder (Tokyo Dylec Corporation, NILU filter folder NL-O) with an impactor and a pump unit (Tokyo Dylec Corporation, MCI sampler) (Fig. 2-5). Filter-pack holder is widely applied to short-term and long-term observations at multiple sites because it is small, lightweight, and is easy to collect multiple components. The flow rate of the pump was set to 20 L min^{-1} in accordance with the $PM_{2.5}$ cut off the impactor. The impactor utilizes the law of inertia to classify and collect particulate matters in specific particle sizes at a specific flow rate. $PM_{2.5}$ was collected on glass fiber filters coated with Teflon. SO_2 was collected on a cellulose filter impregnated with potassium carbonate following the $PM_{2.5}$ filter. NH_3 was collected on a cellulose filter impregnated with phosphoric acid following SO_2 filter.

To obtain daytime and nighttime vertical concentration profiles, I installed filter holders at 4 or 5 heights of the observation tower in the forest (above the forest canopy: 30 m and 23 m, between the leafy canopy layer: 16 m, below the canopy: 8 m and 1 m), and changed the filters twice a day. To sufficiently detect the concentration gradients, I set the sampling time to more than 9-h considering previous measurements at the same site (Yamazaki

et al., 2015). Sampling was conducted continuously, except when it was raining. I obtained 36/38 valid samples in total at each height level for $PM_{2.5}$, and 37/38 valid samples for NH_3. After the sampling, the inorganic ions in each filter were extracted into 10 ml deionized water via ultrasonic extraction, and analyzed using ion chromatography (Thermo Scientific, Dionex ICS-1100).

Table 2-1. Observation periods and strategies of vertical profile measurements.

Season	Observation period	Daytime sampling	Nighttime sampling	Measurement heights
Summer (leafy)	July 21–August 1, 2015	06:00–18:00	18:00–06:00	30 m, 23 m, 8 m, 1m
Winter (leafless)	February 23–29, 2016	08:00–17:00	17:00–08:00	30 m, 23 m, 16 m, 8 m, 1 m
Autumn (leafy)	September 27–October 11, 2016			

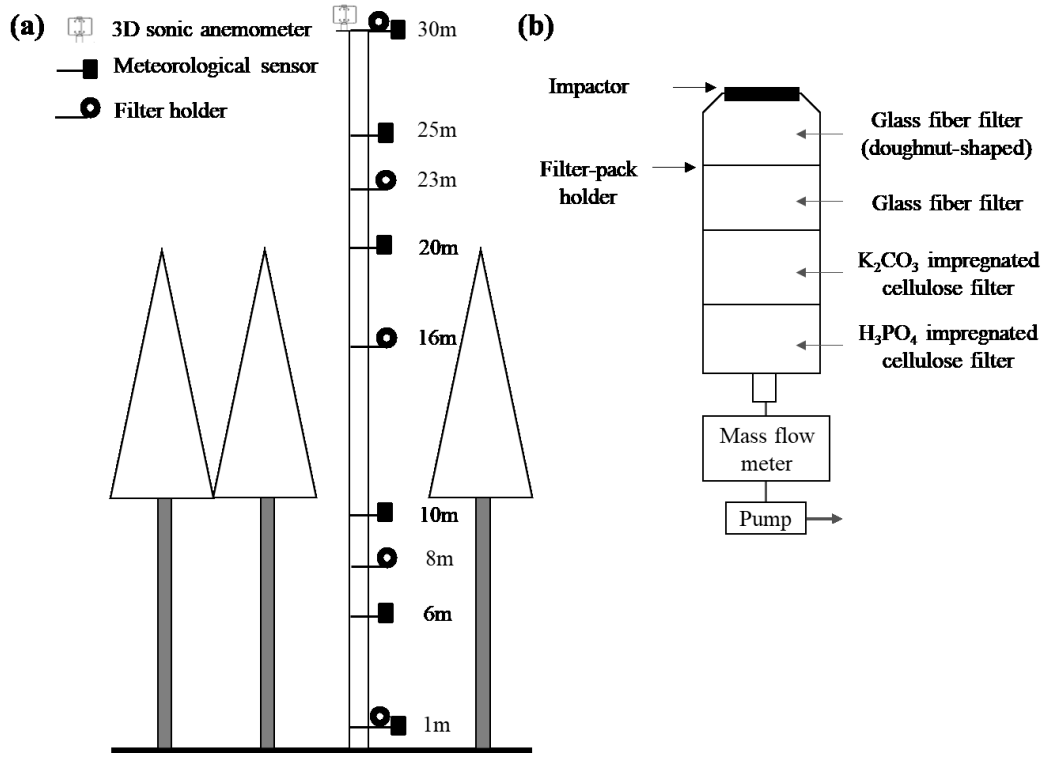

Fig. 2-4. Schematic diagrams of (a) the observation tower and (b) the sampling system for vertical profile measurements.

Fig. 2-5. Photo of filter-pack holder at the 30 m of the tower

Information on instruments for metrological element measurements are given in Fig. 2-6 and Table 2-2. Wind speed (WS) and wind direction (WD) were recorded by a 3D sonic anemometer (YOUNG, 81000) at 30 m. Temperature (Temp) and relative humidity (RH) were observed at heights of 30 m, 25 m, 20 m, 10 m, 6 m, and 1 m using Weather Transmitter (VAISALA, WXT520) and Thermo-hygrometer (VAISALA, HMP45A). Solar radiation (SR) was measured using a pyranometer (PREDE, PCM-01N) at 30 m. Rainfall was measured in 0.5 mm interval using the tipping bucket rain gauge (METIC, R-5) on the open-space ground in the site. All elements were recorded at 10-min intervals except for vertical wind speed, etc. The leaf area index (LAI) of the forest was measured using a plant canopy analyzer (LI-COR LAI-2200).

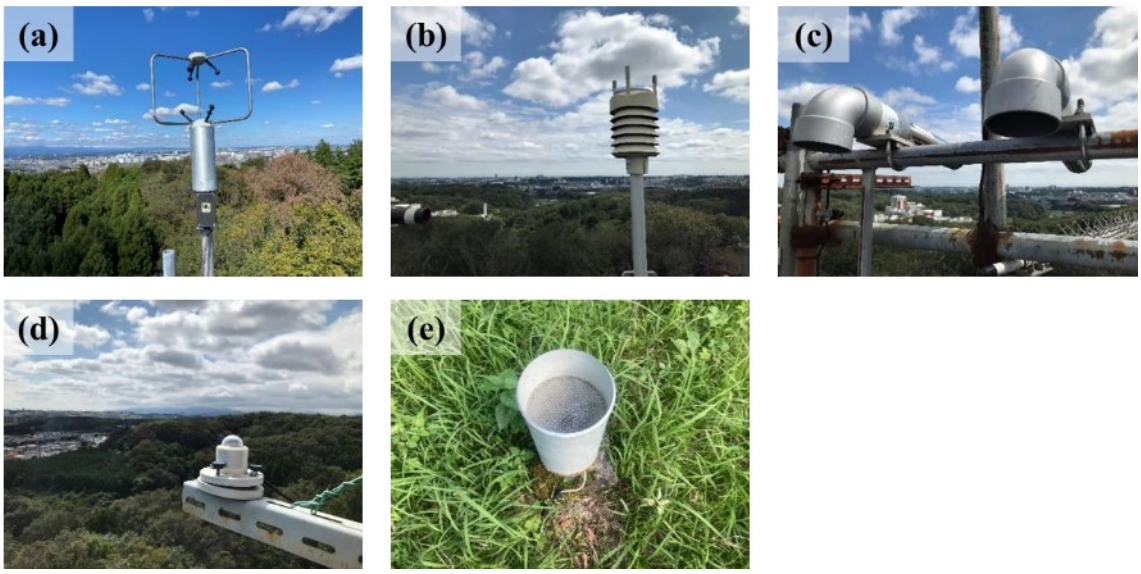

Fig. 2-6. Photo of (a) 3D sonic anemometer, (b) Weather Transmitter, (c) Thermo-hygrometer, (d) Pyranometer, and (e) Tipping bucket rain gauge.

Table 2-2. Information on instruments for metrological element measurements.

Instrument	Parameter	Interval	Unit	Location
3D sonic anemometer (YOUNG, 81000)	U_x wind vector	10 Hz	m s^{-1}	30 m at the tower
	V_y wind vector			
	Vertical wind speed			
	Sonic virtual temperature		°C	
	Wind speed	10 min	m s^{-1}	
	Wind direction		°	
Thermo-hygrometer (VAISALA, HMP45A)*	Air temperature		°C	
	Relative humidity		%	
Pyranometer (PREDE, PCM-01N)	Solar radiation		W m^{-2}	
Weather Transmitter (VAISALA, WXT520)*	Air temperature		°C	30 m, 25 m, 20 m, 10 m, 6 m, and 1 m at the tower
	Relative humidity		%	
Tipping bucket rain gauge (METIC, R-5)	Rainfall		mm	open-space ground in the site

*: The Weather Transmitter at 30 m broke down after 15-summer, and I replaced it with a Thermo-hygrometer.

2.3 Results & Discussion

2.3.1 Overview

LAI was 4.4, 1.7, and 4.3 in 15-summer, 16-winter, and 16-autumn, respectively. LAI (rounded to the nearest whole number) ≥ 4 was defined as leafy and LAI ≤ 2 was defined as leafless period. Atmospheric conditions at the site during the observation periods are listed in Table 2-3. The WS was highest during the daytime in 16-winter; the Temp was highest during the daytime in 15-summer; and the RH was highest during the nighttime in 15-summer. The main WD at the site was south and north. The weather was mostly favorable for measurements except a heavy rain event during the 15-summer. The concentrations of SO_4^{2-} in the $PM_{2.5}$ and NH_3 were highest in 15-summer, while the concentrations of NO_3^- in the $PM_{2.5}$ were highest in 16-winter. This was probably because the formation of SO_4^{2-} was accelerated and semi-volatile NH_4NO_3 particles volatilized and existed as gaseous NH_3 and HNO_3 with the increase in Temp during summer. Moreover, increase in Temp probably accelerated the NH_3 emission from the leaf stomata and soil.

The temporal variations in the concentrations of SO_4^{2-} and NO_3^- in the $PM_{2.5}$ at heights of 30 m, 23 m, 8 m, and 1 m during the observational periods are shown in Fig. 2-7 and Fig. 2-8. A decrease in concentration from the top of the canopy to the forest floor indicates deposition of the substance, and an increase in concentration from the top of the canopy to the forest floor indicates emission, respectively. During the observational periods, there were no differences in the concentrations of SO_4^{2-} between these heights except a small difference between 8 m and 1 m (Fig. 2-7). However, there were significant differences in the concentrations of NO_3^- between these heights (Fig. 2-8). The NO_3^- concentration clearly decreased from the top of the canopy to the forest floor during the observation periods compared to the SO_4^{2-} concentration. The variations in the NH_3 concentrations between these heights were more complicated than those of SO_4^{2-} and NO_3^- in the $PM_{2.5}$ (Fig. 2-9). During the daytime in 15-summer, NH_3 concentration tended to increase from 30 m to 23 m, indicating NH_3 emissions from the forest. During the daytime in 16-winter, NH_3 emissions were frequently observed between 8 m and 1 m. No clear trend was observed during daytime in 16-autumn. On the other hand, NH_3 concentration decreased from 23 m to 1 m at nighttime in all periods. Therefore, there were possibly seasonal and diurnal variations in the NH_3 exchange in the forest.

Table 2-3(a). Concentration for SO_4^{2-}, NO_3^-, and NH_3 with wind speed (WS), main wind direction (WD), air temperature (Temp), relative humidity (RH) at 30 m at the tower, and rainfall during the observation periods. WS, Temp, and RH are given as the means ± standard deviation.

period		SO_4^{2-}	NO_3^-	NH_3	WS	WD	Temp	RH	Rainfall
			μg m^{-3}		m s^{-1}		°C	%	mm
2015	0721_N	–	–	3.99	4.7 ± 1.2	S	27.0 ± 2.2	61.8 ± 8.4	0
	0722_D	0.72	0.46	2.15	7.2 ± 1.8	SSW	28.8 ± 2.1	53.6 ± 6.9	0
	0722_N	1.08	0.12	1.80	5.7 ± 1.1	SSW	26.1 ± 1.5	72.4 ± 9.9	5.0
	0724_D	1.43	1.53	–	1.7 ± 0.6	NNW	27.9 ± 2.1	73.2 ± 9.7	15.5
	0724_N	2.44	2.22	4.12	1.8 ± 0.3	NW	26.0 ± 1.3	82.8 ± 5.2	0
	0725_D	–	–	3.08	1.7 ± 0.7	ESE	29.1 ± 2.4	67.8 ± 9.8	0
	0725_N	4.08	0.56	4.53	2.1 ± 0.3	NW	28.1 ± 1.9	66.0 ± 5.3	0
	0726_D	7.23	0.59	4.06	2.7 ± 1.6	S	30.6 ± 2.3	58.6 ± 8.2	0
	0726_N	6.05	1.93	2.61	3.3 ± 1.5	S	27.1 ± 1.8	71.4 ± 9.0	0
	0727_D	7.29	0.33	3.63	2.3 ± 1.3	ESE	29.8 ± 2.3	63.3 ± 8.0	0
	0727_N	3.26	1.34	4.31	2.0 ± 0.7	N	28.5 ± 1.6	71.1 ± 8.5	0
	0729_N	11.30	4.44	2.64	2.6 ± 0.9	S	26.1 ± 1.1	81.0 ± 5.6	0
	0730_D	9.08	0.46	4.24	2.0 ± 1.0	N	28.0 ± 1.8	72.7 ± 9.3	1.0
	0730_N	9.21	2.67	2.44	2.1 ± 0.6	S	25.9 ± 1.4	81.3 ± 7.4	0
	0731_D	12.06	0.35	2.67	2.3 ± 1.6	S	29.3 ± 2.2	65.9 ± 9.2	0
	0731_N	16.11	2.08	1.86	3.1 ± 1.5	S	26.6 ± 1.1	82.4 ± 6.9	0

Table 2-3(b). Concentration for SO_4^{2-}, NO_3^-, and NH_3 with wind speed (WS), wind direction (WD), air temperature (Temp), relative humidity (RH) at 30 m at the tower, and rainfall during the observation periods. WS, Temp, and RH are given as the means ± standard deviation.

period		SO_4^{2-}	NO_3^-	NH_3	WS	WD	Temp	RH	Rainfall
			μg m^{-3}		m s^{-1}		°C	%	mm
2016	0223_N	3.76	4.91	1.33	2.6 ± 1.6	NNE	5.5 ± 1.4	65.9 ± 15.5	0
	0224_D	2.38	1.29	1.38	3.3 ± 0.7	NNE	4.9 ± 0.2	34.7 ± 2.2	0
	0224_N	1.36	2.73	0.55	1.6 ± 0.5	NE	1.3 ± 2.0	75.2 ± 19.9	0
	0225_D	1.03	3.10	1.38	1.6 ± 0.2	NE	2.4 ± 2.1	60.3 ± 19.9	1.5
	0225_N	1.05	4.15	0.55	2.6 ± 0.6	NW	1.5 ± 1.4	66.6 ± 6.7	0
	0226_D	1.07	1.83	0.71	3.7 ± 1.2	S	5.9 ± 2.3	33.5 ± 12.6	0
	0226_N	1.85	2.29	1.13	2.8 ± 0.7	NNW	3.0 ± 2.4	56.7 ± 6.7	0
	0227_D	2.96	2.37	1.02	5.1 ± 3.2	SSW	7.0 ± 2.7	36.1 ± 10.3	0
	0227_N	7.37	5.37	1.05	4.0 ± 1.9	SSW	6.7 ± 2.1	49.9 ± 10.8	0
	0228_D	5.38	3.58	1.42	3.5 ± 1.5	S	10.0 ± 2.4	37.1 ± 10.2	0
	0228_N	2.49	2.66	1.14	2.9 ± 1.2	N	5.9 ± 2.2	74.8 ± 8.6	0.5
	0229_D	3.00	5.29	1.92	3.0 ± 2.4	SSW	8.7 ± 3.0	69.7 ± 4.5	0
2016	0927_D	3.97	0.75	3.37	1.9 ± 0.9	SE	26.0 ± 1.7	74.5 ± 6.8	0
	0927_N	3.91	2.28	1.53	2.1 ± 1.0	S	24.0 ± 1.2	87.2 ± 5.4	0.5
	0928_D	2.93	2.98	2.82	1.8 ± 0.7	NNE	26.7 ± 1.5	74.1 ± 6.4	0
	0930_D	1.03	1.38	2.16	1.5 ± 0.4	ESE	20.4 ± 0.9	54.0 ± 4.1	0
	1004_D	1.44	1.08	2.56	1.9 ± 0.5	N-NE	27.9 ± 2.4	52.3 ± 10.3	0
	1004_N	3.12	0.69	1.95	2.3 ± 0.4	NW	22.9 ± 2.3	58.1 ± 11.6	0.5
	1005_N	1.54	0.64	1.78	5.2 ± 3.5	S	22.6 ± 1.2	84.6 ± 4.3	0
	1006_D	0.37	1.20	2.58	2.1 ± 1.0	NNE	27.6 ± 1.7	47.9 ± 8.8	0
	1006_N	0.90	0.32	1.56	3.1 ± 0.9	NNE	20.7 ± 2.4	50.3 ± 6.2	0
	1011_N	1.06	0.83	1.62	1.7 ± 0.3	NW	14.7 ± 1.3	75.2 ± 8.3	0

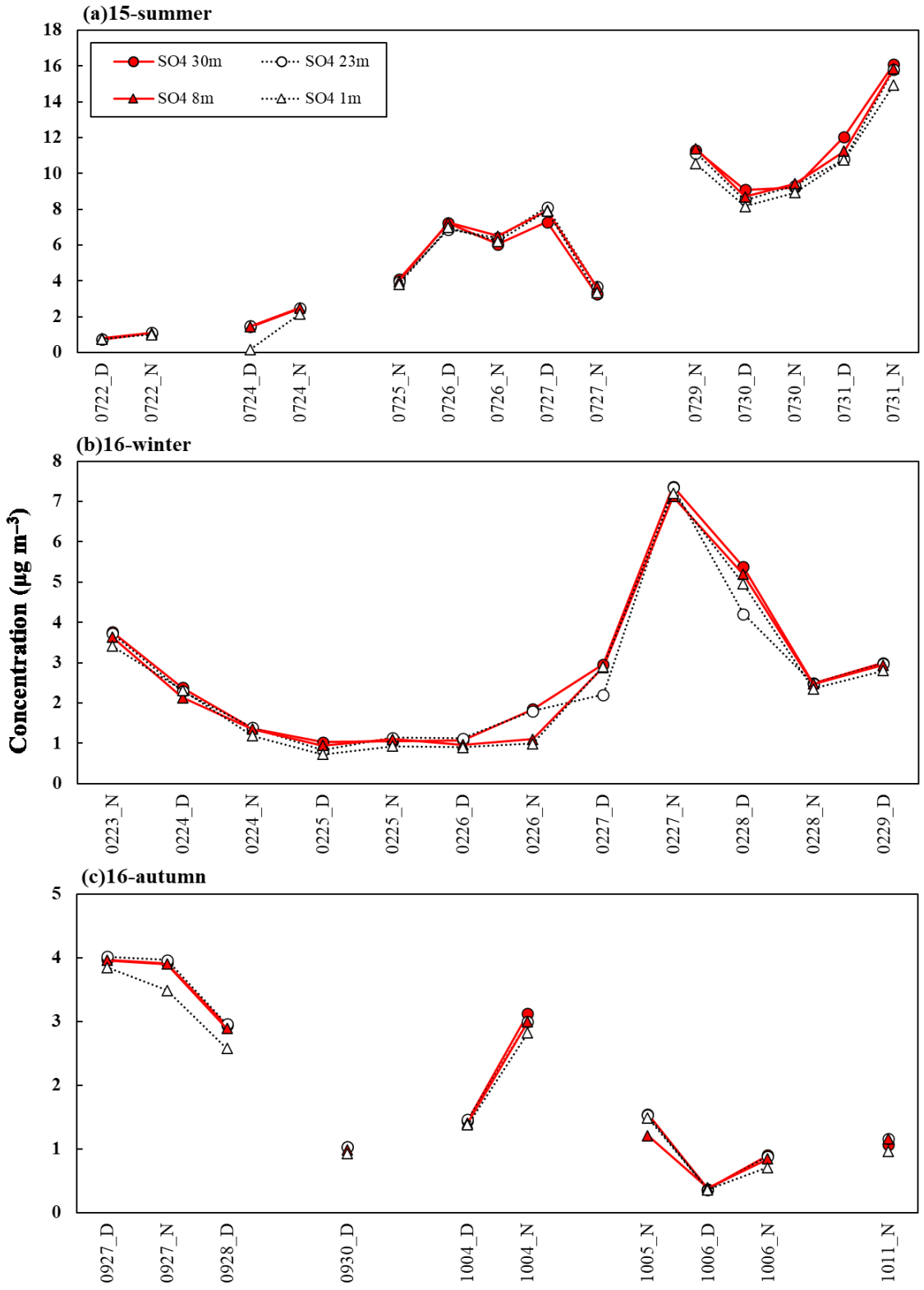

Fig. 2-7. Temporal variations in SO_4^{2-} concentration at 30 m, 23 m, 8 m, and 1 m at the tower during the observation periods. D and N indicate daytime and nighttime, respectively.

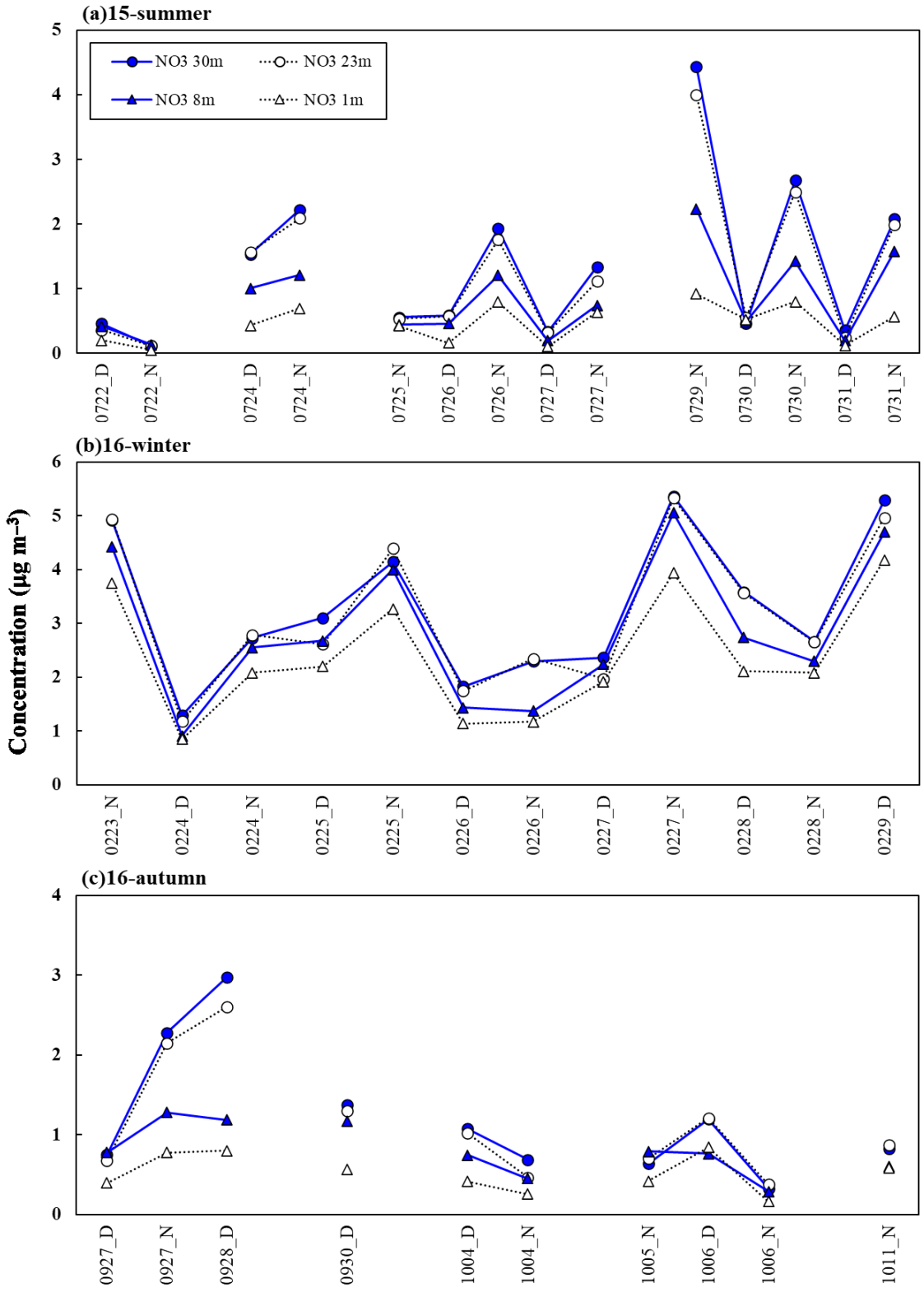

Fig. 2-8. Temporal variations in NO_3^- concentration at 30 m, 23 m, 8 m, and 1 m at the tower during the observation periods. D and N indicate daytime and nighttime, respectively.

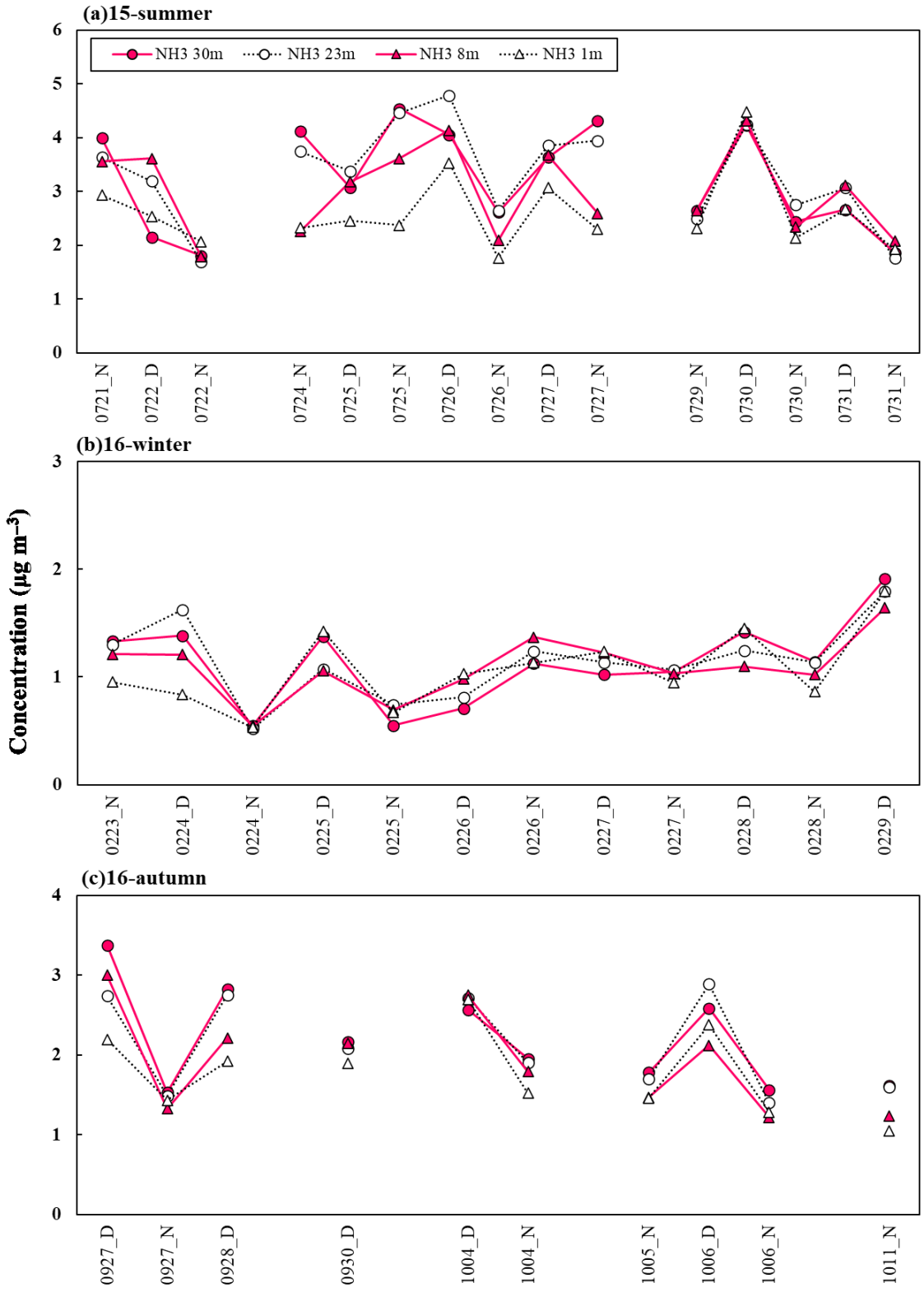

Fig. 2-9. Temporal variations in NH_3 concentration at 30 m, 23 m, 8 m, and 1 m at the tower during the observation periods. D and N indicate daytime and nighttime, respectively.

2.3.2 Vertical concentration profiles

The vertical concentration profiles of SO_4^{2-} and NO_3^- in the $PM_{2.5}$ and those of SO_2 during the daytime and nighttime for the observation periods are shown in Fig. 2-10. The mean concentrations at daytime and nighttime at each height were used to obtain the vertical profiles. The concentrations at all heights were normalized by those at 30 m. As mentioned in Section 1.2, the dry deposition mechanisms of particulate matters are generally assumed to depend on the physical processes at each particle size. In that case, the vertical profiles of SO_4^{2-} and NO_3^- in the $PM_{2.5}$ should show similar tendencies. However, the concentration decreasing of NO_3^- below the canopy was clearly larger than that of SO_4^{2-} during both the daytime and nighttime for all observation periods, especially during the leafy periods. The differences in the vertical profiles of SO_4^{2-} and NO_3^- in the $PM_{2.5}$ decreased in the leafless period due to the smaller decrease in NO_3^- concentration.

The vertical concentration profiles of NH_3 during the daytime and nighttime for the observation periods are shown in Fig. 2-11. During the daytime, emissions occurred above the canopy in 15-summer and near the forest floor in 16-winter. However, NH_3 concentration was decreased from the top of the forest to near the forest floor as a whole during the observation periods. While the diurnal variations in the vertical profiles were larger in 15-summer, there were little changes in 16-autumn. These results suggest that the NH_3 exchange process was different even at the same leafy periods.

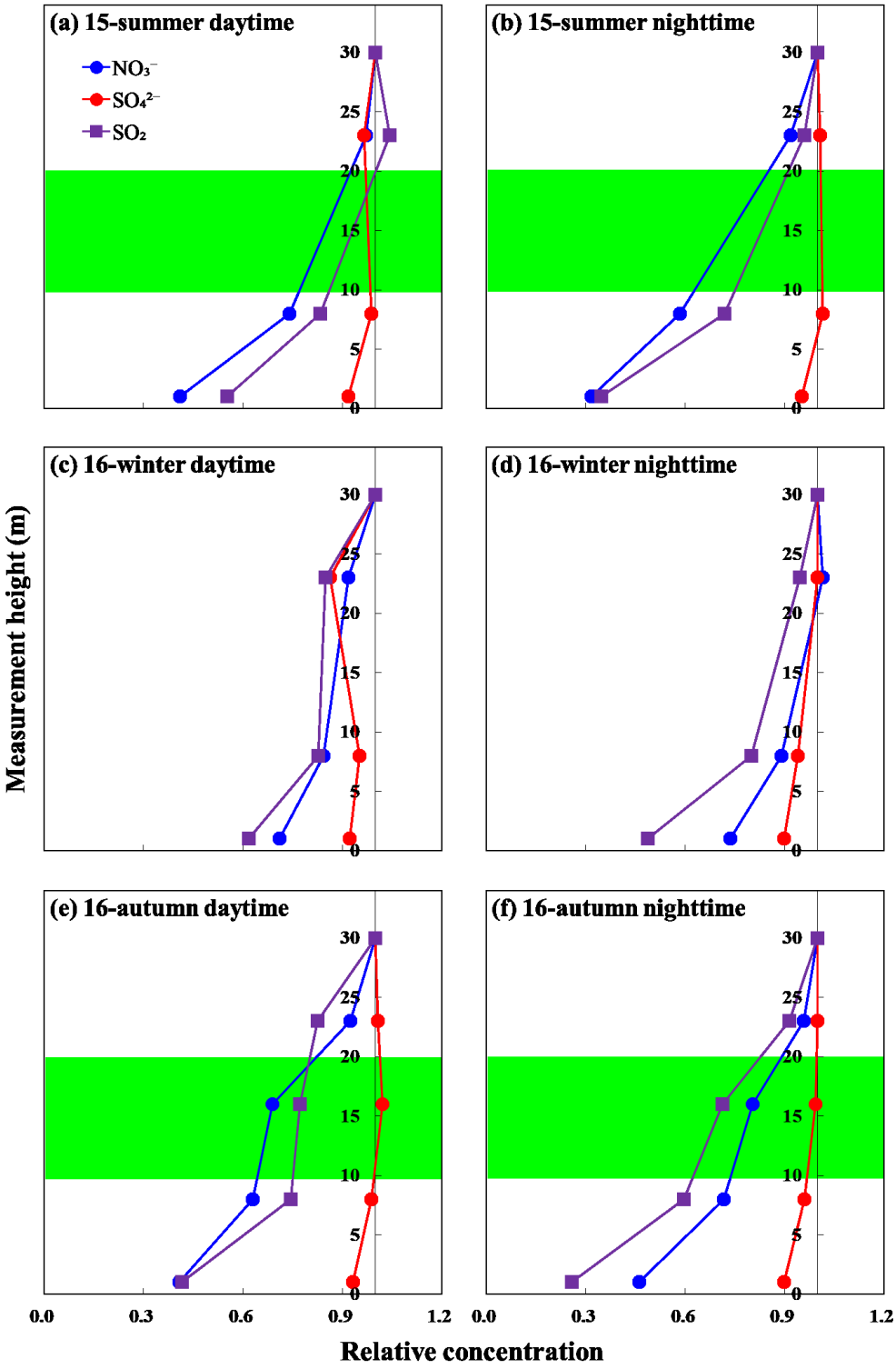

Fig. 2-10. Normalized vertical profiles of the concentrations of SO_4^{2-} (red circles), NO_3^- (blue circles), and SO_2 (purple squares) during the daytime and nighttime for the observation periods. The relative concentration is the concentration ratio with respect to the concentration at 30 m. The green layers indicate the leafy canopies.

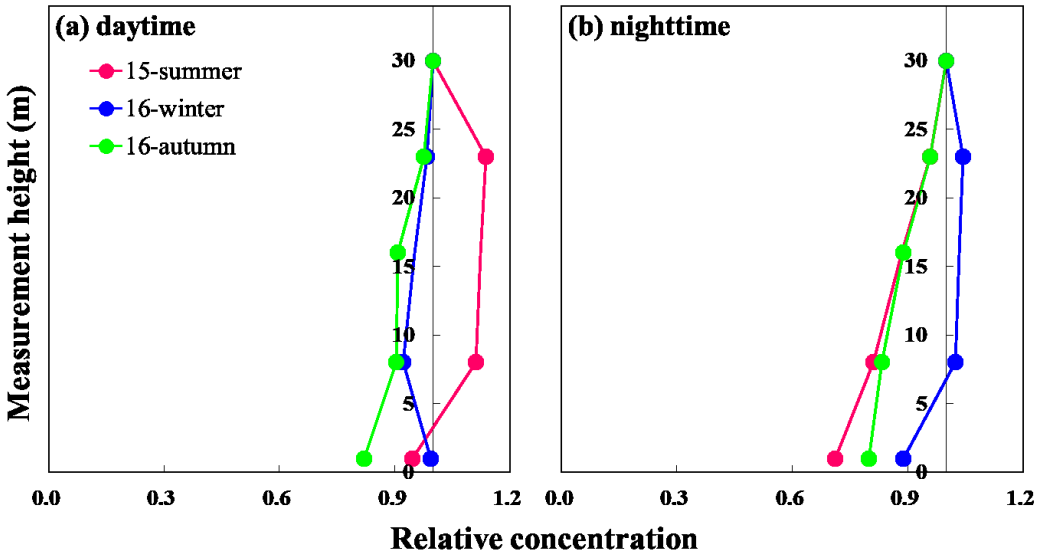

Fig. 2-11. Normalized vertical profiles of the concentrations of NH_3 during the daytime and nighttime for 15-summer (pink circles), 16-winter (blue circles), and 16-autumn (green circles). The relative concentration is the concentration ratio with respect to the concentration at 30 m.

2.3.3 Decreasing rates

The decreasing rate (%) is a proper index to understand the tendency of whether the target component is removed or not between each height (hereafter decreasing rate is referred to as *DR*). The *DR* is defined as follow:

$$DR = \frac{C_{z2} - C_{z1}}{C_{z2}} \times 100 \quad (2\text{-}1)$$

where C_{z2} and C_{z1} is the concentration of the target component at *z2* m and *z1* m (*z2* > *z1*), respectively. Therefore, differences in *DR* indicate the differences in the removal efficiency between components. Since SO_2 is a gas that is easy to deposit on forest surfaces due to its reactive and water-soluble properties, the *DR* for SO_2 is assumed larger than that of fine particulate matter (e.g., Erisman and Draaijers, 1995). This assumption holds in the relationship between SO_2 and SO_4^{2-} profiles under the canopy for all the observation periods (Fig. 2-10). However, the *DR* for NO_3^- in the canopy was close to, sometime larger than, that for SO_2 during the observation periods, especially at daytime in 15-summer and 16-autumn (Fig. 2-10). Even if there was a difference in the particle size distribution for SO_4^{2-} and NO_3^- under 2.5 μm, it cannot cause such a large difference of *DR* between SO_4^{2-} and NO_3^-. In addition to physical processes, there are possibly some factors that enhance the deposition of NO_3^- in $PM_{2.5}$ to the same level as that of gaseous substance.

The distribution of the *DR* of SO_4^{2-} and NO_3^- between each height for the observation periods are shown in Fig. 2-12 and Fig. 2-13. The *DR* values of NO_3^- were clearly larger than those of SO_4^{2-}, particularly in 15-summer and 16-autumn, regardless of daytime and nighttime. Focusing on 16-autumn, I found that the *DR* values of NO_3^- were larger between 23 m and 16 m and between 8 m and 1 m, indicating that the canopy or underlying vegetation contributed to the fast removal of NO_3^-. The *DR* values of SO_4^{2-} varied independently of LAI for all observations. Conversely, the *DR* values of NO_3^- were clearly larger during the leafy periods and smaller during the leafless period. These results also indicated that the variation in the NO_3^- decrease was closely related to the leaf conditions.

The distribution of the *DR* of NH_3 between each height for the observation periods are shown in Fig. 2-14. Although the absolute values of *DR* for NH_3 is smaller than those of NO_3^-, the diurnal variation in *DR* in 15-summer and 16-winter is remarkable. Previous studies have also suggested that there is a seasonal variation in the extent of NH_3 emission due to various factor (Flechard et al. 2013). The difference in results even at the same leafy period and LAI was possibly due to the changes in the emission source and the extent of emission. Main sources of NH_3 in the forest included stomata, soil, fallen leaves and branches, and other organic matters.

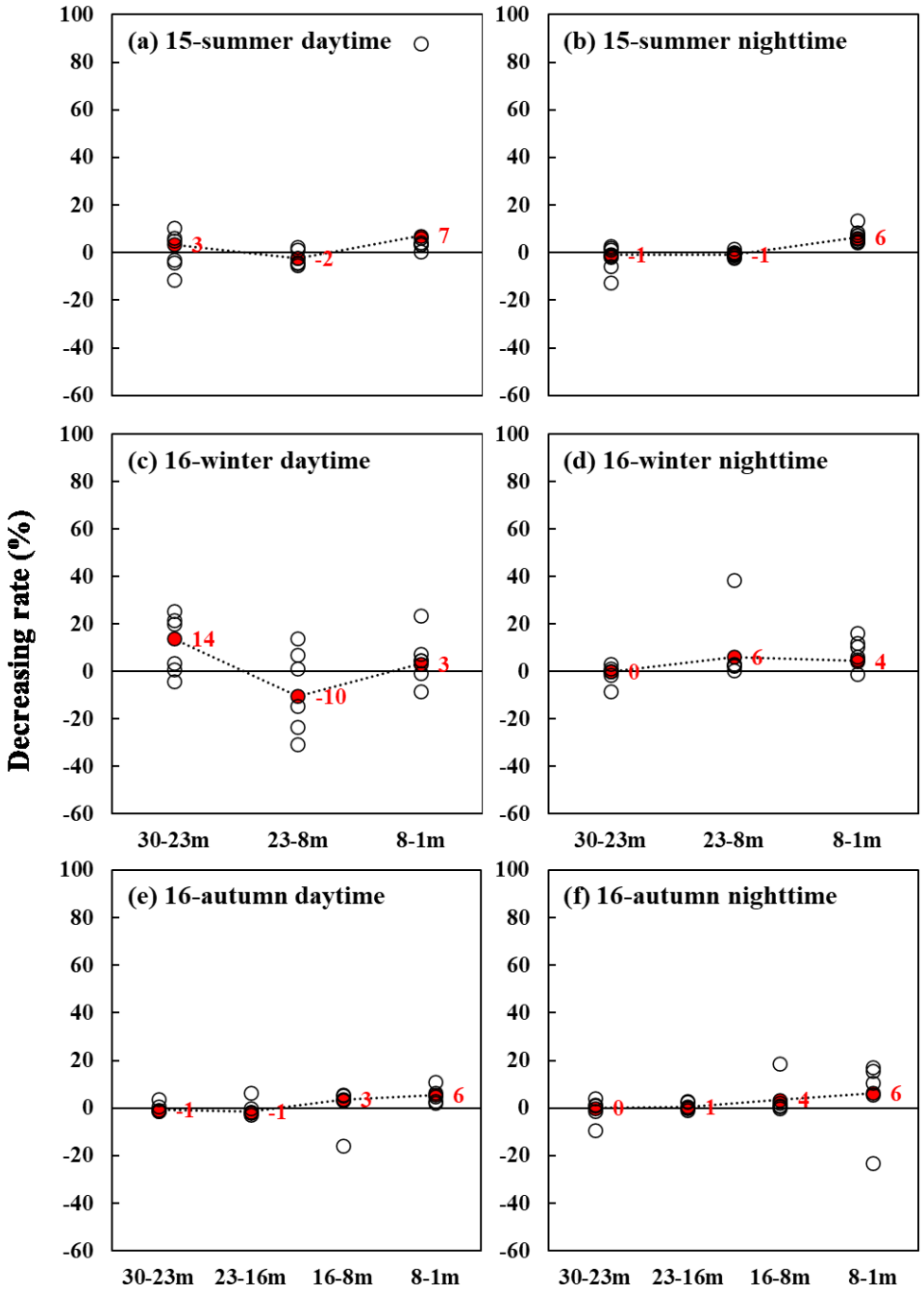

Fig. 2-12. Distribution of the decreasing rates of SO_4^{2-} between each height at the tower during the observation periods. Closed circles and numbers indicate the mean values.

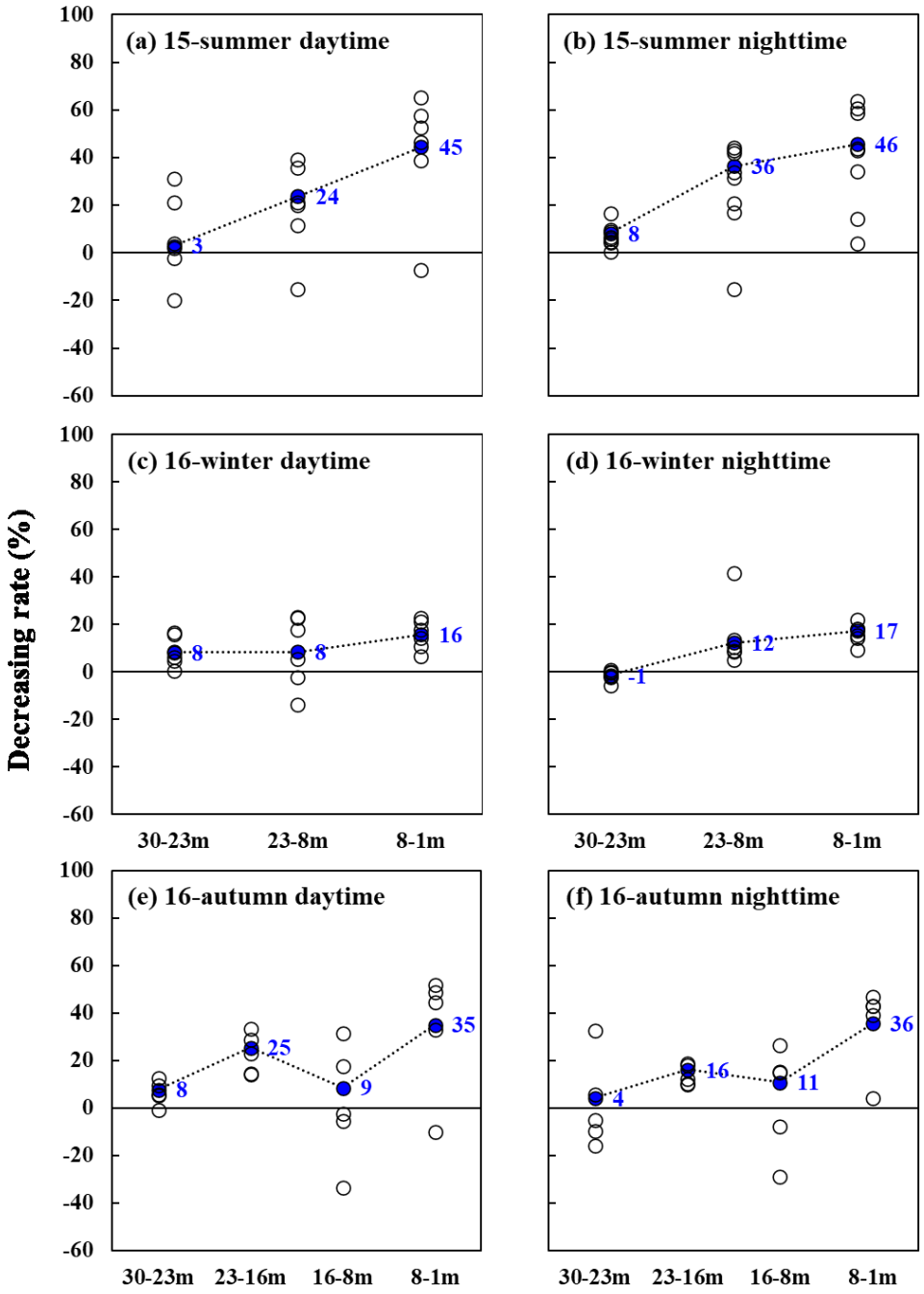

Fig. 2-13. Distribution of the decreasing rates of NO_3^- between each height at the tower during the observation periods. Closed circles and numbers indicate the mean values.

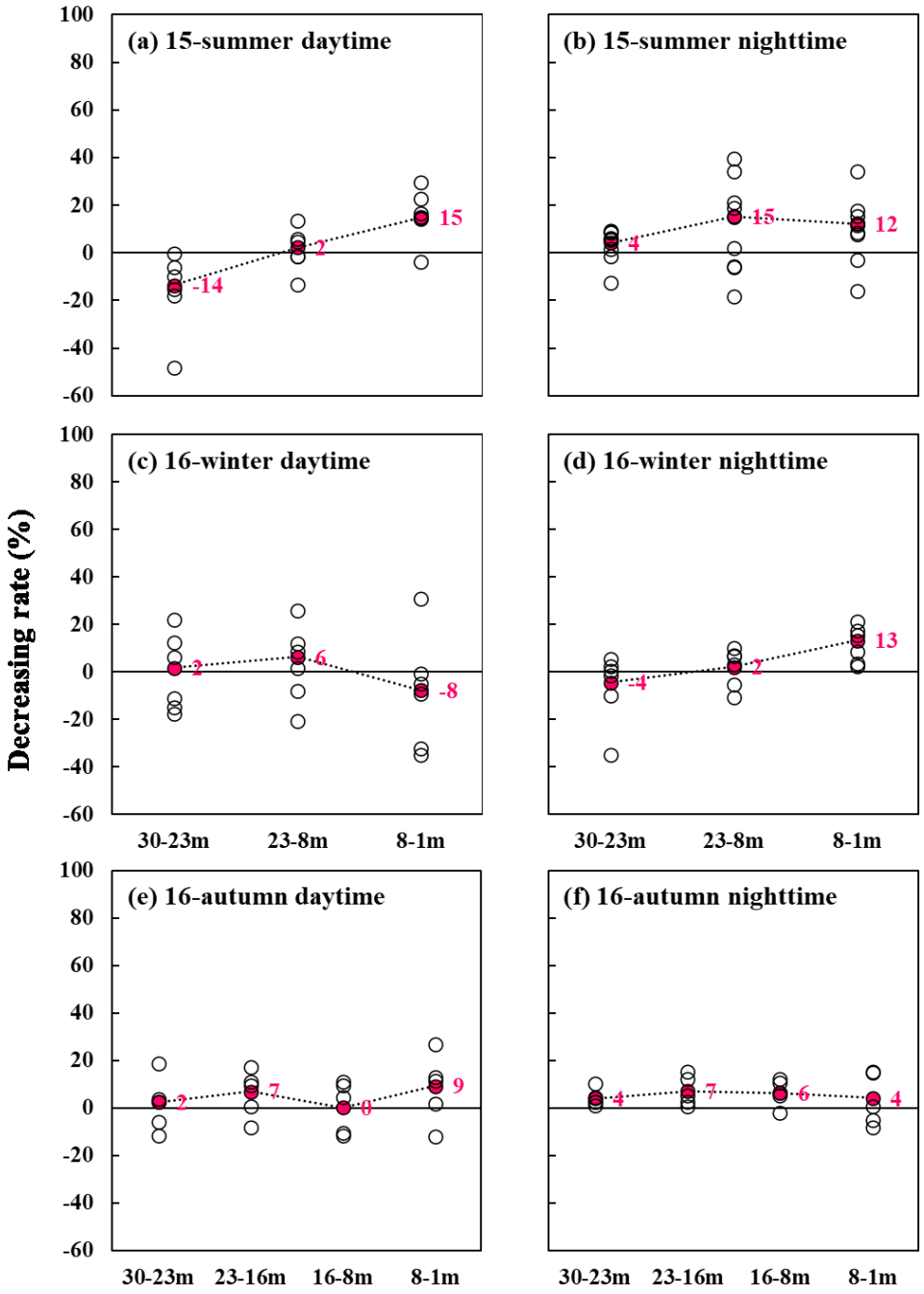

Fig. 2-14. Distribution of the decreasing rates of NH_3 between each height at the tower during the observation periods. Closed circles and numbers indicate the mean values.

2.3.4 Enhancement of dry deposition of ammonium nitrate

Fig. 2-15 and Fig. 2-16 show the relationships between equivalent concentration of total cations ($NH_4^+ + Na^+ + K^+ + Ca^{2+} + Mg^{2+}$) and anions ($SO_4^{2-} + NO_3^- + Cl^-$) and the composition of inorganic components in $PM_{2.5}$ at 30 m, 23 m, 8 m, and 1 m during the observation periods. The ratio of each equivalent concentration was almost 1:1, and about 80% of the inorganic ions in the $PM_{2.5}$ consisted of NH_4^+, SO_4^{2-}, and NO_3^- at all heights. Considering these relationships between the equivalent concentrations, the inorganic components in $PM_{2.5}$ at the site during the observation periods primarily existed as $(NH_4)_2SO_4$ or NH_4NO_3. $(NH_4)_2SO_4$ particles have a very low vapor pressure and exist as solid under atmospheric conditions (Seinfeld and Pandis, 2006). On the other hand, NH_4NO_3 particles are semi-volatile and have an equilibrium relationship with NH_3 and HNO_3 in the atmosphere as shown in Eq. (1-1). Therefore, dry deposition of NH_4NO_3 is affected by the volatilization (equilibrium shift from particle to gas). The volatilization depends on Temp, RH, and the concentrations of either HNO_3 or NH_3. The differences in the *DR* values between SO_4^{2-} and NO_3^- were likely caused by differences in the chemical properties.

There are some previous studies indicate larger removal of NO_3^- particles than those of SO_4^{2-} particles. Over a crested wheatgrass field in the Boulder Atmospheric Observatory, a research facility in Colorado in the United States, Huebert et al. (1988) found that the vertical gradients in concentration of the NO_3^- were larger than those of SO_4^{2-} and sometimes exceeded those of HNO_3. These results are consistent with the model approach in Brost et al. (1988) coupling the volatilization of NH_4NO_3 to the rapid dry deposition of HNO_3. Sievering et al. (1994) conducted similar vertical profile measurements in a spruce forest in Bayerischer Wald National Park (Germany) and obtained large decreases in NO_3^- concentration close to those of HNO_3. The large decreases of NO_3^- concentration is discussed in terms of both particle size distribution and equilibrium shift from particle to gas. Using AGM, Wyers and Duyzer (1993) determined the V_d for SO_4^{2-} and NO_3^- above a coniferous forest at Speulderbos (Netherlands). They found that the V_d of NO_3^- was not only much larger than that of SO_4^{2-}, but also larger than that of the maximum theoretically possible value when the temperature was high (above 20°C). These results were also possibly due to the equilibrium shift from NH_4NO_3 to NH_3 and HNO_3. Van Oss et al. (1998) applied these results in their model, which considered the influence of the equilibrium shift on surface exchange processes above a forest. They also indicated that the volatilization of particulate NH_4NO_3 during the daytime can lead to the emission of HNO_3 and NH_3 above the forest, in addition to the abnormally large V_d for NO_3^-. Based on the observations at a dry heathland in Elspeetsche Veld (Netherlands), Nemiz et al. (2004b) indicated that the chemical conversion of Eq. (1-1) was sufficiently fast to modify the exchange fluxes. From these studies, there are two plausible process which can lead the differences in the dry deposition between $(NH_4)_2SO_4$ or NH_4NO_3:

- An equilibrium shift of NH_4NO_3 due to the higher temperature near the deposition surfaces and/or
- An equilibrium shift of NH_4NO_3 due to the low concentrations of HNO_3 caused by its fast removal near the deposition surfaces.

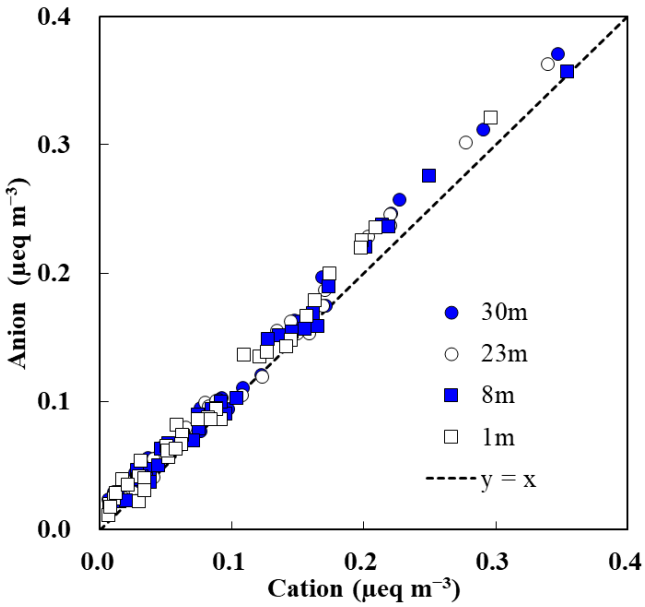

Fig. 2-15. Relationships between equivalent concentration of total cations ($NH_4^+ + Na^+ + K^+ + Ca^{2+} + Mg^{2+}$) and anions ($SO_4^{2-} + NO_3^- + Cl^-$) in the $PM_{2.5}$ at 30 m, 23 m, 8 m, and 1 m at the tower during the observation periods. The dashed line indicates a 1:1 ratio of each equivalent concentration.

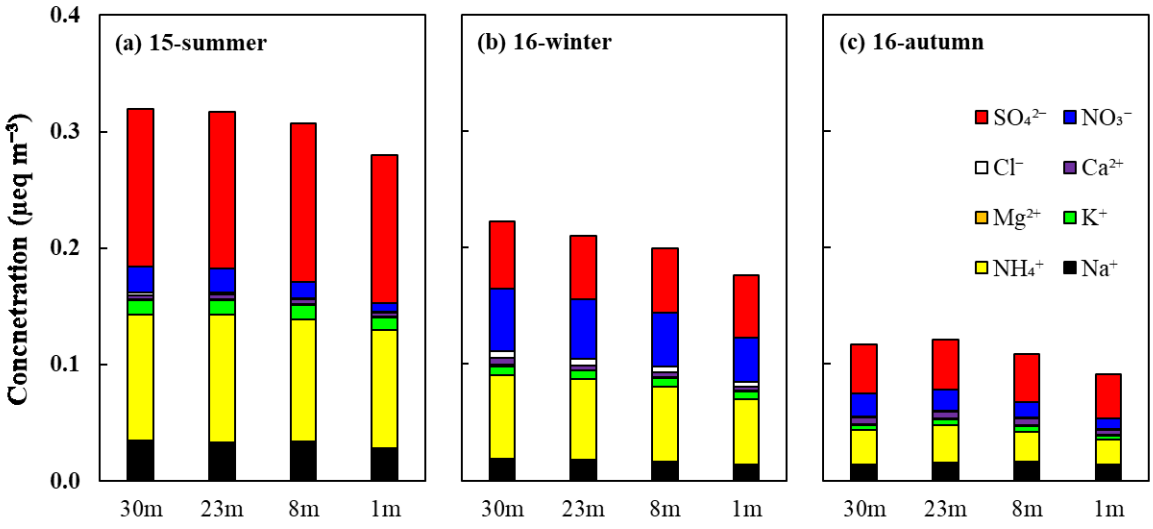

Fig. 2-16. Equivalent concentration of inorganic ions in $PM_{2.5}$ (NH_4^+, Na^+, K^+, Ca^{2+}, Mg^{2+}, SO_4^{2-}, NO_3^-, Cl^-) at 30 m, 23 m, 8 m, and 1 m at the tower during the observation periods.

To verify the first process, I focused on the variations in the ensemble mean Temp over the observation periods (Fig. 2-17). In the daytime, Temp at 30 m was lower than Temp at 20 m (close to the canopy surface) during 15-summer and 16-autumn and was lower than Temp at 1 m (close to the forest floor) during 16-winter. This is because direct sunlight struck the canopy surface during the daytime in the leafy periods and struck the forest floor in the leafless period. In addition, Temp values of canopy surfaces exposed to sunlight tend to be higher than the Temp values near the surfaces at daytime (Nakahara et al., 2019). Therefore, the volatilization of NH_4NO_3 was likely enhanced near the canopy surface during the leafy periods and near the forest floor during the leafless period. This agrees with the larger daytime *DR* values of NO_3^- than those SO_4^{2-} in the canopy during the observation periods (Fig. 2-12 and Fig. 2-13). Conversely, the Temp gradients were not clearly seen in the nighttime, even though the *DR* values of NO_3^- were also larger than those of SO_4^{2-} in the nighttime.

The NH_4NO_3 particles have an equilibrium relationship with the concentrations of the HNO_3 and NH_3 gases in the atmosphere. The V_d for HNO_3 is known to be greatly larger than those of NH_3 and NO_3^-. The V_d calculated by the resistance models are 3 to 10 times higher than those of other gaseous and particulate matter (Ban et al., 2016). During the leafy periods, HNO_3 was quickly removed by the canopy surface due to the large V_d and leaf area. When HNO_3 is quickly removed by the deposition surfaces, HNO_3 concentration near these surfaces drastically decreases. Then, the equilibrium in Eq. (1-1) is shifted to the gas phase. As a result, NH_4NO_3 near the surfaces volatilizes to resupply the decreased HNO_3 concentration and quickly removed by the surfaces as gaseous matter. This process can cause a large removal of NO_3^- just as fast as SO_2 not only at the daytime but also at the nighttime (Fig. 2-10). Therefore, the *DR* of NO_3^- became significantly larger than that of SO_4^{2-}.

Katata et al. (2020) simulated the vertical profiles at FM Tama in 16-autumn using a one-dimensional multi-layer land surface model (SOLVEG), which can consider the equilibrium shift of NH_4NO_3−NH_3−HNO_3 in the canopy and the deposition of each component. Simulations without consideration of the equilibrium shift in SOLVEG showed no difference in SO_4^{2-} and NO_3^- profiles. Conversely, there was a clear difference in SO_4^{2-} and NO_3^- profiles at daytime in the simulations considering the equilibrium shift, and the results were the same as my observations. However, the difference was smaller at nighttime in the model, and this is likely due to the uncertainty in the process of the equilibrium shift of NH_4NO_3 due to the low concentrations of HNO_3 or other nighttime processes. Overall, these results support my hypothesis for the processes that enhance the dry deposition of NO_3^-.

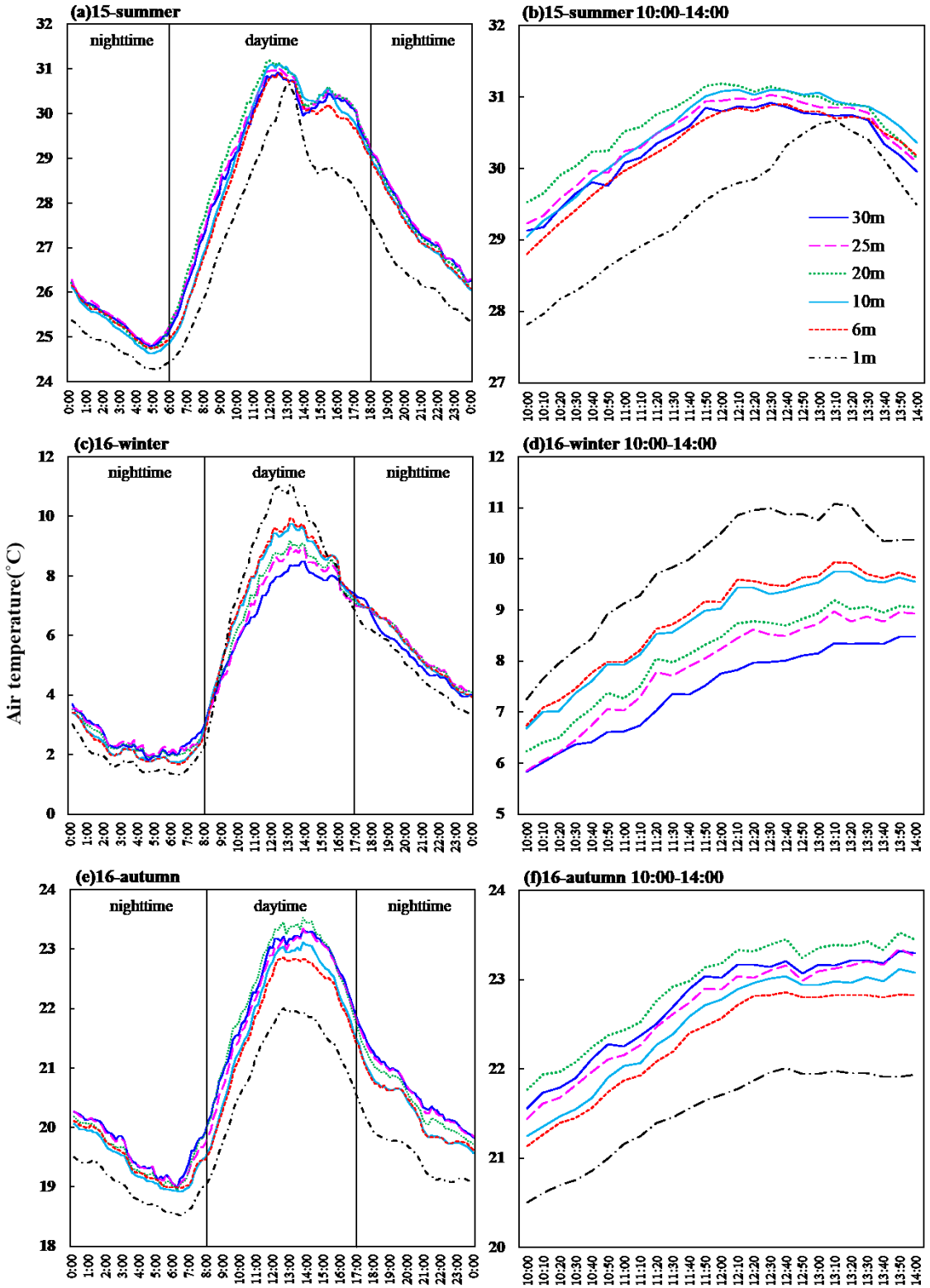

Fig. 2-17. Temporal variations in the ensemble mean values of the air temperature at 30 m, 25 m, 20 m, 10 m, 6 m, and 1 m during the observation periods. The figures ((b), (d), (f)) are an expansion of the period between 10:00 and 14:00 when the temperature is higher.

2.3.5 Uncertainties

The volatilization of NH_4NO_3 due to the higher Temp near the deposition surfaces during the daytime possibly enhanced the dry deposition of NO_3^-. Since the Temp in the filter-pack holders may be higher than their surroundings due to direct sunlight, the volatilization of NH_4NO_3 could also occur in the filter-pack holders. This artifact causes an underestimation of the NH_4NO_3 concentration and an overestimation of the concentrations for NH_3 and HNO_3. According to the Temp profiles at the measurement site, the volatilization of NH_4NO_3 in the filters was likely more intense at 20 m during the daytime in leafy periods, and at 1 m during the daytime in leafless periods. Thus, the concentration of NO_3^- in the $PM_{2.5}$ at those heights should be lower than at other heights. However, the concentrations of NO_3^- in the $PM_{2.5}$ clearly decreased from the top of the canopy to the forest floor in the leafy periods. Since there may not be a close relationship between the concentrations of NO_3^- in the $PM_{2.5}$ and the Temp difference between each of the heights during daytime, we can conclude that the difference in the vertical gradients between NO_3^- and SO_4^{2-} in the $PM_{2.5}$ was not primarily because of the volatilization of NH_4NO_3 in the filter-pack holders.

It is also possible that the daytime NH_3 emissions on the canopy in 15-summer and on the forest floor in 16-winter were affected by this artifact. For the 15-summer, the amount of NH_3 emission is much larger than the amount of NH_4NO_3 volatilization (Fig. 2-18). Therefore, the effect of artifacts was negligible in 15-summer. However, NH_3 concentrations were lower and the amount of NH_3 emissions are also smaller in 16-winter, it is likely that there were some effects of the artifact.

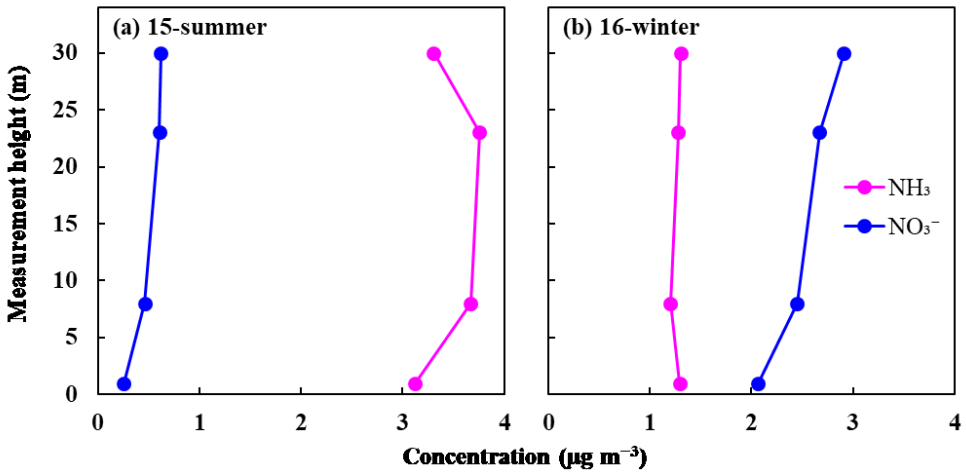

Fig. 2-18. Vertical profiles of the concentrations of NO_3^- (blue circles) and NH_3 (pink circles) during the daytime in (a) 15-summer and (b) 16-autumn.

Chapter 3 Long-term fluxes of nitrate and nitric acid in a deciduous forest

3.1 Introduction

HNO_3 is one of the major Nr and largely contributes to the nitrogen deposition. Although the V_d for HNO_3 is known to be typically larger than that of other Nr due to its higher reactivity, some studies indicated there are HNO_3 emissions in addition to the suppression of HNO_3 deposition (Nemitz, 2015). These results are possibly due to the NH_4NO_3−NH_3−HNO_3 interactions during the deposition process. However, the HNO_3 flux measurements in Europe and the United States from 1990s to the 2010s were conducted only over short periods of time or during the leafy period (Pryor et al., 2002; Pryor and Klemm, 2004; Myles et al., 2007; Hansen et al., 2015). Therefore, there remains a lot of uncertainties in the deposition process of HNO_3 and further measurements are required to address these challenges. Moreover, such flux measurements have rarely been conducted in Asia. Further understanding of the HNO_3 dry deposition process associated with the NH_4NO_3−NH_3−HNO_3 interactions could also improves understanding of NO_3^- dry deposition and NH_3 exchange process, which still has considerable uncertainties.

Against this backdrop, I obtained a long-term (from leafy to leafless periods) flux dataset for HNO_3 and $PM_{2.5}$ inorganic components above a forest. I conducted the flux measurements using the REA method in a forest of suburban Tokyo, Japan. The REA is appropriate method for measuring the flux of HNO_3 and particulate matter, which are difficult to measure quickly, because it is possible to eliminate the need for a fast-response analyzer. To investigate the HNO_3 deposition process, I also compared the V_d of HNO_3 estimated from the measurements with those inferred from the resistance model. This study is the first to evaluate the V_d of HNO_3 associated with the NH_4NO_3−NH_3−HNO_3 interactions based on the long-term flux measurements in the Asian region.

3.2 Methods

3.2.1 Site description

I conducted long-term flux measurements of HNO_3 and $PM_{2.5}$ components in a forest at the FM Tama site of the Tokyo University of Agriculture and Technology, which is located in a western suburb of Tokyo, Japan. More details about the site are described in Section 2.2.1. I also used the same observation tower as for the vertical profile measurements in **Chapter 2**.

3.2.2 Relaxed eddy accumulation sampling system for particle and nitric acid gas

I conducted the measurements from October 14, 2016 to October 3, 2018. I installed an REA system incorporating the denuder/filter-pack sampling technique at the top of the tower (30 m) (Fig. 3-1 (a), (b)). I also installed a denuder/filter-pack sampling system at the same height as the REA system in parallel (Fig. 3-1 (a), (c)) to verify the data measured by the REA system. I carried out continuous samplings and manually changed the denuder tubes and filters on a weekly basis during the long-term measurements.

Micrometeorological elements including WS for the REA system were observed at the top of the tower using a 3D sonic anemometer (GILL, CPR-1590-PK-020 until February 22, 2017; YOUNG, 81000 from September 19, 2017). The measurements were suspended from February 22, 2017 to September 19, 2017 due to mechanical

problems with the anemometer. Weather Transmitter (VAISALA, WXT520) recorded the temp and RH at a height of 25 m. Rainfall was measured in 0.5 mm interval using the tipping bucket rain gauge on the open-space ground in the site. I periodically measured the LAI using a plant canopy analyzer (LI-COR, LAI-2200).

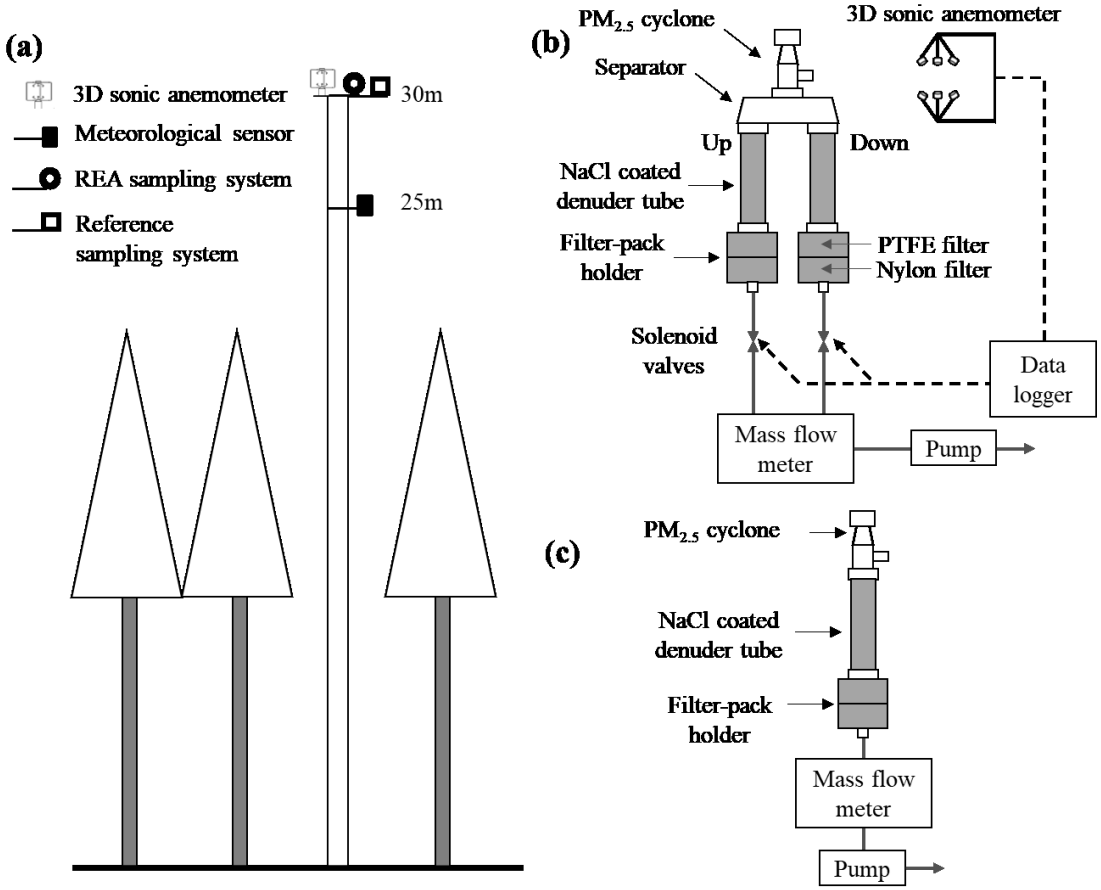

Fig. 3-1. Schematic diagrams of (a) the observation tower, (b) the REA sampling system and (c) the reference sampling system. "Up" and "Down" mean the sampling lines for updraft and downdraft, respectively.

I used the REA system incorporating the denuder/filter-pack sampling technique linked with a 3D sonic anemometer (Sakamoto et al., 2018) to determine the fluxes of HNO_3 and $PM_{2.5}$ components (Fig. 3-2). The REA system was developed based on a previous system for measuring $PM_{2.5}$ sulfate flux in the same site (Matsuda et al., 2015). Generally, the EC is the most direct measurement method for determine the vertical flux. In the EC, the upward and downward mass transfer are measured in a horizontal unit area at a certain height, and the net flux is obtained from the difference between the upward and downward as follow:

$$F = \overline{w'C'} \tag{3-1}$$

where F is flux, and w' and C' are the variations of the vertical wind speed and concentration of target substance, respectively. Since the vertical transfer in the atmosphere is due to turbulence, the upward and downward mass

transfer vary at timescale of about 10 Hz. Therefore, it is necessary to measure the concentration of the target substance with this time resolution in the EC, in addition to measure the vertical wind speed. At present, EC are widely applied to flux measurement of water vapour and carbon dioxide (CO_2).

In REA, target substance is collected and accumulated separately according to the direction of vertical wind (conditional sampling), and the flux is determined from the difference in concentration between the updraft and downdraft, based on the concept of EC. Similar to the EC, REA is required to measure the vertical wind speed with high temporal resolution, however, there is no necessary to measure the concentration of substances instantaneously. Therefore, REA can be applied to air pollutants whose concentrations are much lower than those of CO_2. The fluxes were determined as follows:

$$F = \beta \sigma_w (C_u - C_d) \tag{3-2}$$

where β is an empirical coefficient, σ_w is the standard deviation of the vertical wind speed, and C_u and C_d are the mean concentration of each substance in the updraft and downdraft, respectively. Regarding the conditional sampling, I followed the switching method suggested by Matsuda et al. (2015), while not using their switching frequency. In this study, I set the frequency to 1 Hz to avoid the sampling loss of the denuder/filter-pack system due to frequent switching. I did not employ the "dead-band" sampling to maximize the difference between C_u and C_d (Meyers et al., 2006). I calculate the β from the data obtained by 3D sonic anemometer as follow:

$$\beta = \frac{\overline{w'T'}}{\sigma_w (T_u - T_d)} \tag{3-3}$$

where $w'T'$ is sensible heat flux (w' and T' are the variations of the vertical wind speed and Temp, respectively) determined by the EC, and T_u and T_d are the mean Temp of the updraft and downdraft, respectively. The β coefficient was calculated from the 10-min mean values of $w'T'$ and $\sigma_w(T_u–T_d)$. The V_d was calculated by dividing the flux by the concentration. The concentration was derived from the weighted mean of C_u and C_d by integrated flow rate at each draft.

The REA sampling part comprised a Teflon-coated aluminum cyclone (URG, 2000-30EHB), two annular denuder tubes (URG, 2000-30×150-3CSS), and two Teflon filter-pack holders (URG, 2000-30FG) (Fig. 3-2). The flow rate of pump was set at 5.5 min^{-1} in accordance with the $PM_{2.5}$ cut of the cyclone. The denuder tubes for collecting HNO_3 were coated with 9% NaCl solution (9% (w/v) NaCl + 1% (w/v) glycerin + 50% (v/v) ethanol-water solution) (Nakahara et al., 2019). After coating, the denuder tubes were dried by clean air passing through the desiccant, activated charcoal, and a filter-pack holder (Tokyo Dylec Corporation, NILU filter folder NL-O) comprising a glass fiber filter (Tokyo Dylec Corporation, 2500 QAT-UP 47 mm) and a cellulose filter impregnated with potassium carbonate. HNO_3 was not detected from the coated denuder tubes at the blank test (n = 10). I used a PTFE filter (ADVANTEC, T080A074A) to collect $PM_{2.5}$ on the first stage of the filter-pack holders, and a nylon filter (Pall, ULTIPOR N66) to collect the HNO_3 generated from NH_4NO_3 volatilization followed. The effect of volatilization

of semi-volatile particles within the filter-pack holders mentioned in Section 2.3.5 is thereby negligible. As already mentioned, I also measured the reference concentrations in parallel using the same specifications of $PM_{2.5}$ cyclone and denuder/filter-pack as the REA system for data verification. After the samplings, the inorganic ions in each denuder tube and filter were extracted into deionized water with 20 ml via an ultrasonic method. Then, I used ion chromatography for analyzing the inorganic ions (Dionex, ICS-1100).

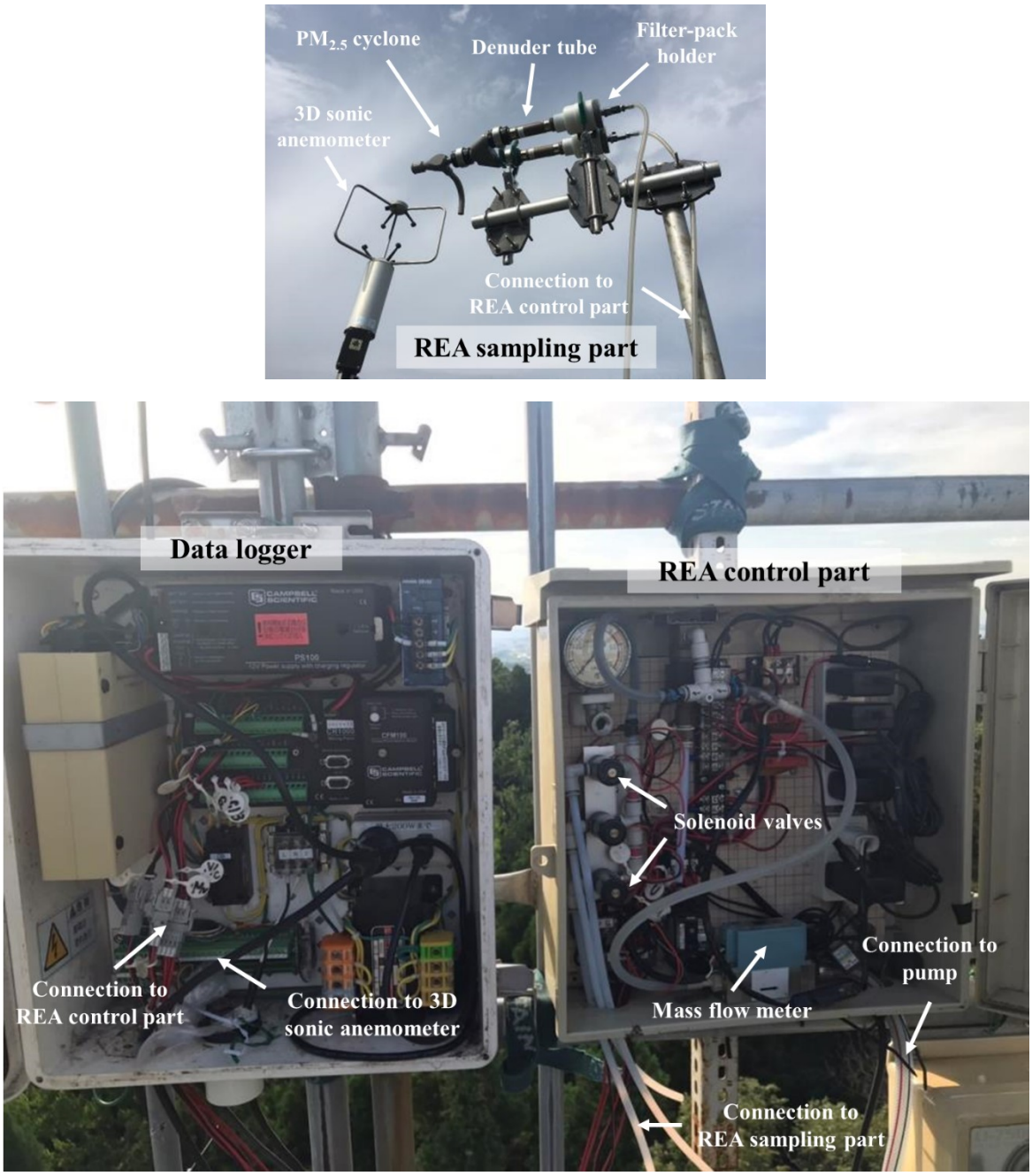

Fig. 3-2. Photo of the REA sampling system.

3.2.3 The resistance model

To analyze the mechanism of deposition process of HNO_3, I compared the REA measurements with the V_d calculated by the current resistance model. In the inferential method, the dry deposition amounts are obtained from the product of the measured concentrations and the inferred V_d as follows (Erisman and Draaijers, 1995):

$$F = C \times V_d \tag{3−4}$$

where F is flux and C is concentration of target component at reference height. The concentration is measured, and the V_d is inferred using the resistance model that models the dry deposition process of particulate matters and gaseous substances. In this study, I used the resistance model adopted by the EANET (Fig. 3-3) to calculate theoretical V_d of HNO_3 for comparison with measurements (EANET, 2010).

The resistance model divides the dry deposition process from the atmosphere to the surface into multiple stages. Each resistance during transport from the atmosphere to the surface is parameterized by the main factors govern each stage. The resistance model defines that gaseous substances pass through three resistances during deposition (Fig. 3-3). The three resistances are aerodynamic resistance (R_a), quasi-laminar resistance (R_b), and surface resistance (R_c), respectively. The surface boundary layer is a layer up to several tens of meters above the ground, and vertical transport in this layer is dominated by turbulent diffusion. R_a is the resistance by this turbulent diffusion and mainly depends on the intensity of the turbulence. The quasi-laminar layer is the layer very close to the deposition surface where is not affected by turbulent diffusion. The thickness of the layer depends on the size and shape of the surface etc. Vertical transport in quasi-laminar layer is dominated by molecular diffusion, and the resistance in this layer is R_b. Gaseous substances pass through the above two resistances and finally deposit on the surface after interaction. The resistance due to this interaction with surface is R_c. For gaseous substances, the reciprocal of the combined resistance of these resistances corresponds to the conductance of Ohm's law, and is defined as V_d as follows:

$$V_d = \frac{1}{R_a + R_b + R_C} \tag{3-5}$$

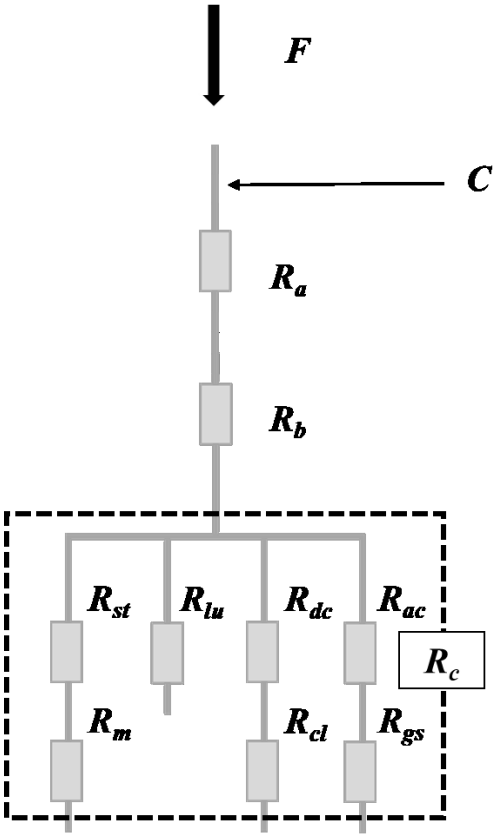

Fig. 3-3. Conceptual diagram of the resistance model based on Wesely (1989). *F* is flux at reference height. *C* is concentration of target at reference height. R_a, R_b, R_c, R_{st}, R_m, R_{lu}, R_{dc}, R_{cl}, R_{ac}, R_{gs} indicate aerodynamic resistance, quasi-laminar resistance, surface resistance, stomatal resistance, mesophyll resistance, cuticular resistance, buoyant convection resistance, lower canopy resistance, surface transfer resistance, and soil resistance, respectively.

- Aerodynamic resistance

R_a is generally determined by the equations of Erisman and Draaijers (1995) as follow:

$$R_a = \frac{1}{ku^*}\left(\ln\frac{z-d}{z_0} - \psi_h\frac{z-d}{L} + \psi_h\frac{z_0}{L}\right) \tag{3-6}$$

where k is von Karman constant (k = 0.41), u^* is friction velocity, z is reference height, d is displacement height, z_0 is roughness length, L is Monin-Obukhov length, and ψ_h is integrated stability function for heat, respectively. u^* is the intensity of turbulence and is obtained from the variations of horizontal and vertical WS recorded by the 3D sonic anemometer as follow:

$$u^* = ((\mathrm{U_x}'\mathrm{W_z}')^2 + \left(\mathrm{V_y}'\mathrm{W_z}'\right)^2)^{1/4} \tag{3-7}$$

where U_x', V_y', and W_z' are the variations of horizontal WS in the east-west direction, horizontal WS in the north-south direction, and vertical wind speed, respectively. d and z_0 were determined from WS at 30 m and 20 m using the logarithmic law of WS. In the FM Tama site, d and z_0 were set at 16 m and 0.8 m for the leafy period, and 15 m and 0.7 m for the leafless period, respectively. L is an index for determining atmospheric stability and is also obtained from elements recorded by the 3D sonic anemometer as follow:

$$L = -\frac{Tu^{*3}}{kg\overline{w'T'}} \tag{3-8}$$

where T is temperature, g is gravitational acceleration (g = 0.98), and $w'T'$ is sensible heat flux, respectively. Since $w'T'$ is nearly 0 at neutral, L has an infinite value. Then, it is possible to determine the atmospheric stability by expressing it as $1/L$. At this time, $1/L$ indicate stable if positive, unstable if negative, and neutral if nearly 0. The formula of ψ_h changes according to the atmospheric stability determined by L. For stable and neutral conditions, ψ_h is calculated as follows:

$$\psi_h \frac{z-d}{L} = -5.2\frac{z-d}{L} \tag{3-9}$$

For unstable condition, ψ_h is calculated as follows:

$$\psi_h \frac{z-d}{L} = 2\ln\frac{1+(x)^2}{2} \tag{3-10}$$

x is calculated as follows:

$$x = \left(1 - 16\frac{z-d}{L}\right)^{0.25} \tag{3-11}$$

- Quasi-laminar resistance

R_b is also determined by the equations of Erisman and Draaijers (1995) as follow:

$$R_b = \frac{2}{ku^*}\left(\frac{Sc}{Pr}\right)^{2/3} \tag{3-12}$$

where Sc is Schmidt number and Pr is Prandtl number. Sc is the ratio of the kinematic viscosity of air to the molecular diffusivity of target substance. Pr is the ratio of the kinematic viscosity of air to the thermal diffusivity (Pr = 0.72).

➢ Surface resistance

R_c is most complicated in the three resistances and various models have been proposed since 1980s. In the resistance model adopted by EANET, the R_c was determined using the parameterization presented by Wesely (1989) as follow:

$$R_c = \left(\frac{1}{R_{st} + R_m} + \frac{1}{R_{lu}} + \frac{1}{R_{dc} + R_{cl}} + \frac{1}{R_{ac} + R_{gs}} \right)^{-1} \tag{3-13}$$

where R_{st} is stomatal resistance, R_m is mesophyll resistance, R_{lu} is cuticular resistance, R_{dc} is resistance to transfer by buoyant convection, R_{cl} is the resistance to removal by leaves, twigs, and other exposed surfaces, R_{ac} is a transfer resistance for process only depend on canopy height and density, and R_g is resistance to removal by the soil, leaf litter, and so on at the ground surface, respectively (Seinfeld and Pandis, 2006). These resistances are calculated as follow:

$$R_{st} + R_m = R_{st} \left(\frac{D_v}{D_{HNO_3}} \right) + \frac{1}{3.3 \times 10^{-4} H^* + 100 f_0} \tag{3-14}$$

$$R_{st} = R_j \left[1 + \left(\frac{200}{SR + 0.1} \right)^2 \left(\frac{400}{T(40 - T)} \right) \right] \tag{3-15}$$

$$R_{lu} = r_{lu} \times \frac{1}{10^{-5} H^* + f_0} \tag{3-16}$$

$$R_{dc} = 100 \left(1 + \frac{1000}{\mathrm{SR} + 10} \right) \left(\frac{1}{1 + 1000\theta} \right) \tag{3-17}$$

$$R_{cl} = \left(\frac{10^{-5} H^*}{R_{clS}} + \frac{f_0}{R_{clO}} \right)^{-1} \tag{3-18}$$

$$R_{gs} = \left(\frac{10^{-5} H^*}{R_{gsS}} + \frac{f_0}{R_{gsO}} \right)^{-1} \tag{3-19}$$

where D_v/D_{HNO3} is the ratio of molecular diffusivity of water vapour to HNO_3, H^* is effective Henry's law constant, f_0 is normalized reactive factor, R_j is minimum R_{st} for water vapour, r_{lu} is an input parameter, θ is the slope of the local terrain, R_{clS} and R_{clO} is R_{cl} for SO_2 and ozone (O_3), and R_{gsS} and R_{gsO} is R_{gs} for SO_2 and O_3, respectively. The values of R_j, r_{lu}, R_{ac}, R_{clS}, R_{clO}, R_{gsS}, and R_{gsO} are given for five season categories and eleven land use categories (LUC). In this study, I adopted these values at mixed forest including wetland for seasonal category of 1, 3, and 5.

The parameters in the resistance model for estimating the V_d of HNO_3 are listed in the Table 3-1. I calculated 1-h value of V_d using meteorological element recorded at the site and obtained mean value of each observation period.

Table 3-1. Setting of the parameters for resistance model adopted by the Acid Deposition Monitoring Network in East Asia (EANET, 2010). Seasonal category 1, 3, and 5 indicate "midsummer with lush vegetation" (from Jun. to Sep.), "late autumn after frost, no snow" (from Nov. to Feb.), and "transitional spring with partially green short annuals" (from Mar. to May. and Oct.).

		Parameter for calculation of deposition velocity of nitric acid	Unit	Seasonal category		
				1	3	5
R_a	z	reference height	m		30	
	d	displacement height	m		16 (leafy period) 15 (leafless period)	
	z_0	roughness length	m		0.8 (leafy period) 0.7 (leafless period)	
R_b	Sc	Schmidt number for HNO_3			1.25	
	Pr	Prandtl number			0.72	
R_{st}	R_j	minimum bulk canopy stomatal resistance for water vapour	s m^{-1}	100	500	190
	D_v/D_{HNO3}	the ratio of molecular diffusivity of water vapour to nitric acid			1.87	
	H^*	effective Henry's law constant for HNO_3	M atm^{-1}		1×10^{14}	
	f_0	normalized reactive factor for HNO_3			0	
R_{lu}	r_{lu}	input parameter	s m^{-1}	2000	8000	3000
R_{dc}	θ	slope of the local terrain	radian		0	
R_{cl}	R_{clS}	resistance to uptake by leaves, twigs, and other exposed surfaces for SO_2	s m^{-1}	2000	6000	3000
	R_{clO}	resistance to uptake by leaves, twigs, and other exposed surfaces for O_3	s m^{-1}	1000	600	700
R_{ac}			s m^{-1}	2000	1500	1500
R_{gs}	R_{gsS}	resistance to uptake by the soil, leaf litter, and so on at the ground surface for SO_2	s m^{-1}	100	200	200
	R_{gsO}	resistance to uptake by the soil, leaf litter, and so on at the ground surface for O_3	s m^{-1}	300	300	300

3.3 Results & Discussion

3.3.1 Verification of REA measurement data

I verified the data from REA sampling system by comparing them with the reference concentrations, because this system has complex sampling lines and sample treatments. I compared the concentrations of HNO_3, NO_3^- (fine NO_3^-) and SO_4^{2-} (fine SO_4^{2-}) in $PM_{2.5}$ derived from REA updraft/downdraft and reference samplings (Fig. 3-4). The concentration of the fine NO_3^- and SO_4^{2-} particles derived from REA and reference samplings were similar; linear regression line was y = 1.03 x − 0.03 (R = 0.97) for fine NO_3^-; y = 0.71 x + 0.37 (R = 0.94) for fine SO_4^{2-}. The concentrations of fine SO_4^{2-} particles derived by REA were slightly lower than the reference concentrations when the concentration is higher than 4 μg m^{-3}, probably because of the loss by updraft/downdraft separator of the REA. The concentration levels of HNO_3 were lower than those of fine particles (less than 1 μg m^{-3}). Despite the good agreements in HNO_3 concentration between REA and reference samplings (linear regression line: y = 1.01 x − 0.01, R = 0.81), the concentration ratios of REA/reference were within ±30% for 65% of the total samples (n = 40/62). This difference in concentrations possibly occurred because HNO_3 was collected by denuder tubes and the operation was more complicated than that of particles.

The measured fluxes using REA potentially have large random errors because they are estimated from many items. Since the flux is particularly dependent on the difference between updraft and downdraft concentrations (C_u–C_d), high precision in concentration measurements is particularly required. In this study, I adopted the REA sample data during the periods the REA/reference ratios were within ±30% for all three components, regarded as valid data (Fig. 3-4). As a result, I obtained 39 valid sample datasets in total. From this screening, correlation in concentration between REA and reference sampling for each component was improved, especially for HNO_3 (Fig. 3-4).

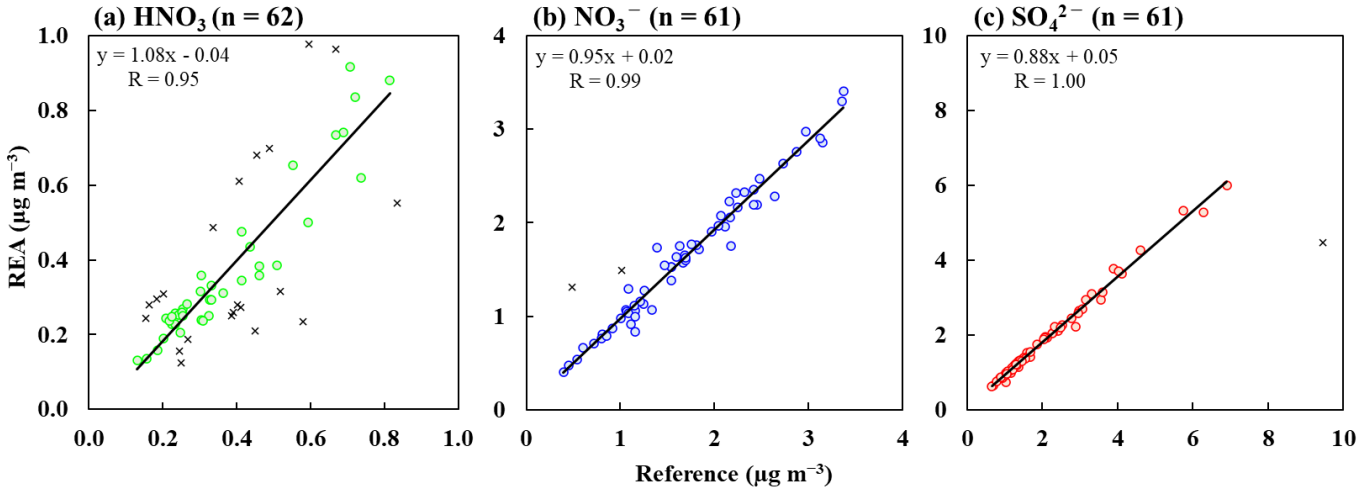

Fig. 3-4. Comparisons of concentrations for HNO_3, NO_3^- and SO_4^{2-} in $PM_{2.5}$ measured using the REA sampling system and the reference sampling system. The linear regression lines and coefficients of correlation were derived from samples which showed the ratios of REA/reference concentration were within ±30%. Circles indicate the ratios of REA/reference concentration were within ±30%, and crosses indicate the ratios of REA/reference concentration were over ±30%.

3.3.2 Fluxes and deposition velocities

C_u, C_d, fluxes, and V_d for HNO_3, fine NO_3^-, and fine SO_4^{2-} with σ_w and β for valid datasets are listed in Table 3-2 and Table 3-3. The data loss due to the screening of concentration mentioned in Section 3.3.1 were about 37%. The β for the valid dataset was 0.53 ± 0.01 (mean ± standard deviation). All β values were within the typical range between 0.40 and 0.63 reported by Milne et al. (1999), and were close to the values (about 0.60) when the "dead-band" sampling was not employed (Bussinger and Oncley, 1990). There was no clear seasonal variation in the value of β. The σ_w was 0.44 ± 0.09 m s^{-1} (mean ± standard deviation), and the variation was larger than that of β. The V_d of HNO_3, fine NO_3^-, and fine SO_4^{2-} ranged between −3.2 and 5.1cm s^{-1}, −2.0 and 8.8 cm s^{-1}, and −4.2 and 2.8 cm s^{-1}, and were 0.63 ± 1.93 cm s^{-1}, 0.93 ± 1.64 cm s^{-1}, and 0.08 ± 1.22 cm s^{-1}, respectively (mean ± standard deviation). In the case of flux or V_d, the median value could be suitable as the representative value, because of their large random errors. In the valid 39 sample datasets, the median values of V_d for HNO_3, fine NO_3^-, and fine SO_4^{2-} were 0.76 cm s^{-1}, 0.71 cm s^{-1}, and −0.01 cm s^{-1}, respectively. Regardless of the difference in mean and median value, the V_d of fine NO_3^- was larger than that of fine SO_4^{2-}, and is same level with that of HNO_3.

Table 3-2(a). Concentrations during updraft (C_u), downdraft (C_d), fluxes, and V_d for HNO_3 with standard deviations of the vertical wind velocity (σ_w) and empirical coefficients (β) for valid datasets. LAI is mean value during each period and gray scales indicate leafy periods.

	period	LAI	C_u	C_d	HNO_3 Flux	V_d	σ_w	β
		$m^2\ m^{-2}$	$\mu g\ m^{-3}$		$\mu g\ m^{-2}\ s^{-1}$	$cm\ s^{-1}$	$m\ s^{-1}$	
2016	10/14-10/21		0.89	0.95	-0.010	1.05	0.30	0.50
	10/28-11/4		0.23	0.25	-0.005	1.87	0.42	0.53
	11/11-11/21	3.9	0.25	0.26	-0.002	0.76	0.35	0.52
	11/21-11/28		0.14	0.13	0.001	-0.97	0.44	0.54
	11/28-12/5		0.21	0.24	-0.006	2.74	0.40	0.54
	12/5-12/14		0.23	0.25	-0.004	1.78	0.46	0.53
	12/14-12/21		0.29	0.33	-0.007	2.25	0.36	0.52
2017	1/6-1/16	1.6	0.26	0.24	0.007	-2.89	0.50	0.53
	1/23-1/30		0.38	0.39	-0.002	0.39	0.42	0.52
	1/30-2/8		0.31	0.28	0.009	-3.23	0.64	0.54
	9/19-9/26		0.37	0.40	-0.005	1.38	0.36	0.52
	10/5-10/12		0.48	0.51	-0.006	1.13	0.35	0.53
	10/12-10/24		0.12	0.14	-0.006	4.21	0.60	0.54
	10/24-10/31	4.4	0.17	0.21	-0.009	4.99	0.50	0.53
	11/7-11/14		0.23	0.24	-0.004	1.63	0.49	0.53
	11/14-11/21		0.15	0.16	-0.001	0.95	0.41	0.52
	11/21-11/28		0.22	0.20	0.004	-1.72	0.36	0.53
	11/28-12/5		0.25	0.25	-0.001	0.26	0.33	0.52
	12/5-12/12		0.23	0.22	0.002	-0.90	0.38	0.53
	12/12-12/22	1.8*	0.27	0.27	0.000	0.00	0.35	0.52
	12/22-1/5		0.26	0.26	-0.002	0.64	0.43	0.52

*: Mean value from Dec. 5, 2017 to Apr. 5, 2018

Table 3-2(b). Concentrations during updraft (C_u), downdraft (C_d), fluxes, and V_d for HNO_3 with standard deviations of the vertical wind velocity (σ_w) and empirical coefficients (β) for valid datasets. LAI is mean value during each period and gray scales indicate leafy periods.

	period	LAI	C_u	C_d	HNO_3 Flux	V_d	σ_w	β
		$m^2\ m^{-2}$	$\mu g\ m^{-3}$		$\mu g\ m^{-2}\ s^{-1}$	$cm\ s^{-1}$	$m\ s^{-1}$	
2018	1/5-1/11	1.8*	0.27	0.30	-0.005	1.80	0.37	0.53
	1/11-1/18		0.46	0.49	-0.005	1.08	0.38	0.52
	1/18-1/30		0.25	0.25	-0.001	0.56	0.42	0.53
	1/30-2/8		0.23	0.25	-0.003	1.24	0.36	0.52
	2/8-2/15		0.43	0.44	-0.001	0.23	0.43	0.52
	2/23-3/1		0.34	0.35	-0.003	0.74	0.44	0.51
	3/1-3/15		0.37	0.35	0.006	-1.75	0.53	0.53
	3/15-3/22		0.30	0.33	-0.009	2.89	0.60	0.52
	3/22-3/29		0.89	0.87	0.004	-0.48	0.38	0.52
	3/29-4/5		0.87	0.80	0.018	-2.15	0.55	0.53
	4/12-4/19	4.6	0.34	0.32	0.008	-2.34	0.60	0.53
	5/17-5/24		0.66	0.82	-0.038	5.13	0.46	0.53
	5/24-5/29		0.65	0.59	0.011	-1.71	0.37	0.55
	8/2-8/9		0.72	0.75	-0.011	1.49	0.66	0.54
	8/16-8/22		0.29	0.30	-0.003	0.88	0.54	0.53
	8/30-9/6		0.30	0.29	0.002	-0.62	0.52	0.53
	9/12-9/20		0.36	0.36	0.000	-0.08	0.32	0.53
	9/20-9/28		0.24	0.25	-0.003	1.28	0.48	0.54

*: Mean value from Dec. 5, 2017 to Apr. 5, 2018

Table 3-3(a). Concentrations during updraft (C_u), downdraft (C_d), fluxes, and V_d for NO_3^- and SO_4^{2-} in $PM_{2.5}$ for valid datasets. The gray scales indicate leafy periods.

		NO_3^-				SO_4^{2-}			
	period	C_u	C_d	Flux	V_d	C_u	C_d	Flux	V_d
		μg m^{-3}		μg m^{-2} s^{-1}	cm s^{-1}	μg m^{-3}		μg m^{-2} s^{-1}	cm s^{-1}
2016	10/14-10/21	1.10	1.16	-0.010	0.90	2.10	2.14	-0.006	0.27
	10/28-11/4	1.02	1.10	-0.020	1.86	0.94	1.05	-0.025	2.51
	11/11-11/21	2.85	2.87	-0.003	0.11	2.08	2.04	0.007	-0.32
	11/21-11/28	1.55	1.64	-0.021	1.29	0.75	0.74	0.001	-0.18
	11/28-12/5	2.19	2.37	-0.039	1.73	1.33	1.48	-0.032	2.28
	12/5-12/14	1.87	2.05	-0.045	2.28	1.00	1.05	-0.011	1.09
	12/14-12/21	1.73	1.80	-0.014	0.77	1.12	1.24	-0.022	1.89
2017	1/6-1/16	1.26	1.29	-0.009	0.67	0.66	0.65	0.002	-0.36
	1/23-1/30	2.02	2.09	-0.014	0.67	1.08	1.11	-0.008	0.70
	1/30-2/8	1.60	1.71	-0.038	2.27	0.94	0.93	0.004	-0.43
	9/19-9/26	1.06	1.08	-0.004	0.39	2.05	2.39	-0.062	2.78
	10/5-10/12	2.16	2.23	-0.013	0.59	2.67	2.63	0.008	-0.30
	10/12-10/24	0.58	0.76	-0.058	8.76	0.60	0.63	-0.010	1.60
	10/24-10/31	1.07	1.07	0.002	-0.14	0.84	0.84	-0.001	0.14
	11/7-11/14	2.12	2.22	-0.027	1.24	1.18	1.18	0.000	-0.01
	11/14-11/21	2.00	1.93	0.017	-0.85	0.92	0.89	0.006	-0.67
	11/21-11/28	1.97	2.17	-0.038	1.82	1.11	1.11	0.001	-0.08
	11/28-12/5	2.42	2.52	-0.018	0.71	1.39	1.40	-0.001	0.04
	12/5-12/12	2.18	2.26	-0.016	0.72	0.84	0.84	-0.001	0.15
	12/12-12/22	2.32	2.34	-0.004	0.16	0.74	0.76	-0.002	0.31
	12/22-1/5	1.50	1.56	-0.013	0.82	0.86	0.88	-0.005	0.52

Table 3-3(b). Concentrations during updraft (C_u), downdraft (C_d), fluxes, and V_d for NO_3^- and SO_4^{2-} in $PM_{2.5}$ for valid datasets. The gray scales indicate leafy periods.

		NO_3^-				SO_4^{2-}			
	period	C_u	C_d	Flux	V_d	C_u	C_d	Flux	V_d
		μg m^{-3}		μg m^{-2} s^{-1}	cm s^{-1}	μg m^{-3}		μg m^{-2} s^{-1}	cm s^{-1}
2018	1/5-1/11	1.53	1.56	-0.006	0.39	0.99	0.99	0.001	-0.06
	1/11-1/18	3.23	3.36	-0.025	0.75	1.01	1.04	-0.005	0.51
	1/18-1/30	1.65	1.62	0.006	-0.39	1.31	1.27	0.008	-0.63
	1/30-2/8	2.65	2.62	0.005	-0.20	1.27	1.21	0.011	-0.89
	2/8-2/15	2.35	2.36	-0.002	0.09	1.95	1.95	0.001	-0.03
	2/23-3/1	3.45	3.37	0.016	-0.47	3.12	3.09	0.007	-0.21
	3/1-3/15	1.94	1.87	0.018	-0.93	2.38	2.18	0.056	-2.48
	3/15-3/22	2.29	2.35	-0.020	0.84	1.97	1.90	0.024	-1.24
	3/22-3/29	2.87	2.94	-0.014	0.47	4.26	4.25	0.002	-0.05
	3/29-4/5	2.18	2.21	-0.011	0.49	5.28	5.36	-0.021	0.39
	4/12-4/19	1.68	1.57	0.032	-1.99	1.45	1.28	0.057	-4.17
	5/17-5/24	1.63	1.84	-0.050	2.89	3.72	3.82	-0.025	0.66
	5/24-5/29	1.71	1.79	-0.016	0.93	3.64	3.64	0.000	0.00
	8/2-8/9	0.79	0.83	-0.014	1.73	6.04	5.94	0.034	-0.57
	8/16-8/22	0.76	0.76	0.002	-0.31	1.06	1.07	-0.004	0.34
	8/30-9/6	0.75	0.82	-0.019	2.47	2.61	2.57	0.009	-0.33
	9/12-9/20	1.35	1.41	-0.009	0.65	2.21	2.17	0.007	-0.34
	9/20-9/28	0.68	0.74	-0.016	2.29	0.96	0.97	-0.003	0.27

Temporal variations of the valid data for V_d of HNO_3, fine NO_3^-, and fine SO_4^{2-} with LAI are shown in Fig. 3-5. From the relationship between canopy situations and measured LAI values, I set the period from early April to early December as leafy (LAI ≥ 4; rounded to the nearest whole number), and the other period as leafless (LAI ≤ 2; rounded to the nearest whole number). The V_d of HNO_3 and fine NO_3^- mostly showed deposition in addition to some emission. For the V_d of fine SO_4^{2-}, the trend of deposition and emission was almost same.

Since it is difficult to understand the seasonal trends in the V_d for each component from Fig. 3-5, the V_d distributions for each component during the leafy and leafless periods are shown in Fig. 3-6. The median values of V_d of HNO_3, fine NO_3^-, and fine SO_4^{2-} during the leafy period were 1.05 cm s^{-1}, 0.93 cm s^{-1} and 0.00 cm s^{-1}, respectively, and those during the leafless period were 0.47 cm s^{-1}, 0.58 cm s^{-1} and −0.04 cm s^{-1}, respectively. As a result, the V_d of HNO_3, fine NO_3^- tended to be larger in the leafy period and smaller in the leafless period. On the other hand, there was no clear seasonal difference in the V_d of fine SO_4^{2-}. The negative median values of the V_d of fine SO_4^{2-} were probably caused by the measurement errors due to the very small V_d levels.

According to the general theories (e.g. Seinfeld and Pandis, 2006), the V_d of reactive gases are much larger than those of fine particles. HNO_3, which is one of the most reactive gases, is theoretically and empirically known for its larger V_d. For example, some previous REA measurements showed the large V_d for HNO_3 above forests. Pryor et al. (2002) have conducted a REA measurement using NaCl coated denuders at a deciduous forest site (canopy height: 25 m, LAI = 4) in USA during summer. They performed short time samplings for daytime (1.5-8 h) and nighttime (8-14 h), and obtained the mean value for the V_d as 3 cm s^{-1} with small u^* up to 0.25 m s^{-1}. Pryor and Klemm (2004) have conducted a REA measurement using the same system of Pryor et al. (2002) at a conifer forest site (canopy height: 19-20 m, LAI = 5.3) in Germany during late spring. They also performed short time samplings for daytime (1.5-5 h), and obtained the mean value for the V_d as 4.6 cm s^{-1} with mean u^* of 0.45 m s^{-1}. Although HNO_3 emissions were sometimes found in both observation, there was no clear conclusion. On the other hand, the V_d measurements of fine particles at various forest sites typically ranged between 0.01 and 1 cm s^{-1} (Petroff et al., 2008). In my measurements, I found the V_d of fine NO_3^- were significantly ($p < 0.05$) larger than that of fine SO_4^{2-} regardless of the leafy and leafless periods, even though the V_d of SO_4^{2-} was within the typical range. Moreover, the median value for the V_d of fine NO_3^- was same level with that of HNO_3. In addition, the mean value of V_d for HNO_3 in my measurements was lower than that reported in the previous studies, and sometimes large HNO_3 emission occurred.

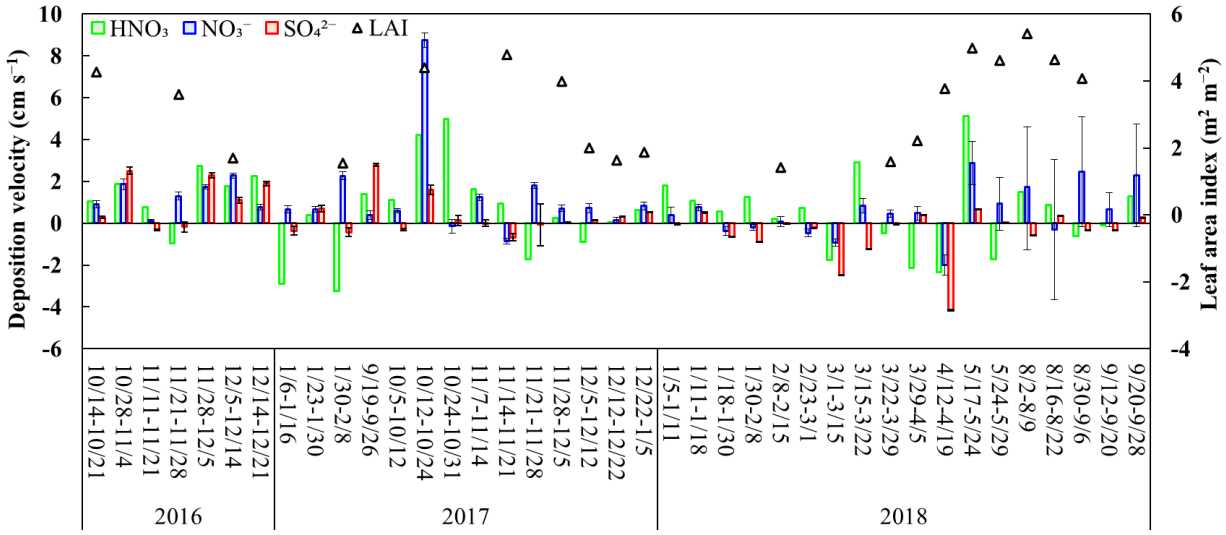

Fig. 3-5. Temporal variations of valid datasets (n = 39) of deposition velocities for HNO_3, NO_3^- and SO_4^{2-} in $PM_{2.5}$ with LAI. Error bars show the measurement precisions of the difference between updraft and downdraft concentrations (C_u–C_d).

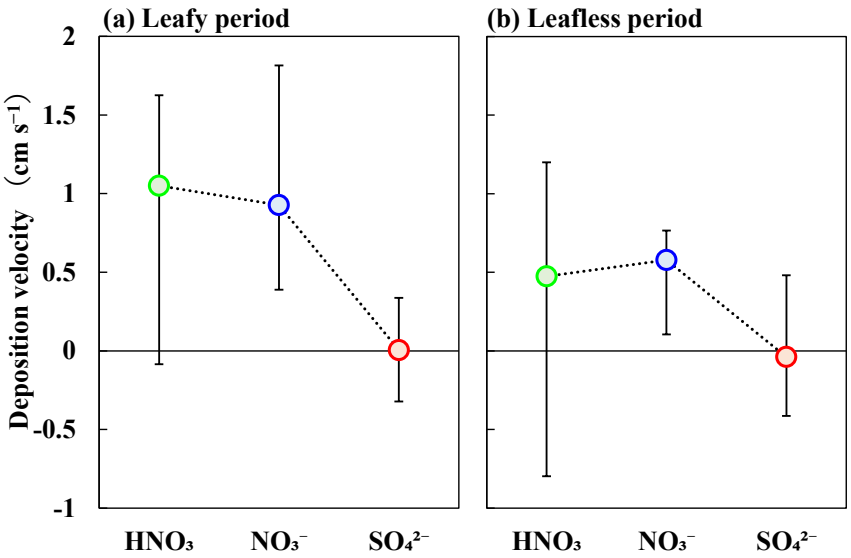

Fig. 3-6. Deposition velocity distributions of deposition velocities for HNO_3, NO_3^- and SO_4^{2-} in $PM_{2.5}$ during (a) leafy (n = 21) and (b) leafless periods (n = 18). Closed circles indicate the median, and top and bottom bars indicate the 75th and 25th percentiles, respectively.

The meteorological conditions during the leafy and leafless periods are shown in Table 3-4. Overall, the measurement site was high-temperature and high-humidity in the leafy periods, and vice versa. There were also some heavy rainfalls during the leafy periods, while the ratios of rainfall duration to sampling time (%-Rainfall) were mostly less than 10% during the measurements. Since the difference of WS and friction velocity (u^*) between the leafy and leafless periods was small, the seasonal difference in V_d was not mainly influenced by aerodynamic conditions. In addition to aerodynamic conditions, canopy wetness and humid condition may have a large impact on the dry deposition process of HNO_3. However, the correlation between V_d of HNO_3 and RH or %-Rainfall were very weak. Moreover, there was also no meteorological elements that have a close relationship with the V_d of HNO_3 as indicated in Table 3-4. It was likely that no obvious trend could be found because weekly basis long-term results were addressed in this study.

As describe in Matsuda et al. (2015), the dominant WD at this site were south and north. Since there is a residential area nearby the north side of this site, the V_d when the main WD is north should be carefully treated. In the valid samples, however, the V_d of HNO_3 showed both deposition and emission regardless of the difference in WD. Therefore, it was considered that the results mentioned above were representative of the characteristic of this forest site.

Table 3-4(a). Wind speed (WS), friction velocity (u^*), temperature (Temp), relative humidity (RH), rainfall and the ratios of rainfall duration to sampling time (%-rainfall) for valid datasets during the total, leafy, and leafless periods. All values except rainfall and %-rainfall are given as the means ± standard deviation. The gray scales indicate leafy periods.

	period	WS	u^*	Temp	RH	Rainfall	%-Rainfall
		m s^{-1}	m s^{-1}	°C	%	mm	%
2016	10/14-10/21	2.0±0.8	0.22±0.17	18±4	68±16	6	1.1
	10/28-11/4	2.1±0.9	0.32±0.23	11±3	70±14	20	4.0
	11/11-11/21	2.1±0.8	0.26±0.19	12±3	73±15	20	2.5
	11/21-11/28	2.3±1.0	0.29±0.25	8±5	76±16	48	8.5
	11/28-12/5	2.2±0.8	0.32±0.18	9±3	65±16	14	2.1
	12/5-12/14	2.5±1.1	0.34±0.27	8±4	56±15	34	3.1
	12/14-12/21	2.6±1.0	0.27±0.25	7±4	52±15	0	0.0
2017	1/6-1/16	2.7±1.2	0.37±0.25	4±3	53±17	28	3.7
	1/23-1/30	2.5±1.3	0.30±0.19	5±4	44±16	0	0.0
	1/30-2/8	2.8±1.3	0.47±0.32	5±3	40±15	0	0.0
	9/19-9/26	2.2±1.1	0.29±0.18	21±2	73±13	31	4.6
	10/5-10/12	2.0±0.9	0.29±0.18	19±4	76±11	66	7.2
	10/12-10/24	2.5±1.0	0.49±0.23	14±3	85±13	461	26.9
	10/24-10/31	2.5±1.1	0.41±0.31	13±3	72±19	105	12.7
	11/7-11/14	2.7±1.4	0.40±0.31	13±3	61±16	4	0.6
	11/14-11/21	2.2±0.9	0.34±0.26	9±3	64±14	2	0.3
	11/21-11/28	2.3±1.2	0.28±0.15	8±3	61±17	22	3.6
	11/28-12/5	2.0±0.7	0.27±0.16	9±3	69±15	3	0.5
	12/5-12/12	2.6±1.1	0.30±0.20	6±3	54±17	2	0.4
	12/12-12/22	2.3±1.0	0.28±0.25	5±3	50±12	0	0.0
	12/22-1/5	2.4±1.1	0.35±0.26	5±3	48±16	13	0.9

Table 3-4(b). Wind speed (WS), friction velocity (u^*), temperature (Temp), relative humidity (RH), rainfall and the ratios of rainfall duration to sampling time (%-rainfall) for valid datasets during the total, leafy, and leafless periods. All values except rainfall and %-rainfall are given as the means ± standard deviation. The values in parentheses indicate the correlation coefficient between each element and the V_d of HNO_3. The gray scales indicate leafy periods.

	period	WS	u^*	Temp	RH	Rainfall	%-Rainfall
		m s^{-1}	m s^{-1}	°C	%	mm	%
2018	1/5-1/11	2.6±1.3	0.28±0.17	5±3	50±18	7	1.6
	1/11-1/18	2.4±0.9	0.30±0.19	4±3	47±20	9	1.3
	1/18-1/30	2.4±1.1	0.34±0.23	3±3	52±21	8	0.9
	1/30-2/8	2.3±0.9	0.28±0.20	3±2	56±22	15	2.2
	2/8-2/15	2.7±1.4	0.33±0.23	5±3	42±15	0	0.0
	2/23-3/1	2.5±1.4	0.36±0.20	6±3	59±15	44	5.0
	3/1-3/15	2.9±1.7	0.42±0.26	9±4	58±19	150	7.1
	3/15-3/22	2.9±1.5	0.05±0.26	9±5	66±18	71	9.6
	3/22-3/29	2.5±1.3	0.28±0.17	13±4	58±14	7	1.1
	3/29-4/5	3.0±1.6	0.44±0.33	15±4	54±16	0	0.0
	4/12-4/19	3.0±2.0	0.49±0.30	14±3	61±22	34	5.8
	5/17-5/24	2.5±1.3	0.37±0.28	19±4	59±18	8	1.3
	5/24-5/29	2.5±1.5	0.28±0.17	21±2	68±10	0	0.0
	8/2-8/9	3.1±1.5	0.53±0.35	26±4	78±12	61	9.6
	8/16-8/22	3.1±1.9	0.41±0.35	24±3	63±16	0	0.0
	8/30-9/6	3.5±3.4	0.36±0.25	25±3	78±12	71	6.5
	9/12-9/20	1.9±0.9	0.26±0.16	21±2	78±13	23	4.1
	9/20-9/28	2.2±0.9	0.39±0.24	19±4	83±11	160	18.5
Total	(n = 39)	2.5±0.4	0.35±0.08	12±7	62±12	39	4.0±5.5
		(-0.23)	(0.05)	(0.14)	(0.30)	(0.32)	(0.35)
Leafy	(n = 21)	2.4±0.4	0.35±0.09	16±6	70±8	55	5.7±6.7
		(-0.10)	(0.28)	(0.02)	(0.11)	(0.39)	(0.34)
Leafless	(n = 18)	2.6±0.2	0.34±0.07	7±3	52±6	21	2.0±2.7
		(-0.42)	(-0.36)	(-0.20)	(0.29)	(-0.04)	(0.21)

3.3.3 Enhancement of dry deposition of ammonium nitrate

Relationships between equivalent concentration of (a) total cations ($NH_4^+ + Na^+ + K^+ + Ca^{2+} + Mg^{2+}$) and anions ($SO_4^{2-} + NO_3^- + Cl^-$) and (b) NH_4^+ and $SO_4^{2-} + NO_3^-$ in the measured $PM_{2.5}$ during the observation periods are shown in Fig. 3-7. There was a good agreement between the NH_4^+ cations and the $SO_4^{2-} + NO_3^-$ anions as well as between the total cations and anions. Moreover, about 89% of the inorganic ions in the $PM_{2.5}$ comprised NH_4^+, SO_4^{2-}, and NO_3^-, indicating that the inorganic components of the $PM_{2.5}$ at the forest site were mainly existed as $(NH_4)_2SO_4$ and NH_4NO_3. These results were similar to those of vertical profile measurements in **Chapter 2**.

There are a lot of evidence for larger removal of NO_3^- than SO_4^{2-} at various sites in Europe and United states (Nemitz, 2015). The same results have also been reported by REA measurements (Honjo et al., 2016; Sakamoto et al., 2018) and by vertical profile measurements (Yamazaki et al., 2015; Nakahara et al., 2019) at forest sites in Japan over the past few years, as already mentioned in **Chapter 2**. These studies founded that the NH_4NO_3–NH_3–HNO_3 interactions influences the dry deposition process of NO_3^-. When the equilibrium shifts from solid to gas phase due to higher surface temperature in daytime or low HNO_3 concentrations near the deposition surface, volatilized fine NO_3^- is quickly removed and eventually have a larger V_d value than that of SO_4^{2-}. In this study site, higher temperatures near the deposition surface in daytime possibly induced the equilibrium shift in both leafy and leafless periods (Fig. 2-17). Since the HNO_3 concentrations were also low at the site, HNO_3 is possibly depleted near the surface and also promoted the equilibrium shift. Therefore, this long-term measurement obtained larger V_d for fine NO_3^- probably caused by the volatilization of NH_4NO_3, as well as previous short-term measurement conducted at the same site (Honjo et al., 2016). These results also confirmed that the results of vertical profile measurements in **Chapter 2** are not due to the artifacts in filter-pack holders.

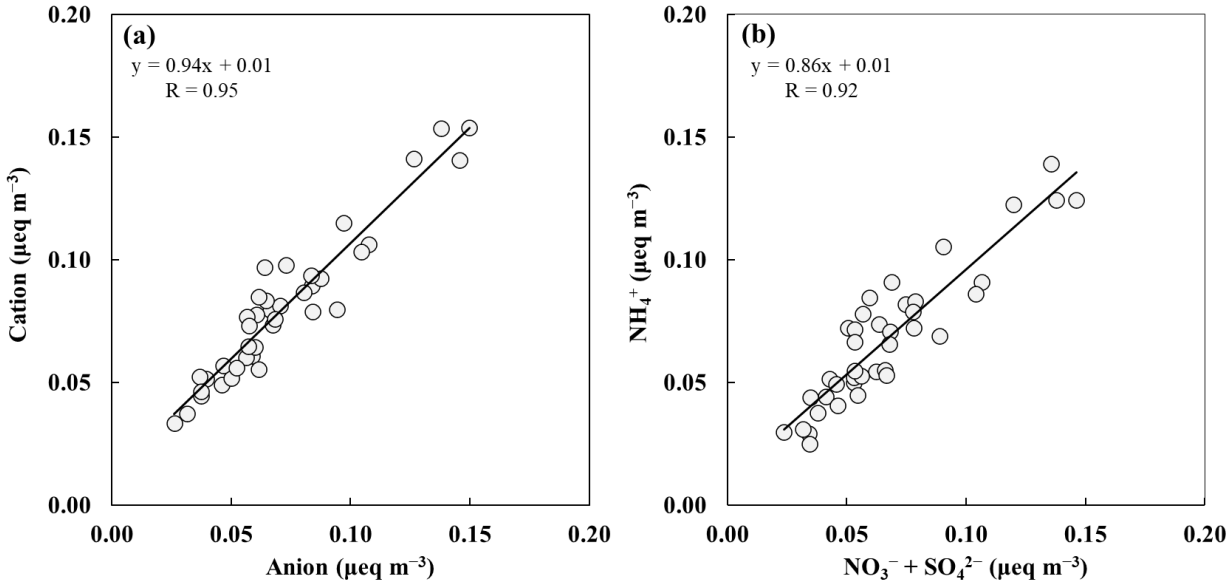

Fig. 3-7. Equivalent concentration relationships between (a) total cations ($NH_4^+ + Na^+ + K^+ + Ca^{2+} + Mg^{2+}$) and anions ($SO_4^{2-} + NO_3^- + Cl^-$), and (b) NH_4^+ and $SO_4^{2-} + NO_3^-$ in the $PM_{2.5}$ during the observation periods.

3.3.4 Emission of nitric acid gas associated with the equilibrium shift of ammonium nitrate

The HNO_3 deposition process associated with the equilibrium shift of NH_4NO_3–NH_3–HNO_3 has rarely been researched in Asian region. The equilibrium shift of NH_4NO_3 generates HNO_3 and NH_3 near the surface, which are thought to be efficiently removed compared to NH_4NO_3. On the other hand, if the gas concentrations near the deposition surfaces were high, the gas could not be completely removed by the surface (suppressed deposition) and some of them could be emitted to the atmosphere through the upward turbulence (apparent emission).

I compared the V_d measured by REA (V_d–REA) with the V_d inferred from the resistance model (V_d–Inf) to evaluate the measured V_d of HNO_3 (Fig. 3-8). The V_d–Inf were in the range of 1.55 to 3.89 cm s^{-1}, and the median values were 2.40 cm s^{-1} during the measurements, 2.27 cm s^{-1} in the leafy periods, and 2.53 cm s^{-1} in the leafless periods, respectively. The V_d–REA values were broadly distributed from emission to deposition than the V_d–Inf, and their median values were smaller than those for V_d–Inf in both the leafy and leafless periods. These differences between V_d–REA and V_d–Inf clearly appeared in the leafless periods. Since the resistance model does not take into account the emission process, the smaller V_d–REA value could be caused by suppressed deposition or apparent emission due to high HNO_3 concentration near the surface due to the equilibrium shift. In addition, the small V_d–REA in the leafless periods was likely caused by the small removal due to the small deposition surface (small LAI). In fact, large emissions were mainly appeared in the leafless periods (Fig. 3-8).

The suppressed deposition or apparent emission of HNO_3 is reported based on some observations by Nemitz (2015). In a REA flux measurement conducted by Hansen et al. (2015) at a mixed deciduous forest site in USA during late summer/autumn, about 70% of the total samples showed emission of HNO_3. In my long-term measurements, about 30% of the total samples of HNO_3 showed emissions (n = 12/39). Since the fine NO_3^- concentrations were much higher than those of HNO_3, NH_4NO_3 could act as a sufficient source of HNO_3. Moreover, the HNO_3 emissions almost coincided with the cases that in which the V_d of fine NO_3^- were higher than those of fine SO_4^{2-} (n = 10/12). This finding strongly supports that the small V_d–REA compared with the V_d–Inf was caused by suppressed deposition or apparent emission of HNO_3 due to the equilibrium shift of NH_4NO_3.

Relationship between the V_d of HNO_3 measured by REA and u^* during the emission and deposition cases are shown in Fig. 3-9. The V_d of HNO_3 well correlate with u^* regardless of the emission/deposition cases ($p < 0.05$). This indicates that the emissions might be enhanced by the turbulence as well as the depositions. The larger HNO_3 emissions during the leafless periods were probably caused due to the high HNO_3 concentrations near the canopy due to the large generation and small removal were emitted by the larger upward turbulence. In this study, the measured V_d of HNO_3 were relatively small compared to those measured in previous studies (Section 3.3.2), although the turbulent (u^*) values was the same levels. This may be due to the previous studies only being conducted in the daytime or for short periods of time during the spring/summer. It is also suggested that the HNO_3 emission might depend on the types of forest.

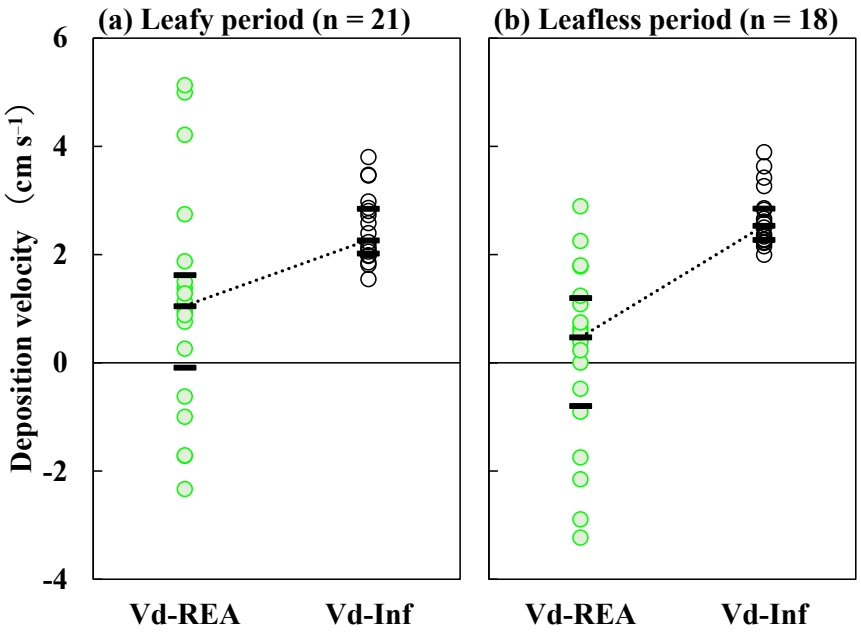

Fig. 3-8. Distributions of deposition velocity for HNO_3 measured by REA (V_d–REA) and inferred from the resistance model (V_d–Inf) during (a) leafy and (b) leafless periods. Middle, top, and bottom bars indicate the median, 75th and 25th percentiles, respectively.

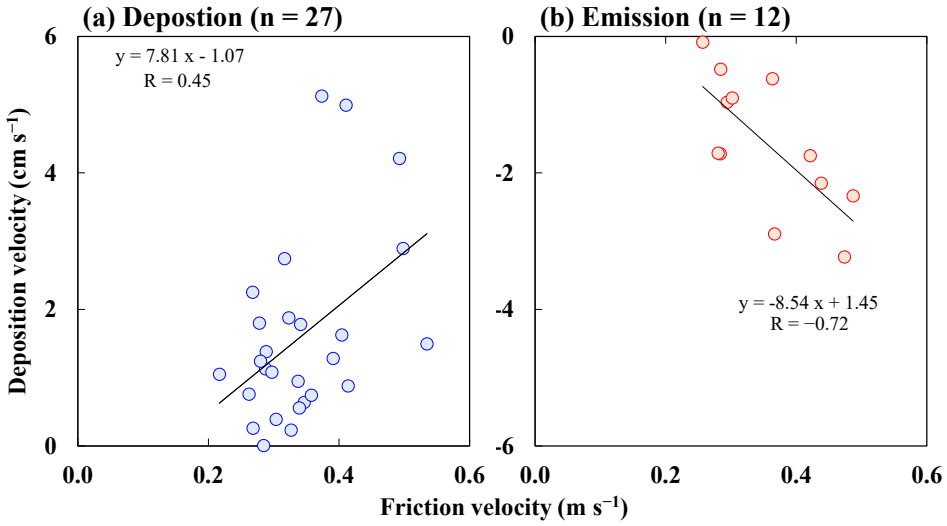

Fig. 3-9. Relationships between deposition velocity of HNO_3 measured by REA and friction velocity during (a) deposition cases and (b) emission cases.

3.3.5 Uncertainties

As described in Eq. (3-2), the determination of flux is dependent on β, σ_w, and $C_u - C_d$ (ΔC). At the site, it is difficult to measure the ΔC of HNO_3 precisely in a high temporal resolution (hourly, day/night etc.) because of the low concentration. Therefore, I set the sampling time as one week and focused on the long-term variations. Since the fluxes determined in this study were based on weekly samplings, the diurnal variations in β, σ_w, and ΔC were possibly averaged, and there might be over or under estimation for fluxes if there were some typical diurnal variations. The diurnal variations in the ensemble mean of β and σ_w during specific periods are shown in Fig. 3-10. These periods were selected taking into account seasons and HNO_3 deposition/emission trends. There were no clear variations in the β regardless of the deposition or emission of HNO_3. On the other hand, σ_w was mostly high in daytime and low in nighttime during both leafy and leafless periods. The σ_w in nighttime was, however, mostly larger than 0.2 m s^{-1} for all cases. Therefore, the flux measurements are available in nighttime, if the ΔC is detected. From previous REA measurements at the same site (Matsuda et al., 2015), there was no typical diurnal variations in ΔC of fine SO_4^{2-}, although HNO_3 and fine NO_3^- were not measured. If only the σ_w has the typical diurnal variation, the influence of weekly average on the flux could be not so large, although there might be some over or under estimations. However, it also should be note that β and σ_w do not determine the direction of flux. Measurements in high time resolution with a high sensitivity instrument are required for further investigation of diurnal variation in the fluxes.

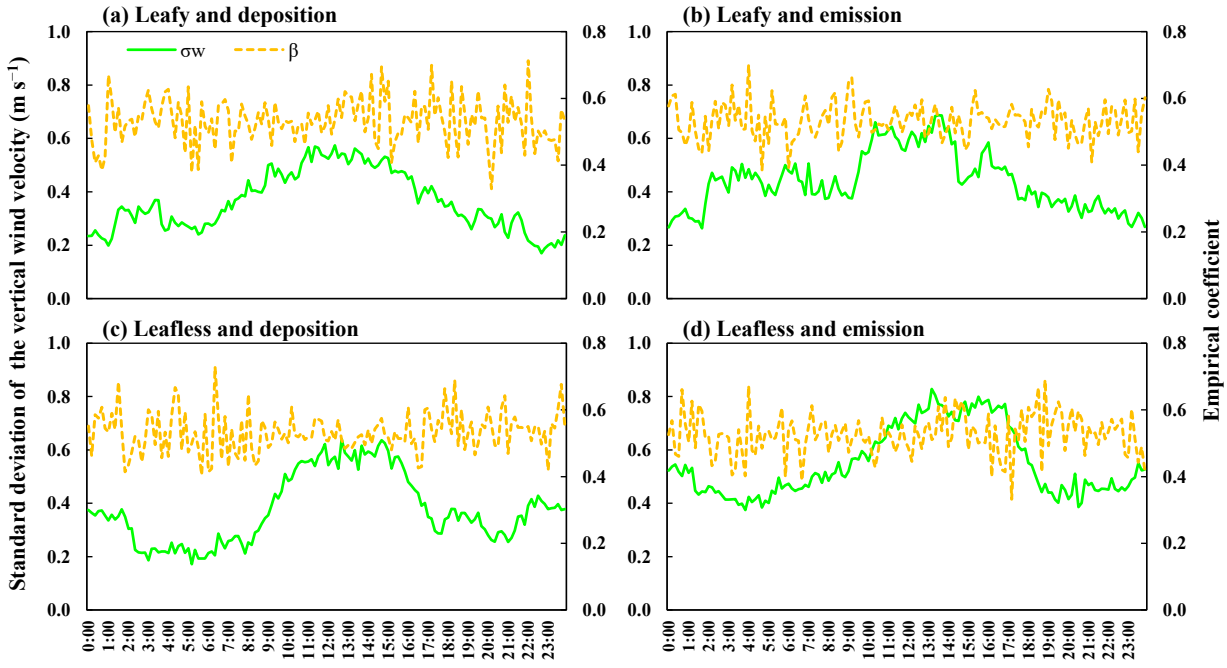

Fig. 3-10. Diurnal variations in the ensemble mean of β and σ_w during (a) leafy and deposition period (from Sep. 19, 2017 to Sep. 26, 2017), (b) leafy and emission period (from Nov. 11, 2016 to Nov. 28, 2016), (c) leafless and deposition period (from Jan. 11, 2018 to Jan. 18, 2018), and (d) leafless and emission period (from Mar. 29, 2018 to Apr. 5, 2018). Deposition and emission indicate the result of the V_d of HNO_3.

Since HNO_3 is a major trace gas involved in various chemical reactions in the atmosphere, it is important to discuss about the sources and sinks to validate the measured fluxes at this forest site. During the daytime, HNO_3 is formed through the oxidation of nitrogen dioxide (NO_2) by hydroxyl radical (OH radical). This chemical reaction occurs not only with the soil surface but also with the leaf surface (Hayashi et al., 2012). This disproportionation reaction is accelerated under sunlight irradiation, therefore the emission of HNO_3 was possibly enhanced in summer at the site. The main sinks of HNO_3 are its removal through dry or wet deposition to the surface and the formation of NH_4NO_3 with NH_3 in the atmosphere. Further sinks have also been suggested in recent years. Zhou et al. (2011) indicated that the photolysis of deposited HNO_3 on the forest canopy may acts as a sink of HNO_3, through their summertime experiments. This daytime photochemical process also produces nitrous acid (HONO) which is a source of OH radicals in the atmosphere.

Since I only performed long-term measurements for HNO_3 and $PM_{2.5}$ components, it was difficult to discuss these sources and sinks quantitatively or qualitatively. However, large emission of HNO_3 were mostly found in the leafless period (winter), and the enhanced fine NO_3^- deposition were also found simultaneously in both leafy and leafless periods. Therefore, the emissions of HNO_3 in my measurement were more likely due to the equilibrium shift of NH_4NO_3.

Chapter 4 Seasonal fluxes of ammonia in an agricultural field

4.1 Introduction

NH_3 is a principal component of Nr and has been deeply involved in human activities such as agriculture. While sulfur and NO_x emissions have been significantly reduced in Europe, the United States, and East Asia in recent years due to the emission control strategies, NH_3 emissions have continuously increased (Fowler et al., 2020; Kurokawa and Ohara, 2020). Thus, the world faces dramatic changes in air pollution; from acid pollution to alkaline pollution (Sutton et al., 2020).

Measurements at various vegetation in Europe and the United States since the 1980s show that NH_3 has not only a one-way deposition behavior from the atmosphere to the surface, but also has a property of bi-directional exchange; emission from plants and soil to the atmosphere (Flechard et al., 2013). To describe this complicated NH_3 bi-directional exchange, several bi-directional exchange models devolved from a simple resistance model were introduced (Sutton et al., 1998; Nemitz et al., 2001; Massad et al., 2010; Zhang et al., 2010). Some attempts have combined this model with a chemical transport model to evaluate NH_3 emission, transport, and deposition at a regional scale (Bash et al., 2013). On the other hand, only a few studies focused on the bi-directional exchange of NH_3 in Asia. For example, flux measurements and modeling over rice paddy fields were conducted in Japan (Hayashi et al., 2012; Katata et al., 2013; Hayashi et al., 2017). To apply these bi-directional exchange models to Asian regions, further measurement-based studies are required because the models depend on regional characteristics.

In this study, I investigate the NH_3 bi-directional exchange based on field measurements in Japan and aims to contribute to the development of a bi-directional exchange model applicable for East Asia. I determined NH_3 fluxes over an agricultural field in soybean-growing and fallow periods in Tokyo, Japan using REA method. The REA was also used for NH_3 flux measurements over cropland in the United States since 2000s (Meyers et al., 2006; Nelson et al., 2017; Nelson et al., 2019). I also compared the fluxes obtained from my observations with those inferred from a bi-directional exchange model to examine the applicability of the model in this region for the first time in East Asia.

4.2 Methods

4.2.1 Site description

I conducted NH_3 flux measurements using REA in an agricultural field of the Field Museum Fuchu (FM Fuchu) of the Tokyo University of Agriculture and Technology (35°40′N, 139°29′E), in the west of central Tokyo. The agricultural field is flat and surrounded by university buildings with trees, residential areas, and traffic roads (Fig. 4-1). The soil of the cropland was Andosols, which is primarily derived from volcanic ash and is typically black due to the accumulated organic matter. I set up an observation point in the southeast field (about 0.9 ha) of the cropland. I conducted measurements in soybean-growing (July 28–August 5, 2020) and fallow (March 4–March 10, 2021) periods. Before the soybean-growing period (20-summer), soybean seeds were planted on the southeast field. The

soybean height was on average about 0.7 m during the observation of 20-summer. Maize was planted on the north and west fields of the cropland. Vegetables were cultivated in the northwest field. A small dairy barn was situated on the east side across a road. The WD in July on the cropland was south from analysis of previous meteorological data. Therefore, I set up the observation point to obtain sufficient fetch (about 40 m) from the south side. The ratio of flux measurement height to the fetch was about 3%. During the fallow period (21-winter), I conducted observations at the same point as 20-summer. In 21-winter, the field including the observation point and the north side became bare land, and the west field became a low grassland.

Soybean seeds (*Enrei* and *Tsukui Native*) were planted on June 17 and 24, 2020. Before planting, the field was fertilized on June 2, 2020, with 200 kg nitrogen and potassium chemical fertilizer with urea (N: K = 16: 16), containing 70% of its N as ammonium-N. Then, 300 kg fused phosphate and 40 kg potassium sulfate fertilizers were applied, and the soil surface layer (about 15–20 cm) was mixed with fertilizer using a rotary. Pesticides and herbicides were sprayed and weeding was conducted irregularly until the harvest. Soybean was harvested on October 21 and between November 1 and 5, 2020. After the harvest, cow dung compost (19.6 t) was sprayed on the field on November 18, 2020 and mixed with the soil surface layer. The amount of N fertilizer in the soybean field was about 36 kg ha^{-1} during the year. The application of chemical fertilizer is irregular and the amount is not fixed because the crops cultivated in this field differ every year. Cow dung compost is mainly used based on recycle-based agriculture.

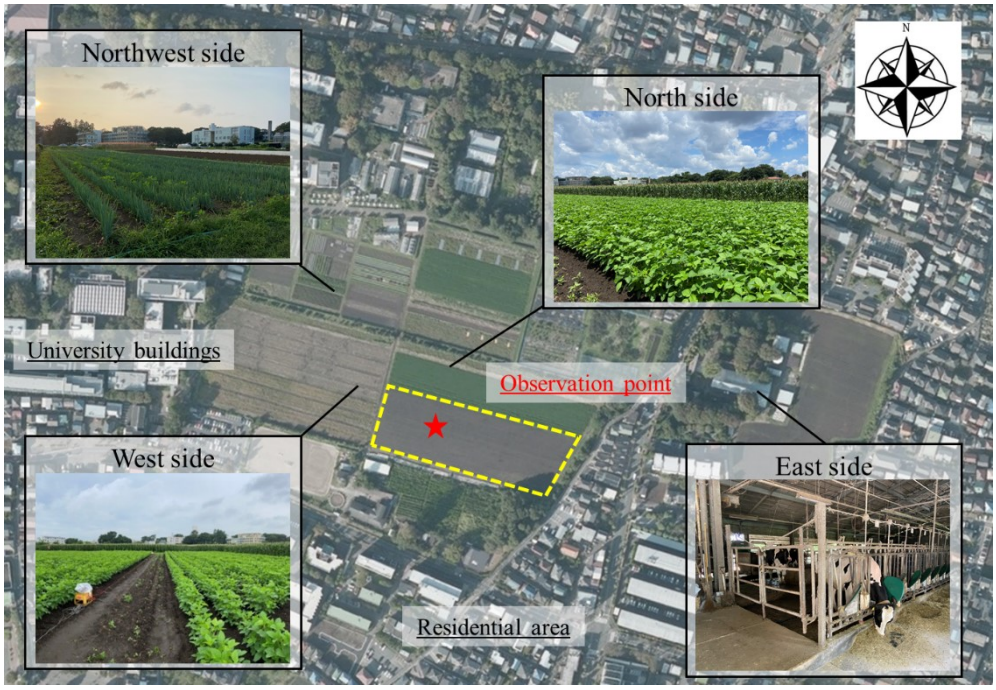

Fig. 4-1. Location of the observation site with surrounding environment during the soybean-growing periods. This aerial photograph is taken by Geospatial Information Authority of Japan (2019).

4.2.2 Relaxed eddy accumulation sampling system for ammonia

I determined the NH_3 fluxes using the REA system incorporating the denuder/filter-pack sampling technique linked with a 3D sonic anemometer (Fig. 4-2). The REA sampling system was the same as Section 3.2.2, except that I added other annular denuder tubes (URG, 2000-30×150-3CSS) for collecting NH_3. The denuder tubes were set between the annular denuder tubes for collecting HNO_3 and filter-pack holders for collecting $PM_{2.5}$ (Fig.3-1 (b)). The coating solution of denuder tubes for NH_3 was 0.85% phosphoric acid (0.85% (w/v) H_3PO_4 + 1% (w/v) glycerin + 50% (v/v) ethanol-water solution). After coating, the denuder tubes were also dried by clean air. I conducted the blank tests using the tubes directly after the coating at each observation (n = 5). The median of these contents in the blank was subtracted when calculating the NH_3 concentration. The travel blank can be ignored because the laboratory for the coating process was within 200 m of the observation point. The sampling part of REA system was installed 1.2 m above the ground. I also measured the reference concentration for verifying the data obtained from the REA system by installing another denuder/filter-pack sampling system (reference) at the same height as the REA system in parallel. To determine daytime (10:00 to 17:00) and nighttime (18:00 to 9:00) NH_3 fluxes, I conducted continuous sampling and manually changed the denuder tubes and filters twice a day. After sampling, the NH_4^+ ion in each denuder tube was extracted into deionized water with 20 ml (20-summer) or 10 ml (21-winter) via an ultrasonic method. I used ion chromatography to analyze the NH_4^+ content (Dionex, ICS-1100). Before running the analysis, I calibrated the system using an NH_4^+ standard solution (Kanto Chemical Corporation, 01802-96).

The fluxes were determined from Eq. (3-2) as in Section 3.2.2. I also estimated the uncertainty of measured flux (σ_F) and the detection limit of difference in concentration between updraft and downdraft (ΔC) by REA sampling system on the basis of Wolff et al. (2010b) and Walker et al. (2013). However, it should be noted that I did not conduct side-by-side concentration measurements using same sampling system. Instead, the results of parallel concentration measurements using REA and reference sampling system were used. I plotted the measured concentrations using REA and reference sampling system and made an orthogonal linear regression. I defined the residuals of the orthogonal linear regression as random error in the concentration and regarded the standard deviation of the residuals ($\sigma_{\Delta C}$) as the detection limit of ΔC. I also regarded ΔC in REA system was significant if it was larger than $\sigma_{\Delta C}$. σ_F can be obtained by combining the uncertainty in the ΔC ($\sigma_{\Delta C}$) and the uncertainty in the β and σ_w (σ_{vtr}) following Gaussian error propagation as follow:

$$\sigma_F = F\sqrt{\left(\frac{\sigma_{v_{tr}}}{v_{tr}}\right)^2 + \left(\frac{\sigma_{\Delta C}}{\Delta C}\right)^2} \tag{4-1}$$

I calculated σ_F only using $\sigma_{\Delta C}$ because it was clear that a major part of σ_F was governed by $\sigma_{\Delta C}$ in Wolff et al. (2010b).

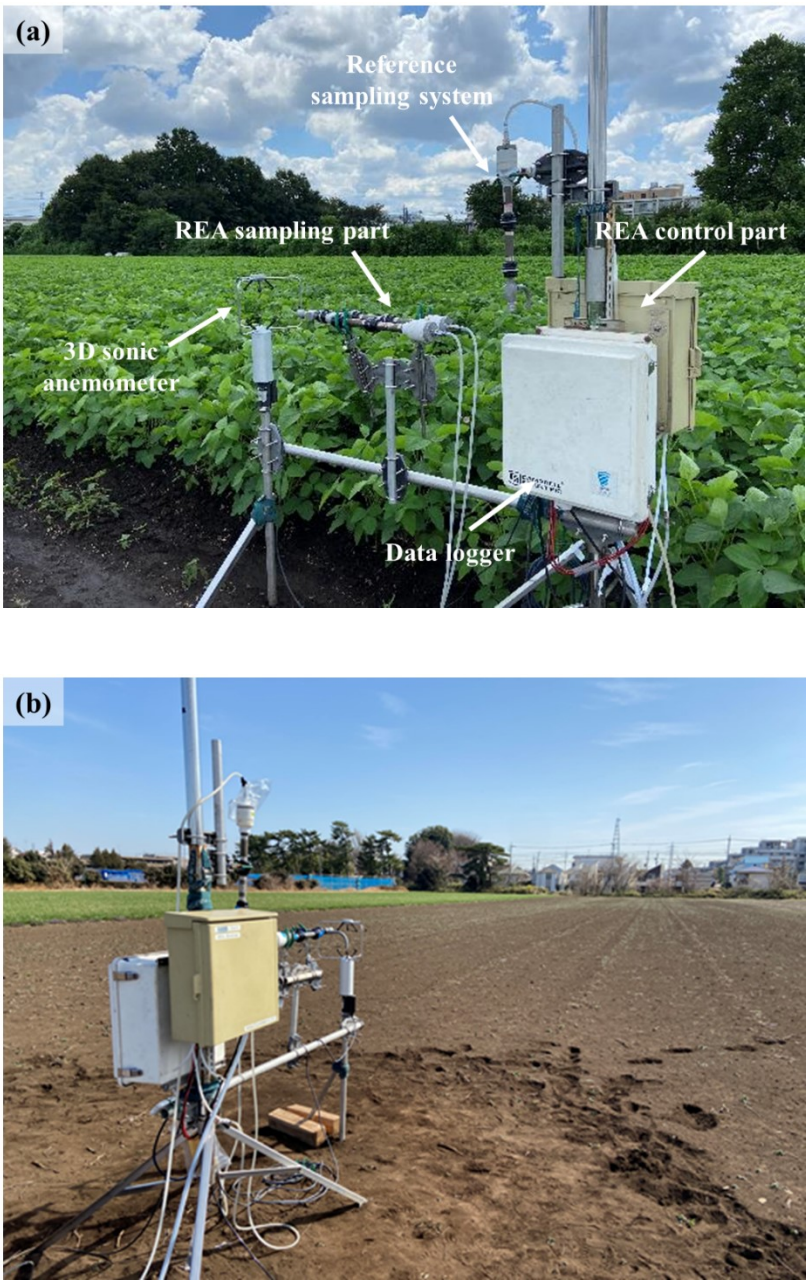

Fig. 4-2. Photo of the REA sampling system in (a) soybean-growing and (b) fallow periods.

4.2.3 The ammonia bi-directional exchange model

As mentioned in Section 1.3, I verified the applicability of the current bi-directional exchange model compared with the REA measurements. In the resistance model, concentration of target substance at deposition surface is assumed to be zero (Erisman and Draaijers, 1995). Thus, the direction of flux is assumed only toward deposition, and emission from surface cannot be reproduced (Fig. 4-3(a)). However, observations and experiments over 40 years since the 1980s have reported the NH_3 emission from plant stomata and soil (Flechard et al. 2013). Since the emission process brings uncertainty to the estimation of nitrogen deposition, various bi-directional exchange models which can reproduce the NH_3 emission from surface have been developed and validated based on observations, starting with Sutton et al. (1995). In this study, I used the bi-directional exchange model of Zhang et al. (2010) to infer NH_3 flux in the FM Fuchu site. This model is developed from the resistance model of Zhang et al. (2003) and is similar to the two-layer model of Nemtiz et al. (2001), in which emission from stomata and soil are assumed (Fig. 4-3(b)).

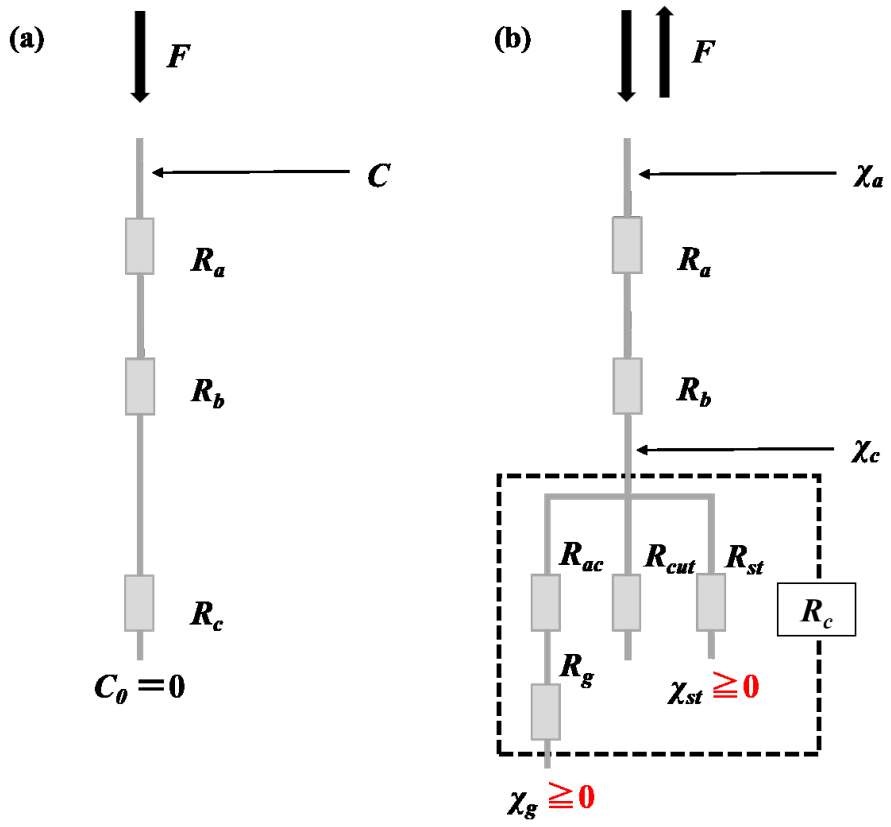

Fig. 4-3. Conceptual diagram of (a) the resistance model and (b) bi-directional exchange model based on Zhang et al. (2010). F is flux at reference height. C and χ_a are concentration of target at reference height. R_a, R_b, R_c, R_{ac}, R_g, R_{cut}, and R_{st} indicate aerodynamic resistance, quasi-laminar resistance, surface resistance, in-canopy aerodynamic resistance, soil resistance, cuticular resistance, and stomatal resistance, respectively. C_0 is concentration at deposition surface. χ_a, χ_{st}, and χ_g indicate canopy, stomatal, and soil compensation point, respectively.

Unlike the resistance model, the bi-directional exchange model infers the canopy compensation point (χ_c) as a new parameter. χ_c is air concentration at top of the canopy at which the direction of flux change, and this concept is proposed by Farquhar et al. (1980). Therefore, the net exchange flux above the canopy can be calculated as follows:

$$F = -\frac{\chi_a - \chi_c}{R_a + R_b} \tag{4-2}$$

where χ_a is air concentration. When χ_a is lower than χ_c, the flux indicates emission (positive), and vice versa. χ_c is determined from χ_a and each compensation point and resistance as follow:

$$\chi_c = \left(\frac{\chi_a}{R_a + R_b} + \frac{\chi_{st}}{R_{st}} + \frac{\chi_g}{R_{ac} + R_g}\right) \cdot \left(\frac{1}{R_a + R_b} + \frac{1}{R_{st}} + \frac{1}{R_{ac} + R_g} + \frac{1}{R_{cut}}\right)^{-1} \tag{4-3}$$

where χ_{st} and χ_g are stomatal and soil compensation points, R_{st}, R_{cut}, R_{ac}, and R_g indicate stomatal resistance, cuticular resistance, in-canopy aerodynamic resistance, and soil resistance, respectively. χ_{st} and χ_g are presented in Nemitz et al. (2004a) as follow:

$$\chi_{st} = \left(\frac{161500}{T_{st}}\right) \mathrm{e}^{\left(-\frac{10378}{T_{st}}\right)} \Gamma_{st} (1.703 \times 10^{10}) \tag{4-4}$$

$$\chi_g = \left(\frac{161500}{T_g}\right) \mathrm{e}^{\left(-\frac{10378}{T_g}\right)} \Gamma_g (1.703 \times 10^{10}) \tag{4-5}$$

where T_{st} and T_g are stomata and soil temperature, and Γ_{st} and Γ_g are stomata and soil emission potential, respectively. Emission potential is an index for the intensity of NH_3 emission and is calculated as follow:

$$\Gamma_{st} = \frac{\left[NH_4{}^+\right]_{\mathrm{st}}}{[H^+]_{\mathrm{st}}} \tag{4-6}$$

$$\Gamma_g = \frac{\left[NH_4{}^+\right]_{\mathrm{g}}}{[H^+]_{\mathrm{g}}} \tag{4-7}$$

where $[NH_4{}^+]_{\mathrm{st}}$ and $[NH_4{}^+]_{\mathrm{g}}$ are the $NH_4{}^+$ concentration in the leaf apoplast and soil, and $[H^+]_{\mathrm{st}}$ and $[H^+]_{\mathrm{g}}$ are the H^+ concentration in the leaf apoplast and soil, respectively. Emission potentials are usually determined through foliage and soil analysis, however, it is difficult due to technical difficulties. Therefore, Zhang et al. (2010) reviewed a wide range of previous measurements and set emission potentials for each LUC. Although the values of emission

potentials for forests widely vary considering the nitrogen load, I used these literature values at first. R_a and R_b were determined following Section 3.2.3.

- Stomatal resistance

R_{st} is calculated from a sunlit/shade R_{st} sub-model presented by Zhang et al. (2002) as follow:

$$R_{st} = \left(G_s(PAR)f(T)f(D)f(\psi)\frac{D_i}{D_v}\right)^{-1} \tag{4-8}$$

where G_s(PAR) is the unstressed leaf stomatal conductance and is a function of photosynthetically active radiation (PAR), $f(T)$ is the conductance-reducing effects of air temperature, $f(D)$ is the conductance-reducing effects of water vapour pressure deficit, $f(\psi)$ is the conductance-reducing effects of water stress, and D_i/D_v is the ratio of molecular diffusivity of target gaseous substance to water vapour, respectively. G_s(PAR) is calculated as follow:

$$G_s(\mathrm{PAR}) = \frac{F_{\mathrm{sun}}}{r_{\mathrm{st}}(\mathrm{PAR}_{\mathrm{sun}})} + \frac{F_{\mathrm{shade}}}{r_{\mathrm{st}}(\mathrm{PAR}_{\mathrm{shade}})} \tag{4-9}$$

$$r_{\mathrm{st}}(\mathrm{PAR}) = r_{\mathrm{st\,min}}\left(1 + \frac{b_{\mathrm{rs}}}{\mathrm{PAR}}\right) \tag{4-10}$$

$$F_{\mathrm{sun}} = 2\cos\theta\left(1 - \mathrm{e}^{\left(\frac{-0.5\mathrm{LAI}}{\cos\theta}\right)}\right) \tag{4-11}$$

$$F_{\mathrm{shade}} = \mathrm{LAI} - F_{\mathrm{sun}} \tag{4-12}$$

where F_{sun} and F_{shade} are the total sunlit and shaded LAI, r_{st} is the unstressed R_{st}, $r_{\mathrm{st\,min}}$ is the minimum R_{st}, b_{rs} is empirical constant, and $\mathrm{PAR}_{\mathrm{sun}}$ and $\mathrm{PAR}_{\mathrm{shade}}$ are PAR received by sunlit and shaded leaves, respectively. When LAI < 2.5 or SR < 200 W m^{-2}, $\mathrm{PAR}_{\mathrm{sun}}$ and $\mathrm{PAR}_{\mathrm{shade}}$ are calculated as follow:

$$\mathrm{PAR}_{\mathrm{sun}} = R_{\mathrm{dir}}\frac{\cos\alpha}{\cos\theta} + \mathrm{PAR}_{\mathrm{shade}} \tag{4-13}$$

$$\mathrm{PAR}_{\mathrm{shade}} = R_{\mathrm{diff}}\mathrm{e}^{(-0.5\mathrm{LAI}^{0.7})} + 0.07R_{\mathrm{dir}} \times (1.1 - 0.1\mathrm{LAI})\mathrm{e}^{-\cos\theta} \tag{4-14}$$

Under all other conditions, $\mathrm{PAR}_{\mathrm{sun}}$ and $\mathrm{PAR}_{\mathrm{shade}}$ are calculated as follow:

$$\mathrm{PAR_{sun}} = {R_{\mathrm{dir}}}^{0.8}\frac{\cos\alpha}{\cos\theta} + \mathrm{PAR_{shade}} \tag{4-15}$$

$$\mathrm{PAR_{shade}} = R_{\mathrm{diff}}\mathrm{e}^{(-0.5\mathrm{LAI}^{0.8})} + 0.07R_{\mathrm{dir}} \times (1.1 - 0.1\mathrm{LAI})\mathrm{e}^{-\cos\theta} \tag{4-16}$$

where R_{diff} and R_{dir} are the downward visible radiation fluxes above the canopy from diffuse and direct-beam radiation, θ is the solar zenith angle, and α is the angle between the leaf and the sun ($\alpha = 60°$ for a canopy assumed to have a spherical leaf angle distribution), respectively. R_{diff} and R_{dir} are inferred from Kamii et al. (1996) as follow:

$$R_{\mathrm{dir}} = \mathrm{SR} - R_{\mathrm{diff}} \tag{4-17}$$

$$R_{\mathrm{diff}} = K_{\mathrm{S}} \times Q_0 \tag{4-18}$$

$$K_{\mathrm{S}} = \mathrm{A} \times {K_{\mathrm{T}}}^{\mathrm{B}} \times (1 - K_{\mathrm{T}})^{\mathrm{C}} \tag{4-19}$$

$$K_{\mathrm{T}} = \frac{\mathrm{SR}}{Q_0} \tag{4-20}$$

$$\mathrm{A} = 0.878 + 13.8\cos\theta - 19.32\cos^2\theta + 10.03\cos^3\theta \tag{4-21}$$

$$\mathrm{B} = 1.33 + 0.476\cos\theta \tag{4-22}$$

$$\mathrm{C} = 1.60 + 4.11\cos\theta - 7.36\cos^2\theta + 3.76\cos^3\theta \tag{4-23}$$

where Q_0 is extra-terrestrial horizontal radiation, K_{S} and K_{T} indicate standardized diffuse and global radiation. All other formula for calculating R_{st} are presented as follow:

$$f(T) = \frac{T - T_{\mathrm{min}}}{T_{\mathrm{opt}} - T_{\mathrm{min}}}\left(\frac{T_{\mathrm{max}} - T}{T_{\mathrm{max}} - T_{\mathrm{opt}}}\right)^{b_{\mathrm{t}}} \tag{4-24}$$

$$b_{\mathrm{t}} = \frac{T_{\mathrm{max}} - T_{\mathrm{opt}}}{T_{\mathrm{opt}} - T_{\mathrm{min}}} \tag{4-25}$$

$$f(D) = 1 - b_{\mathrm{vpd}}D \tag{4-26}$$

$$D = e^*(T) - e \tag{4-27}$$

$$f(\psi) = \frac{\psi - \psi_{c2}}{\psi_{c1} - \psi_{c2}} \tag{4-28}$$

$$\psi = -0.72 - 0.0013\mathrm{SR} \tag{4-29}$$

where T_{min} and T_{max} are minimum and maximum temperatures which stomata will close, T_{opt} is optimum temperature for maximum stomatal opening, b_{vpd} is a water vapour pressure deficit constant, D is the vapour pressure deficit, $e^*(T)$ is the saturation water vapour pressure at T, e is the ambient water vapour pressure, ψ is leaf water potential, and ψ_{c1} and ψ_{c2} are parameters specifying leaf water potential dependency, respectively. $f(\psi) = 1$ when $\psi > \psi_{c1}$: no leaf water potential stress. It should be note that R_{st} was set at infinite value during nighttime because the leaf stomata is completely closed when there is no SR (Zhang et al., 2003).

- Cuticular resistance

R_{cut} is calculated for SO_2 and O_3 and then scaled for other gaseous substance as follow:

$$\frac{1}{R_{cut}} = \frac{\alpha}{R_{cut}(\mathrm{SO_2})} + \frac{\beta}{R_{cut}(\mathrm{O_3})} \tag{4-30}$$

where α and β are scaling factors based on the solubility and reactivity and have different values for each gaseous substance (Wesely, 1989). For NH_3, $\alpha = 1$ and $\beta = 0$ (Zhang et al., 2002). This means that the R_{cut} values of NH_3 is the same as that of SO_2. R_{cut} is determined for dry and wet conditions as follow:

$$R_{cut-\mathrm{dry}} = \frac{R_{cutd0}}{\mathrm{e}^{0.03\times \mathrm{RH}}\ \mathrm{LAI}^{1/4}\ u^*} \tag{4-31}$$

$$R_{cut-\mathrm{wet}} = \frac{R_{cutw0}}{\mathrm{LAI}^{1/4}\ u^*} \tag{4-32}$$

where R_{cutd0} and R_{cutw0} are reference values for dry and wet R_{cut}, and their values for SO_2 and O_3 at different LUC are presented in Zhang et al. (2003).

- In-canopy aerodynamic resistance

R_{ac} is same for all gaseous substances and is calculated as follow:

$$R_{ac} = \frac{R_{ac0} \times \mathrm{LAI}^{1/4}}{u^{*2}} \tag{4-33}$$

$$R_{ac0} = R_{ac0}(min) + \frac{\mathrm{LAI} - \mathrm{LAI}(min)}{\mathrm{LAI}(max) - \mathrm{LAI}(min)} \times [R_{ac0}(max) - R_{ac0}(min)] \quad (4\text{-}34)$$

where R_{ac0} is the reference value for R_{ac}, $R_{ac0}(min)$ and $R_{ac0}(max)$ are minimum and maximum values of R_{ac0}, and LAI(min) and LAI(min) are minimum and maximum LAI values during the year, respectively. The values of R_{ac0} at difference LUC are also presented in Zhang et al. (2003).

- Soil resistance

R_g is also calculated for SO_2 and O_3 and then scaled for other gaseous substance as follow:

$$\frac{1}{R_g} = \frac{\alpha}{R_g(\mathrm{SO_2})} + \frac{\beta}{R_g(\mathrm{O_3})} \quad (4\text{-}35)$$

R_g is determined for dry and wet conditions in the same way as R_{cut}. R_g for SO_2 varies at each LUC in dry condition, and is set at 50 s m^{-1} in wet condition. R_g for O_3 is set at 200 s m^{-1} in dry and wet conditions for vegetated surfaces. Compared to other resistance, information on R_g is limited and the parameterization is very simple.

The parameters in the bi-directional exchange model for estimating the NH_3 flux at cropland (LUC = 15) are listed in the Table 4-1. In the 21-winter observation, χ_{st}, R_{st}, R_{cut}, and R_{ac} were not considered for the flux calculation because there was no vegetation canopy. I calculated 1-h value of NH_3 using meteorological and other elements recorded at the site.

Table 4-1. Setting of the parameters for bi-directional exchange model based on Zhang et al. (2010).

	Parameter		Unit	20-summer	21-winter
R_a	z	reference height	m	1.25	1.15
	d	displacement height	m	0.46	0
	z_0	roughness length	m	0.17	0.01
R_b	Sc	Schmidt number for NH_3		0.75	
	Pr	Prandtl number		0.72	
R_{st}	$r_{\text{st min}}$	minimum stomatal resistance	s m^{-1}	120	–
	b_{rs}	empirical light response constant for stomatal resistance	W m^{-2}	40	–
	T_{min}	minimum temperature for stomatal opening	°C	5	–
	T_{opt}	optimum temperature for stomatal opening	°C	27	–
	T_{max}	maximum temperature for stomatal opening	°C	45	–
	b_{vpd}	water vapour pressure deficit constant	kPa^{-1}	0	–
	Ψ_{c1}	leaf-water-potential dependency	Mpa	−1.5	–
	Ψ_{c2}	leaf-water-potential dependency	Mpa	−2.5	–
	D_{NH3}/D_v	the ratio of molecular diffusivity of ammonia to water vapour		0.97	–
R_{ac}	R_{ac0}(min)	minimum in-canopy aerodynamic resistance	s m^{-1}	10	–
	R_{ac0}(max)	maximum in-canopy aerodynamic resistance	s m^{-1}	40	–
R_g	R_{gd} SO_2	dry soil resistance for SO_2	s m^{-1}	200	
	R_{gw} SO_2	wet soil resistance for SO_2	s m^{-1}	50	
R_{cut}	R_{cutd0} SO_2	dry cuticle resistance for SO_2	s m^{-1}	1500	–
	R_{cutw0} SO_2	wet cuticle resistance for SO_2	s m^{-1}	50	–
χ_{st}	Γ_{st}	stomatal emission potential		800	–
χ_g	Γ_g	soil emission potentials		5000	5000

4.2.4 Meteorological element, soil, and foliage measurements

- Meteorological element measurement

I installed a 3D sonic anemometer (YOUNG, 81000) 1.2 m above the ground at the observation point to measure WS, WD, and other elements for determine NH_3 flux. I used the Temp and rainfall data collected by the Automated Meteorological Data Acquisition System (AMeDAS) introduced by the Japan Meteorological Agency in FM Fuchu, which is located about 200 m northwest of the observation point. The thermometer was installed 1.5 m above the ground in this system. Near the AMeDAS, a Thermo Recorder (T&D Corporation, TR-72U) was installed 1 m above the ground to record RH. Soil Temp was recorded using a sheath-type temperature probe (HIOKI, 9472-50) at 0.15 m below the ground next to the 3D sonic anemometer. SR was measured using a pyranometer (PREDE, PCM-01N) at an observation tower (30 m) in the FM Tama, 11 km from FM Fuchu (Fig. 2-6(d)). All meteorological and soil elements were recorded at 10-min intervals except elements for determine flux.

- Soil measurement

I collected soil samples to measure the pH and NH_4^+ concentrations in the soil of the cropland. Samples were collected at three points near the observation point (from the apex of a right-angled isosceles triangle with a hypotenuse of 5 m). I dug a hole with a width and depth of 30 cm for each point, and evenly collected soil from the layer at depths of 0–10 cm and 10–20 cm after removing the surface layer (EANET, 2000). After soil sampling, gravel and plant roots were removed and sieved with a 2 mm mesh. To measure soil pH, the soil was mixed with deionized water at a ratio of 1:2.5 (25 mL solution for 10 g soil) and continuously shaken for 1-h. Then, the pH of supernatant was measured using a glass electrode pH meter (HORIBA, F-71) after standing for a while. The NH_4^+ concentration was measured by mixing the soil with 2M KCl at a ratio of 1:10 (50 mL solution for 5 g soil) and continuously shaken for 1-h (Yamashita et al., 2010). The supernatant was filtered using a disposable syringe filter with a 0.45 μm membrane filter (GL Sciences, 5040-28508) after standing for a while. The NH_4^+ content was quantified using an ion chromatograph (Dionex, ICS-1100). The mean values of three locations were used. As shown in Eq. (4-7), Γ_g was calculated from the NH_4^+ concentration and H^+ concentration derived from pH.

- Foliage measurement

I measured the LAI using a plant canopy analyzer (LI-COR, LAI-2200) in 20-summer. LAI was measured at 3 to 5 points around the observation points on the start, middle, and last observation dates. The mean values were used for LAI. The canopy height was also recorded simultaneously. I collected soybean leaf samples twice on August 6 and September 9, 2020. Leaf samples were refrigerated until analysis. The fresh leaves were washed with deionized water, gently air-dried, and frozen down for measuring bulk tissue NH_4^+ concentrations (Mattsson et al., 2009; Personne et al., 2015). The frozen leaves were ground in liquid nitrogen using a mortar and 1 g of the ground material was shaken with 15 mL of 10 mM formic acid or 15 mL deionized water for measuring NH_4^+ or pH, respectively. The suspensions were centrifuged at 3,000 rpm for 30 min, and the supernatants were filtered using a disposable syringe filter with a 0.45 μm membrane filter (Advantec, DISMIC 25AS). The bulk tissue NH_4^+ concentration and pH were measured using an ion chromatograph (Dionex, ICS-1100) and glass electrode (HORIBA, F-72), respectively. The bulk foliar NH_4^+ concentration could relate to the Γ_{st} based on the apoplast

solution analysis (Mattsson et al., 2009). Massad et al. (2010) proposed empirical equation to estimate Γ_{st} using the bulk foliar NH_4^+ concentration ($[NH_4^+]_{\mathrm{bulk}}$) based on the meta-analysis of existing data as follow:

$$\Gamma_{st} = 19.3 \times \mathrm{e}^{(0.0506 \times [NH_4^+]_{\mathrm{bulk}})} \tag{4-36}$$

Since it was technically difficult to conduct apoplast solution analysis, I estimated Γ_{st} using Eq. (4-36). For comparison, I also calculated the bulk foliar NH_3 emission potential (Γ_{bulk}) as follows:

$$\Gamma_{bulk} = \frac{[NH_4^+]_{\mathrm{bulk}}}{[H^+]_{\mathrm{bulk}}} \tag{4-37}$$

where $[H^+]_{\mathrm{bulk}}$ is the H^+ concentration in the bulk foliar (Mattsson et al., 2009).

4.3 Results & Discussion

4.3.1 Overview

As described in Section 4.2.1, soybean was planted on the observation field before the observation of 20-summer. The canopy height was about 0.6–0.7 m on the observation start date and reached about 0.7–0.9 m at the end of the observation because the soybean was under growth stage during the observation periods. The LAI value also increased from 3.0 to 4.7 along with the canopy growth.

Hourly variations of meteorological and soil conditions during the two observation periods are shown in Fig. 4-4. Daytime WS was larger than nighttime WS most of the time by ~60% on average, and the WS in 21-winter was larger than in 20-summer. The main WD in 20-summer was north in the first half of the observation period and south in the second half. The north WD was dominant in 21-winter. Since the rainy season continued at the end of July in the year, rainfall and RH were high in the first half of 20-summer. In the second half, air temperature increased, and RH decreased. It was relatively dry in 21-winter, except for some rainfall periods. Regardless of the observation period, the soil temperature variation was small and remained within a certain range.

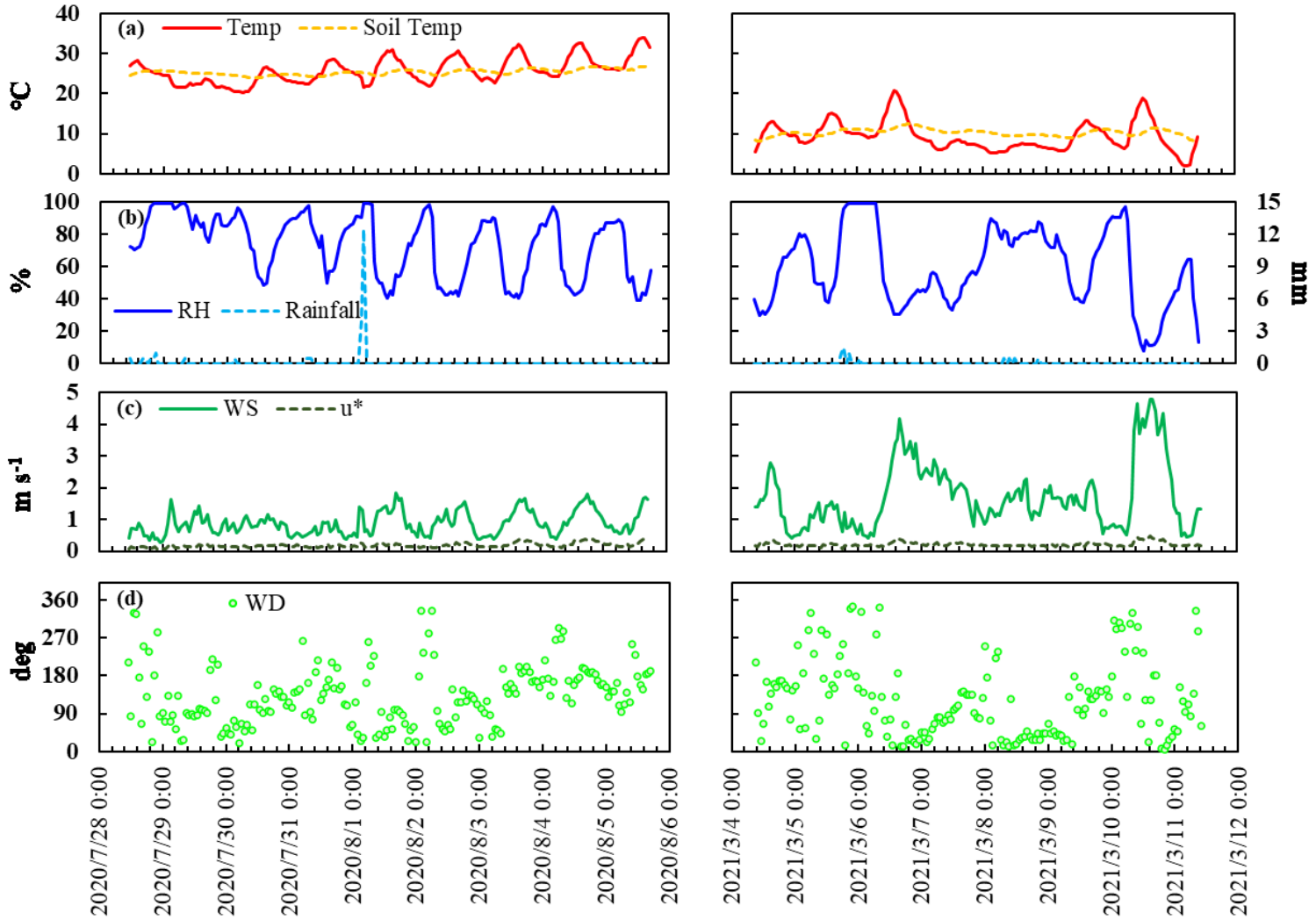

Fig. 4-4. Hourly variations of (a) air temperature (Temp) and soil temperature (Soil Temp), (b) relative humidity (RH) and rainfall, (c) wind speed (WS) and friction velocity (*u**), and (d) wind direction (WD).

4.3.2 Flux and deposition velocity

I verified REA measurements by comparing NH_3 concentrations measured using REA with those measured by the reference sampling system (Fig. 4-5). Some data could not be obtained due to concentrations below detection limits or not being quantified. Although the NH_3 concentrations derived from REA were similar to the reference concentrations; the linear regression line was y = 1.32 x − 1.01 (R = 0.84), the REA concentrations were lower than the reference concentrations when the concentration below 1 μg m^{-3}. Since an updraft/downdraft separator is used in REA for conditional sampling, the effect of loss due to this separator cannot be ignored at low concentrations. The error in REA system could also be larger than that of the reference because the REA concentrations were derived from the weighted mean of concentrations in updraft and downdraft. However, the tendency of concentration variations was consistent, and the REA measurements were successful except when the concentration was low.

C_u, C_d, fluxes, and V_d for NH_3 with σ_w and β during the observation periods are listed in Table 4-2. The σ_w was between 0.22 and 0.64 m s^{-1}, and the median was 0.33 m s^{-1}. β was between 0.50 and 0.61, and the median was 0.57. All β values were between 0.40 and 0.63 as reported by Milne et al. (1999), and similar to those reported by Nelson et al. (2017) in a corn field. While σ_w was larger in 21-winter than 20-summer, no clear difference occurred in the β value. The flux was between −0.197 and 0.055 μg m^{-2} s^{-1} (positive indicates emission), indicating that both NH_3 emission and deposition were observed. The V_d of NH_3 was between −3.2 and 27.0 cm s^{-1} (positive indicates deposition), and the median was 4.9 cm s^{-1}. Although most samples showed V_d less than 10 cm s^{-1}, three samples extremely exceeded. Since concentrations of these samples were less than 1 μg m^{-3}, the V_d could be inaccurate than those of other samples. Myles et al. (2011) also indicated that low NH_3 concentrations could lead to high uncertainty in V_d from their flux measurements.

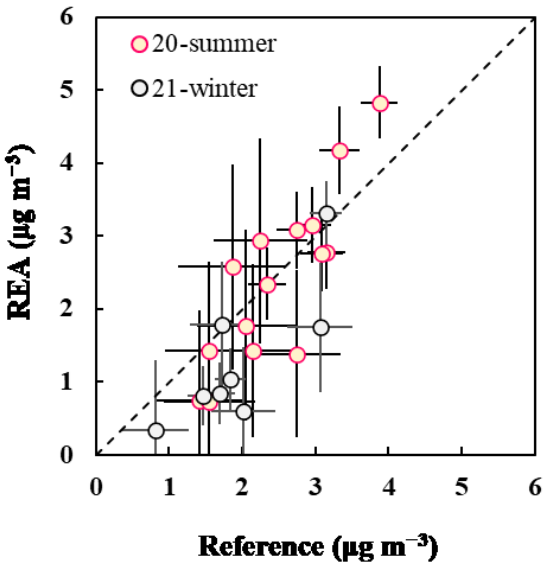

Fig. 4-5. Comparison between NH_3 concentrations measured using the REA and reference sampling systems in 20-summer (pink circles) and 21-winter (white circles). The dashed line indicates a 1:1 ratio of each concentration. Error bars indicate the errors of the concentration measurements due to the variability of blank values. Only corresponding samples are displayed (n = 23).

Table 4-2. Concentrations during updraft (C_u) and downdraft (C_d), fluxes, and V_d for NH_3 with standard deviations of vertical wind velocity (σ_w) and empirical coefficients (β). The bars indicate fluxes that could not be determined due to C_u or C_d below detection limits or not being quantified. D and N indicate daytime and nighttime, respectively.

Period		Start time	End time	NH_3					
				σ_w	β	C_u	C_d	Flux	V_d
				m s^{-1}		μg m^{-3}		μg m^{-2} s^{-1}	cm s^{-1}
2020	0728_D	10:53	18:01	0.25	0.58	2.55	3.90	−0.197	6.01
	0728_N	19:02	9:19	0.22	0.58	–	9.32	–	–
	0729_D	10:41	17:03	0.29	0.60	0.24	1.16	−0.163	22.05
	0729_N	17:56	9:29	0.28	0.57	2.72	3.49	−0.120	3.83
	0730_D	10:43	17:00	0.29	0.58	2.94	2.93	0.003	−0.10
	0730_N	17:59	8:46	0.27	0.57	3.60	4.64	−0.157	3.77
	0731_D	11:26	16:58	0.28	0.54	2.03	3.06	−0.156	6.04
	0731_N	17:54	9:58	0.28	0.57	4.39	5.18	−0.126	2.60
	0801_D	11:03	16:59	0.34	0.58	1.60	1.95	−0.069	3.91
	0801_N	18:05	9:22	0.28	0.53	3.04	3.12	−0.012	0.38
	0802_D	10:21	16:51	0.30	0.58	1.23	1.62	−0.068	4.74
	0802_N	18:07	9:25	0.27	0.54	2.35	3.09	−0.107	3.86
	0803_D	10:26	16:58	0.35	0.59	1.18	1.66	−0.099	6.95
	0803_N	18:05	9:17	0.30	0.55	2.52	2.95	−0.070	2.55
	0804_D	10:09	16:57	0.37	0.61	1.13	1.63	−0.111	8.02
	0804_N	18:01	9:29	0.31	0.59	2.18	2.48	−0.055	2.35
	0805_D	10:25	16:55	0.38	0.57	0.58	0.88	−0.063	8.62
2021	0304_D	10:10	17:21	0.41	0.56	0.39	0.79	−0.093	15.62
	0304_N	18:25	9:00	0.30	0.53	2.72	3.73	−0.164	4.96
	0305_D	10:11	17:20	0.34	0.54	1.31	2.19	−0.162	9.10
	0305_N	18:20	9:01	0.30	0.53	–	0.47	–	–
	0306_D	10:10	17:20	0.50	0.60	1.84	1.65	0.055	−3.15
	0306_N	18:22	9:01	0.44	0.60	0.83	0.86	−0.008	0.96
	0307_D	10:13	17:19	0.39	0.56	–	–	–	–
	0307_N	18:34	9:07	0.33	0.58	–	–	–	–
	0308_D	10:27	17:19	0.37	0.58	–	–	–	–
	0308_N	18:14	9:10	0.35	0.60	–	–	–	–
	0309_D	10:11	17:16	0.36	0.56	–	–	–	–
	0309_N	18:17	9:14	0.34	0.53	0.72	1.28	−0.101	9.80
	0310_D	10:21	17:19	0.64	0.58	0.22	0.46	−0.090	27.04
	0310_N	18:20	9:40	0.39	0.50	0.61	0.97	−0.070	8.70
Median				0.33	0.57	1.72	2.07	−0.096	4.85
SD				0.08	0.03	1.13	1.29	0.061	6.80

Temporal variations in NH_3 concentrations and flux during the observation periods are shown in Fig. 4-6. NH_3 concentrations had a diurnal variation and tended to be low during daytime and high during nighttime, especially in 20-summer. The WS and u^* variations were opposite of the variations in concentration. NH_3 concentration possibly increased at nighttime because NH_3 was not diffused due to the small WS and u^* and was stagnated near the surface. Contrary to the concentration, there was no diurnal variation in the NH_3 flux. These results suggest that V_d in the daytime was larger than in the nighttime. There was no clear relationship between the flux and WD. The fluxes mostly showed deposition throughout the two observation periods. Although two cases showed emission, the magnitude of fluxes was much less than those of deposition cases. The soybean or the ground surface were considered to be the main sink of NH_3 during the two observation periods.

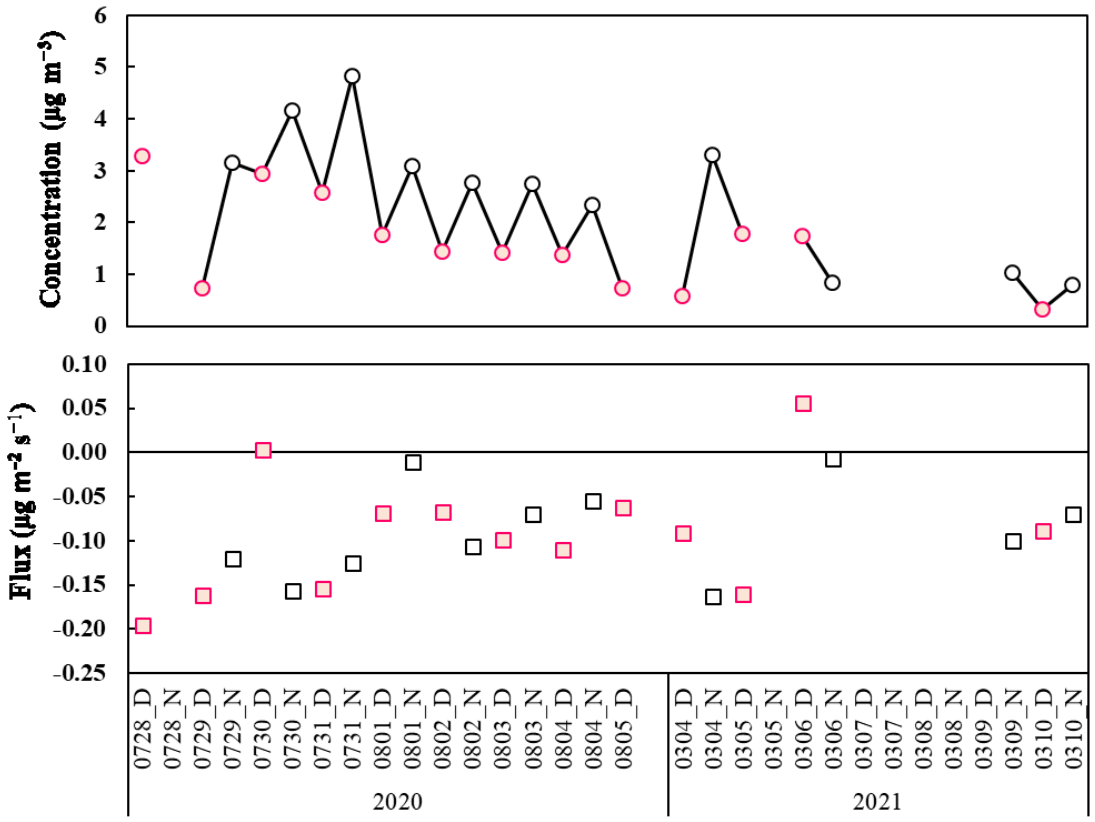

Fig. 4-6. Temporal variations of NH_3 concentration and flux. D and N indicate daytime and nighttime, respectively. Pink symbols indicate daytime values and white symbols indicate nighttime values, respectively.

V_d distribution of NH_3 during the two observation periods are shown in Fig. 4-7. The median values of V_d were 3.9 cm s^{-1} in 20-summer and 8.9 cm s^{-1} in 21-winter. The V_d level was much larger than that calculated using general resistance models which was between 0.6 to 1.3 cm s^{-1} (e.g., Ban et al., 2016; Yamaga et al., 2021); however, slightly lower than the V_d over an unfertilized soybean field measured using AGM (Myles et al., 2011). Although the studies were limited in cropland, it can be seen from Table 4-3 that the V_d were mostly larger than those of other studies. Since the amount of N fertilizer in the site was much lower than that of other studies except Myles et al. (2011), the difference in the amount of N fertilizer may have some effects on the magnitude V_d. The V_d in 20-summer was lower than that in 21-winter, even excluding the three uncertain values exceeded 10 cm s^{-1} mentioned above. The larger V_d in 21-winter was possibly caused by the larger u^* than that in 20-summer. There could be also some unknown processes enhancing NH_3 deposition in 21-winter.

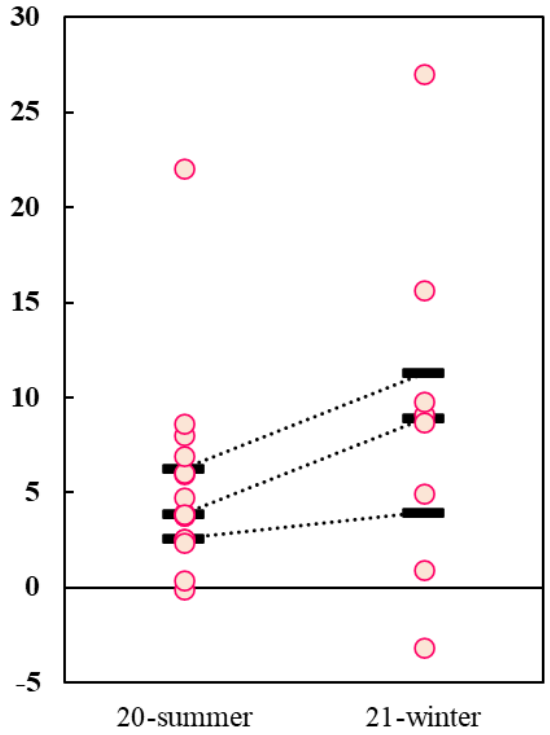

Fig. 4-7. Deposition velocity distributions of NH_3 in 20-summer (n = 16) and 21-winter (n = 8). Top, middle, and bottom bars indicate the 75th percentiles, median, and 25th percentiles, respectively.

Table 4-3. Ammonia concentrations, fluxes, and deposition velocity in croplands.

Reference	Canopy	Method	Period		Concentration	Flux	V_d	Fertilizer
					nmol m^{-3}	nmol m^{-2} s^{-1}	cm s^{-1}	kg N ha^{-1}
[1]	rice	AGM	28 Jul. to 4 Aug. 2010	D	129 ± 91*	−4.2~6.0	0.6**	77.9 (8 Apr. 2010)
				N	109 ± 49*	−0.7~0.3	0.2**	
			5 to 13 Dec. 2009	D	288 ± 124*	−4.6~0.6	0.2**	
				N	203 ± 88*	−1.7~−0.2	0.2**	
					μg m^{-3}	μg m^{-2} s^{-1}		
[2]	maize	REA	12 to 14 Jun. 2001	D	14.42~43.54	0.463~2.652	—	105 (on Jun. 2001)
			26 Jul. to 28 Aug.	D/N	0.28~4.81	−0.203~0.128	—	
[3]	soybean	AGM	8 to 16 Sep. 2006	D	1.61 ± 1.01*	−0.28~0.09	7.09 ± 9.83*	unfertilized
[4]	corn	REA	7 May. to 8 Jun. 2014	D	2.70 ± 1.38*	−0.009~0.800	—	168 (6 May. 2014)
			9 Jun. to 30 Sep. 2014	D	1.20 ± 0.73*	−0.161~0.185	—	
[5]	soybean	MBR	17 Jun. to 22 Aug. 2002		0.01~43.9	−0.448~0.327	0.43 ± 0.50*	65 (May. 2002)
[6]	corn	MBR	29 May. to 29 Jun. 2007		10.3 ± 7.2*	−0.043~6.906	—	20 (18 to 23 Apr. 2007)
								134 (on 25 to 29 May. 2007)
			30 Jun. to 1 Aug. 2007		2.2 ± 1.7*	−0.230~3.125	—	
[7]	soybean	REA	28 Jul. to 5 Aug. 2020	D/N	2.46 ± 1.16*	−0.197~0.003	3.88**	36 (2 Jun. 2020)
			4 to 10 Mar. 2021	D/N	1.31 ± 0.96*	−0.164~0.055	8.90**	

Reference: [1] Hayashi et al. (2012), [2] Meyers et al. (2006), [3] Myles et al. (2011), [4] Nelson et al. (2017), [5] Walker et al. (2006), [6] Waller et al. (2013), [7] This study.

Method: AGM, MBR, and REA indicates the aerodynamic gradient method, the modified Bowen ratio method, and the relaxed eddy accumulation method, respectively. *: mean ± standard deviation. **: median. D and N indicate daytime and nighttime, respectively.

4.3.3 Bi-directional exchange of ammonia

According to Flechard et al. (2013), many factors control the bi-directional exchange of NH_3, such as meteorological, chemical, biological, and anthropogenic processes. In this Section, I investigated the factors controlling the bi-directional exchange of NH_3 in the observation site and considered suitable parameters for the bi-directional exchange model.

Active vertical mixing might enhance both deposition and emission of air pollutant when turbulence is large. For example, as described in Section 3.3.4, the REA measurements confirmed that an increase in $u*$ promotes HNO_3 deposition and emission over a forest (Fig. 3-9). Relationship between V_d of NH_3 and u^* during the two observation periods are shown in Fig. 4-8. Overall, the V_d of NH_3 and u^* had a positive correlation; the linear regression line was y = 46.79 x − 3.64 (R = 0.46). A positive correlation occurred in 20-summer when exclude three uncertain cases and two emission cases; the linear regression line was y = 23.01 x − 0.40 (R = 0.64). However, the correlation was unclear in 21-winter due to insufficient samples (n = 5). NH_3 showed deposition, except for one case, in the observations at unfertilized soybean field by Myles et al. (2011). The V_d of NH_3 positively correlated with u^* and this result is in good agreement with my results. Turbulence could mostly control NH_3 deposition in some conditions.

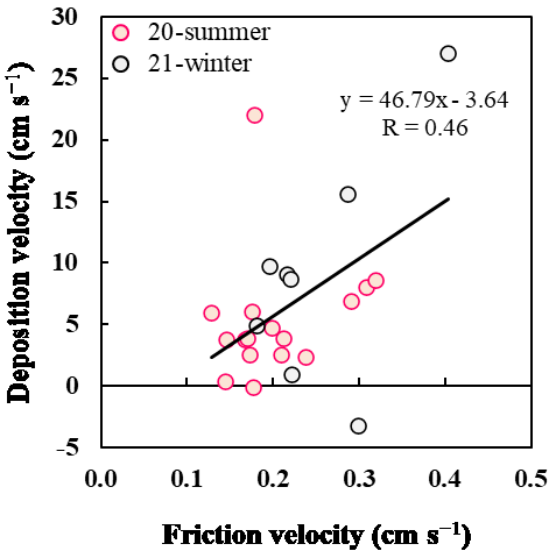

Fig. 4-8. Relationship between NH_3 deposition velocity and friction velocity. The linear regression line and coefficient of correlation was derived from the two observation periods (n = 24).

The wet surface is known to play a significant role as a sink of NH_3. For example, the flux measurements over a soybean field in the United States by Walker et al. (2006) using the Bowen-ratio method showed that the NH_3 deposition rate was higher when the canopy was wet. There are also resistance models that set the R_c of NH_3 to correspond to RH considering the high solubility of NH_3. However, there was no correlation between the V_d of NH_3 and RH in my two observations periods. While the wet surface enhances NH_3 deposition, it is also reported that NH_3 emitted when the wet surface dries. In the flux measurements over a deciduous forest in the United States using the REA method by Hansen et al. (2015), NH_3 emission typically occurred after rainfall. In addition, Wentworth et

al. (2016) observed NH_3 emissions at morning from dew evaporations. I observed two NH_3 emission cases (0730_D and 0306_D) during the observation periods. In both periods, dry conditions directly after the rainfall sharply decreased RH and increased temperature (Fig.4-4). A small deposition of 0306_N possibly followed the emission of 0306_D. These results strongly support the possibility that the NH_3 emissions observed in my observation were not from plants and/or soil emission but were due to the desorption of NH_3 that adsorbed on the surface through rainfall. This process is not considered in typical bi-directional exchange models.

The appropriate setting of emission potential, which indicates the magnitude of NH_3 emission, is crucial for estimating NH_3 flux because this parameter has large influence in the model. From the calculations using the default values of emission potential for crops LUC proposed by Zhang et al. (2010) (Γ_{st} = 800, and Γ_g = 5000), the inferred flux estimated from the bi-directional exchange model was between 0.005 and 0.191 μg m^{-2} s^{-1} and mean value is 0.054 μg m^{-2} s^{-1} (Fig. 4-9). This result indicates that only NH_3 emissions were estimated in the model. On the other hand, NH_3 flux determined from the REA mostly showed depositions (mean value is −0.091 μg m^{-2} s^{-1}). The large difference between measured and inferred flux could be due to the large default values of Γ_{st} and Γ_g for the cropland. Therefore, I obtained the Γ_{st} and Γ_g values suitable for the observation site from analysis of pH and NH_4^+ concentrations in the soil and soybean leaf.

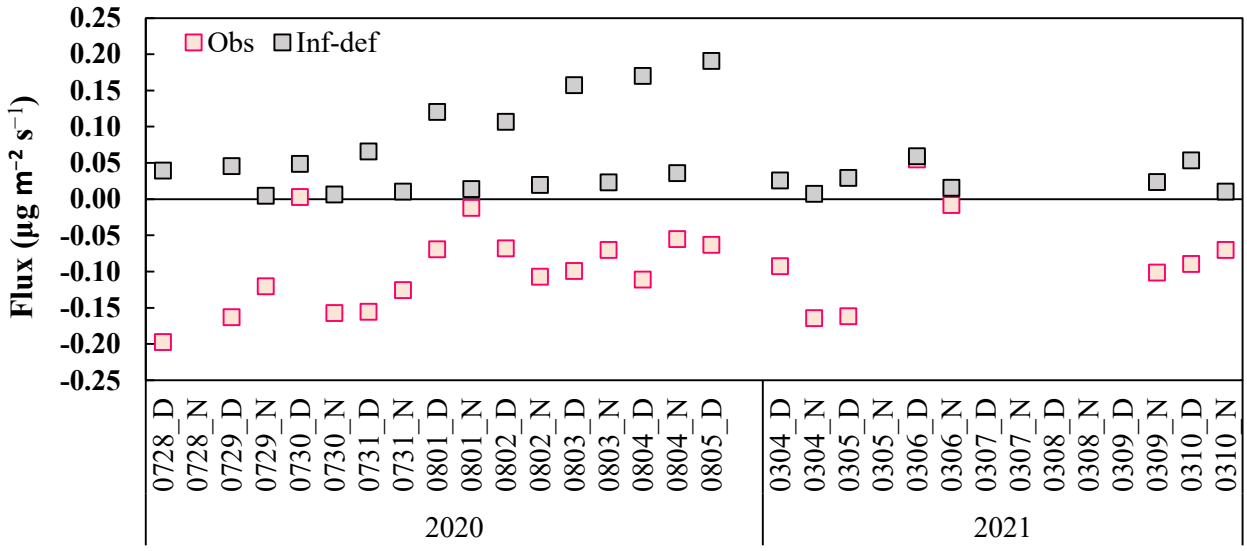

Fig. 4-9. Comparison of the measured NH_3 flux from the REA (Obs) and inferred from the bi-directional exchange model using the default parameters (Inf-def). D and N indicate daytime and nighttime, respectively.

Soil pH and NH_4^+ concentrations are listed in Table 4-4. Regardless of the difference in soil layers, the pH were similar and near neutral. NH_4^+ was detected in 20-summer, and Γ_g = 582 was calculated using Eq. (4-7). The default value (Γ_g = 5000) in the literature was about 8.5 times larger than the measured value and was an excessive value for the observation site. This measured value was also much smaller than those of Massad et al. (2010) which was between 1514 and 13000 at arable ecosystems using extraction method (n = 4). However, NH_4^+ was not detected in 21-winter, and Γ_g = 0 was calculated. Therefore, no emission occurred from the soil in 21-winter theoretically. This

might be due to the nitrification of NH_4^+, which caused the substantial increase in NO_3^- in 21-winter. There is evidence indicates that the nitrification rate of Andosols is higher than those of other soils (Fueki et al., 2006). Because Andosols comprise volcanic ash and humus, it has a high cation exchange capacity (CEC). For this property, Andosols gave a high potential for fertilizer retention, and the loss of NH_4^+ through emission is unlikely. Hayashi et al. (2009) reported that the volatilization loss of NH_3 was suppressed due to the high CEC of Andosols from dynamic chamber measurements in Japan. Therefore, the observation site of this study was a cropland, where the NH_3 emissions from the soil was smaller than those of other studies.

Table 4-4. Soil pH and NH_4^+ and NO_3^- concentrations (mmol L^{-1}).

	pH		NH_4^+		NO_3^-	
	0–10 cm	10–20 cm	0–10 cm	10–20 cm	0–10 cm	10–20 cm
20-summer	6.7	6.8	0.02	0.02	0.02	0.03
21-winter	6.8	6.6	n.a	n.a	0.08	0.15

The NH_4^+ concentration of bulk tissue in the soybean leaves was larger in August than in September, and Γ_{st} and Γ_{bulk} had the same tendency (Table 4-5). Similar to the Γ_g, the Γ_{st} estimated from Eq. (4-36) were much smaller than the default value of the literature (Γ_{st} = 800) and the measured value at a soybean field by Walker et al. (2006). However, the values were not calculated from the apoplast solution but estimated from the empirical equation using bulk leaf tissue. To use bulk tissue NH_4^+ concentration as a proxy of the apoplast solution for evaluating the emission potential, relevant data should be accumulated (Walker et al., 2019). The Γ_{st} is much smaller than the Γ_g in general cropland (Zhang et al., 2010; Walker et al., 2013), and I observed same tendency in this study.

Table 4-5. Bulk tissue NH_4^+ concentration, Γ_{st}, and Γ_{bulk} in the soybean leaves. Γ_{st} was estimated using the empirical equation by Massad et al. (2010).

Sampling date	NH_4^+ (μg g^{-1} fresh leaf)	Γ_{st}	Γ_{bulk}
August 6, 2020	50 ± 6	267 ± 94	139 ± 21
September 9, 2020	25 ± 1	69 ± 3	104 ± 16

Since the Γ_{st} is known to depend on the growth stage of each plant, as also suggested by my results, we should discuss it and set a proper value for Γ_{st}. Temporal variations also occur in χ_{st} and Γ_{st} as reviewed in Flechard et al. (2013). For example, some plants have larger Γ_{st} in young or aged leaves and smaller Γ_{st} in leaves during the growth stage, depending on the capacity of NH_4^+ assimilation. Nitrogen assimilation of soybean primarily occurs during the reproductive stage, and continuous nitrogen assimilation after the initial flowering stage is required for growth (Ohyama, 2017). The amount of nitrogen required for soybean assimilation is larger and is about four times larger than that of rice. Thus, during the soybean growth stage in 20-summer, the nitrogen uptake is probably enhanced rather than the NH_3 emission. Soybean harvesting in the study field started in October 2020, suggesting soybeans

gradually accumulated nitrogen in the seeds in September. Nitrogen redistribution from leaf to seed might have occurred during the seed-filling stage and this might decrease the leaf nitrogen concentration (Zhao et al., 2014). The decrease in the NH_4^+ concentration of bulk tissue (Table 4-5) might reflect this nitrogen redistribution.

I compared the NH_3 flux determined from REA with that inferred from the bi-directional exchange model after I revised the parameters based on the above considerations (Fig. 4-10). The Γ_g was set at 582 in 20-summer and 0 in 21-winter. The Γ_{st} was set at 0 in 20-summer. Furthermore, the parameters presented by Baldocchi et al. (1987) for soybean were used for calculating R_{st}; the minimum stomatal resistance ($r_{\mathrm{st\ min}}$) was set at 65, and the empirical light response constant for stomatal resistance (b_{rs}) was set at 10. The inferred flux after revising the parameters was between −0.042 and −0.001 μg m^{-2} s^{-1}, indicating that only NH_3 deposition was estimated contrary to the flux before revising the parameters. Although the tendency of estimated flux was similar to the measured flux, the magnitude was much smaller. Even I assumed a slight emission from soil and plants, the flux level was not reproduced. These results implied that there could be other processes enhancing NH_3 deposition. For example, in the presence of sufficient gaseous or particulate acids (e.g., organic acids) in the canopy or above the soil, NH_3 might react with them and transform into less volatile form. In addition, the formation of NH_4NO_3 near the surfaces also can be a sink for NH_3. Here, the deposition of NH_3 could be enhanced.

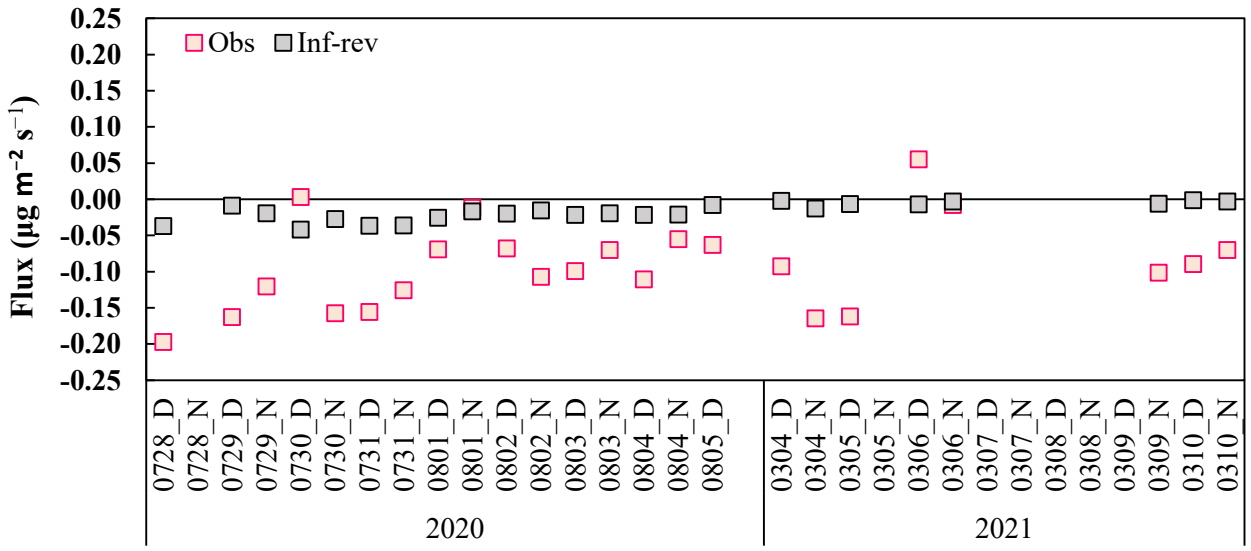

Fig. 4-10. Comparison of the measured NH_3 flux from the REA (Obs) and inferred from the bi-directional exchange model after revising the parameters (Inf-rev). D and N indicate daytime and nighttime, respectively.

The application of N fertilizer is also a vital factor for increasing the Γ_{st} and Γ_g and contributes to the large NH_3 emissions (Flechard et al., 2013). The effect is particularly large when urea or organic manure is contained. In the flux measurements over a maize field in the United States using the REA method, Meyers et al. (2006) reported large NH_3 emissions for a few days after applying urea–ammonium–nitrate (UNA). Walker et al. (2013) also observed a large increase in NH_3 emission flux after applying UNA during the flux measurements over a maize field in the United States using the Bowen-ratio method. However, fertilizer applied to the observation site of this study

contained lower urea, and the fertilizer amount was much lower than those of previous study (Table 4-3). Moreover, both observation periods were further separated in time from the periods of fertilization than previous study. Due to these differences with previous studies, large NH_3 emissions were possibly not observed. Therefore, the fertilizer type and amount as well as the timing of fertilizer application have a large influence on the NH_3 emissions over croplands.

4.3.4 Uncertainties

I estimated the detection limit of ΔC were about 0.50 μg m^{-3} following Section 4.2.2. As a result, about 46% of the total samples were above the detection limit of ΔC and considered as significant. This value was similar to that of Wolff et al. (2010b) for NH_3 (51~54%). The flux for samples with significant ΔC were between −0.197 and −0.101 μg m^{-2} s^{-1}. The median for percentage of flux errors to the measured flux (σ_F/F) was about 57%. Therefore, it can be concluded that the discrepancy between measured and estimated fluxes was not primarily due to the uncertainty in flux measurements. However, more precise and high-resolution flux observation is required for further understanding.

Chapter 5 Attempts to update the bi-directional exchange model

5.1 Introduction

As discussed in **Chapter 4**, the bi-directional exchange model using default input parameters did not reproduce the observation results which mostly indicated NH_3 deposition, but only showed emission. Although the results of the model after revising parameters were improved, the inferred fluxes were still smaller than the measured fluxes even I considered the on-site soil and foliage information. These results suggest that the structure of the model, which is biased towards reproduction of emissions, should be improved. In this study, I verified the applicability of the NH_3 bi-directional exchange model for the FM Tama forest based on observation results in **Chapter 2** and introduce attempts to update the NH_3 bi-directional exchange model for application in East Asia region.

5.2 Methods

To calculate the theoretical NH_3 fluxes, I used the bi-directional exchange model developed by Zhang et al. (2010). The concept of this model was already described in Section 4.2.3. The parameters in the bi-directional exchange model for estimating the NH_3 flux at deciduous broadleaf trees (LUC = 7) are listed in the Table 5-1. I calculated 1-h value of NH_3 using meteorological and other elements recorded at the site.

Table 5-1. Setting of the parameters for bi-directional exchange model based on Zhang et al. (2010).

	Parameter		Unit	15-summer
R_a	z	reference height	m	30
	d	displacement height	m	16
	z_0	roughness length	m	0.8
R_b	Sc	Schmidt number for NH_3		0.75
	Pr	Prandtl number		0.72
R_{st}	$r_{\text{st min}}$	minimum stomatal resistance	s m^{-1}	150
	b_{rs}	empirical light response constant for stomatal resistance	W m^{-2}	43
	T_{min}	minimum temperature for stomatal opening	°C	5
	T_{opt}	optimum temperature for stomatal opening	°C	27
	T_{max}	maximum temperature for stomatal opening	°C	45
	b_{vpd}	water vapour pressure deficit constant	kPa^{-1}	0.36
	Ψ_{c1}	leaf-water-potential dependency	Mpa	−1.9
	Ψ_{c2}	leaf-water-potential dependency	Mpa	−2.5
	D_{NH3}/D_v	the ratio of molecular diffusivity of water vapour to ammonia		0.97
R_{ac}	R_{ac0}(min)	minimum in-canopy aerodynamic resistance	s m^{-1}	100
	R_{ac0}(max)	maximum in-canopy aerodynamic resistance	s m^{-1}	250
R_g	R_{gd} SO_2	dry soil resistance for SO_2	s m^{-1}	200
	R_{gw} SO_2	wet soil resistance for SO_2	s m^{-1}	50
R_{cut}	R_{cutd0} SO_2	dry cuticle resistance for SO_2	s m^{-1}	2500
	R_{cutw0} SO_2	wet cuticle resistance for SO_2	s m^{-1}	50
χ_{st}	Γ_{st}	stomatal emission potential		3000
χ_g	Γ_g	soil emission potentials		2000

5.3 Results & Discussion

Temporal variations of 1-h NH_3 flux inferred from the bi-directional exchange model using default input parameter and of measured daytime and nighttime relative concentration of NH_3 at 23 m against to 30 m during 15-summer are shown in Fig. 5-1. The trends of NH_3 emission were mostly in agreement between model and observation at daytime. However, inferred nighttime mean flux was nearly 0 μg m^{-2} s^{-1} and the model failed to reproduce the nighttime deposition trend of the observation, in contrast to consistent large daytime emission. REA flux measurement for NH_3 at the same site in Jul. 2018 showed the averaged NH_3 fluxes were 0.073 μg m^{-2} s^{-1} in daytime and −0.087 μg m^{-2} s^{-1} in nighttime (Morioka et al., 2020). Even compared to this result, the nighttime deposition flux in the model was considerably smaller.

The value of the emission potential is set to a uniform value regardless of daytime and nighttime in the bi-directional exchange model. At nighttime in the forest, stomata completely close, the intensity of turbulence becomes small, and the Temp decreases. Then, NH_3 emission from the stomata and the soil will be suppressed. Thus, the extremely small nighttime NH_3 flux in the model suggests that the setting of emission potentials in the forest (Γ_{st} = 3000, and Γ_g = 2000) was possibly incorrect as in **Chapter 5**. Therefore, I tested the sensitivity of the inferred NH_3 fluxes to changes in the emission potentials in the model (Fig. 5-2). Contrary to my prediction, lowering the emission potential in the model led to a large decrease in daytime fluxes and had little effect on nighttime fluxes.

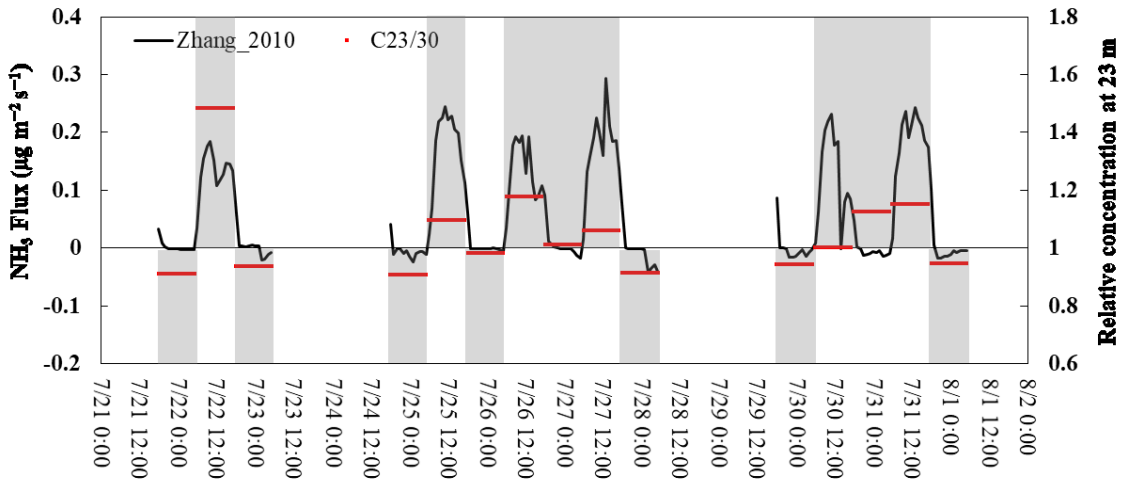

Fig. 5-1. Temporal variations in NH_3 flux inferred from the bi-directional exchange model of Zhang et al. (2010) (black line) and measured relative concentration of NH_3 at 23 m (red line) during 15-summer. The relative concentration is the concentration ratio with respect to the concentration at 30 m. The gray layers indicate the trend of NH_3 emission or deposition based on measurements and concentration higher than 1 implies NH_3 emission.

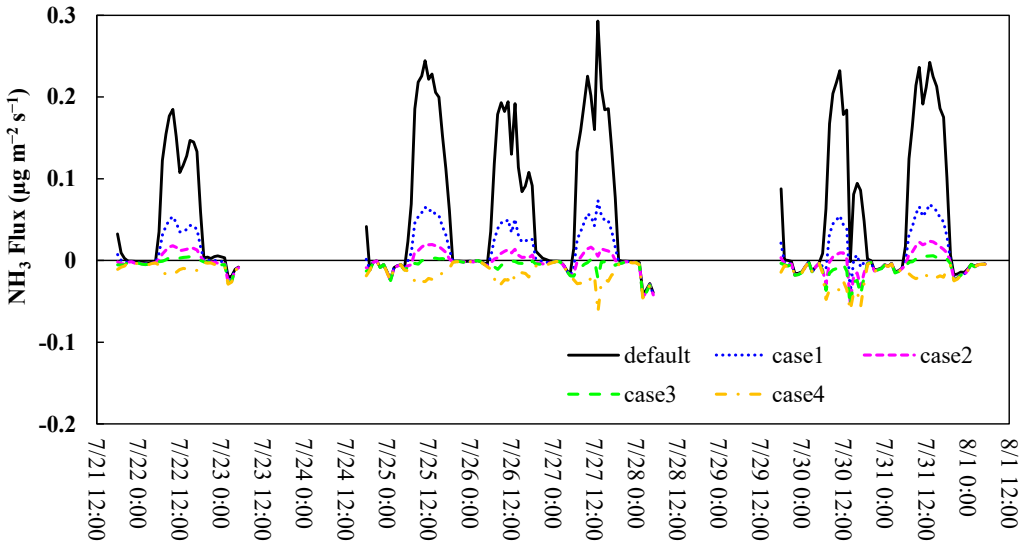

Fig. 5-2. Sensitivity of NH_3 flux inferred from the bi-directional exchange model to changes in stomatal and soil emission potential. Default, case1, case2, case3, and case4 indicate stomatal emission potential was set at 3000, 1000, 500, 300, and 0, and soil emission potential was set at 2000, 1000, 500, 300, and 0, respectively.

As mentioned in Eq. (4-2) and Eq. (4-3), the direction of inferred flux is determined by the magnitude correlation between χ_c and χ_a, and χ_c is calculated from χ_a and each resistance and emission potential in the model. Therefore, I investigated the temporal variations in each resistance and found that the values of R_{st} and R_{ac} were considerably larger than that of the emission potentials (χ_{st} and χ_g) at nighttime in the forest site. Therefore, Eq. (4-3) can be replaced by Eq. (5-1) at nighttime, and the Eq. (5-1) clearly indicates that χ_c is independent of the emission potentials. As the results of sensitivity test of χ_c against to the parameters of Eq. (5-1), χ_c strongly depended on the magnitude of R_{cut} at nighttime. Therefore, the small fluxes at nighttime perhaps due to the large χ_c driven by inappropriate setting of R_{cut}.

$$\chi_c = \left(\frac{\chi_a}{R_a + R_b}\right) \cdot \left(\frac{1}{R_a + R_b} + \frac{1}{R_{cut}}\right)^{-1} \tag{5-1}$$

Then, I compared R_{cut} estimated from the major formulas proposed by Wesely (1989), Sutton et al. (1998), Smith et al. (2000), and Massad et al. (2010) with that estimated from the formula of Zhang et al. (2003) used in this study. The formulas are listed in Table 5-2. It can be seen from Table 5-2 that RH is a main parameter in all equations except Wesley (1989). In Wesley (1989), the R_{cut} is set to be a constant value and is the most primitive of these formulas. Although the formula of Sutton et al. (1998) is a simple function of RH, this is based on laboratory experiments and field measurements which suggest that the removal of NH_3 by leaf cuticular enhances in wet conditions because water films can be a sink for NH_3. The formula of Smith et al. (2000) is developed from that of Sutton et al. (1998) and is used in the resistance model of EANET (EANET, 2010) for estimating NH_3 V_d. Temp is added to the formula from empirical relationship. The formula of Massad et al. (2010) is also developed from that of Sutton et al. (1998). In addition to RH, Massad et al. (2010) focused on the leaf cuticular chemistry and introduced an acid ration (AR) as a new parameter. AR is the ratio of molar concentration of acid gas (SO_2, HNO_3, and hydrogen chloride) to NH_3. This setting is based the concept of "co-deposition", which indicates that R_{cut} decrease with increasing in the ratio of molar concentration of SO_2 to NH_3 in the atmosphere from various measurements (Nemitz, 2015). Moreover, Massad et al. (2010) determined an empirical factor for four surfaces: forests, arable crops, short semi-natural, and grassland from review of previous measurements at these sites. Introducing these parameter makes it possible to calculate the R_{cut} including the on-site information at each site. This approach is much more flexible than that of Sutton et al. (1998), which was derived only from information at a unique site.

Table 5-2. Major formulas for calculating cuticular resistance. r_{lu} is input parameter for cuticular resistance (r_{lu} = 2000), H^* is effective Henry's law constant (H^* = 20000 for NH_3), and f_0 is normalized reactive factor (f_0 = 0 for NH_3), AR is the molar concentration ratio of acid gas (SO_2, HNO_3, and hydrogen chloride) to NH_3, and a is empirical factor (a = 0.0318 ± 0.0179 for forest), respectively.

Reference	Formulas for calculating R_{st}	
Wesely (1989)	$r_{lu} \times (10^{-5}H^* + f_0)^{-1}$	(2-47)
Sutton et al. (1998)	$2e^{(100-RH)/12}$	(2-48)
Smith et l. (2000)	$10^{log(T+2)}e^{(100-\mathrm{RH})/7}\ (T > 0)$	(2-49)
Massad et al. (2010)	$\frac{31.5}{AR} \times e^{a(100-\mathrm{RH})}$ $AR = \frac{2[SO_2] + [HNO_3] + [HCl]}{[NH_3]}$	(2-50)

Temporal variations of R_{cut} calculated from formula of Zhang et al. (2003) (default) and formulas in Table 5-2 during 15-summer are shown in Fig. 5-3. The default values of R_{cut} were in most cases much lower than the values of Smith et al. (2000) and Wesley (1989) and higher than the values of Massad et al. (2010) and Sutton et al. (1998). Relationships between R_{cut} calculated from these formulas and RH are shown in Fig. 5-4. Although the magnitudes of the R_{cut} values were different, Smith et al. (2000), Massad et al. (2010), and Sutton et al. (1998) showed similar variations since RH is the dominant parameter. On the other hand, default values showed a different variation, even though RH was used as a parameter. Relationships between the default values of R_{cut} and RH and u^* at wet and dry conditions are shown in Fig. 5-5. It can be seen that the default values were clearly independent of RH and strongly dependent on u^* regardless of dry and wet conditions. The characteristic of R_{cut} in Zhang et al. (2003) was clearly different from other models described here.

The purpose of this approach is to reproduce the deposition flux at nighttime in the bi-directional exchange model. I considered that this purpose is possibly achieved by using the formulas of Massad et al. (2010) and Sutton et al. (1998), which calculates R_{cut} much less than the default values, instead of Zhang et al. (2003). Temporal variations in 1-h NH_3 flux inferred from the bi-directional exchange model using R_{cut} calculated from Zhang et al. (2003), Sutton et al. (1998), and Massad et al. (2010) during 15-summer are shown in (Fig. 5-6). Although the daytime NH_3 emission became less than the default values, nighttime deposition could be reproduced to some extent, especially when using the formula of Sutton et al. (1998). As mentioned in Section 4.2.3, the formula of Zhang et al. (2003) is not obtained based on the property of NH_3 and R_{cut} for each gaseous substance is calculated based on the R_{cut} of SO_2 and O_3. It is highly possible that the nighttime deposition could not be reproduced in the model using the formula of Zhang et al. (2003) to calculate R_{cut} because the response of NH_3 to RH was not reflected. In order to improve the prediction accuracy of the model, it is possibly necessary to develop a unique formula for R_{cut} based on observations in the East Asian region.

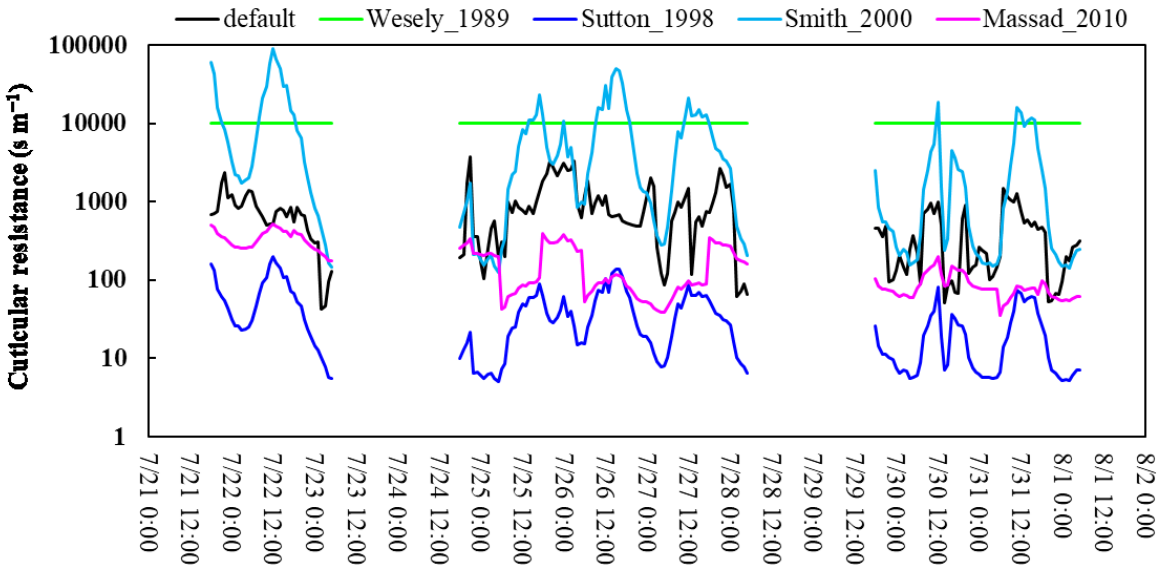

Fig. 5-3. Temporal variations in cuticular resistance calculated from formulars of Zhang et al. (2003) (default), Wesely (1989), Sutton et al. (1998), Smith et al. (2000), and Massad et al. (2010) during 15-summer.

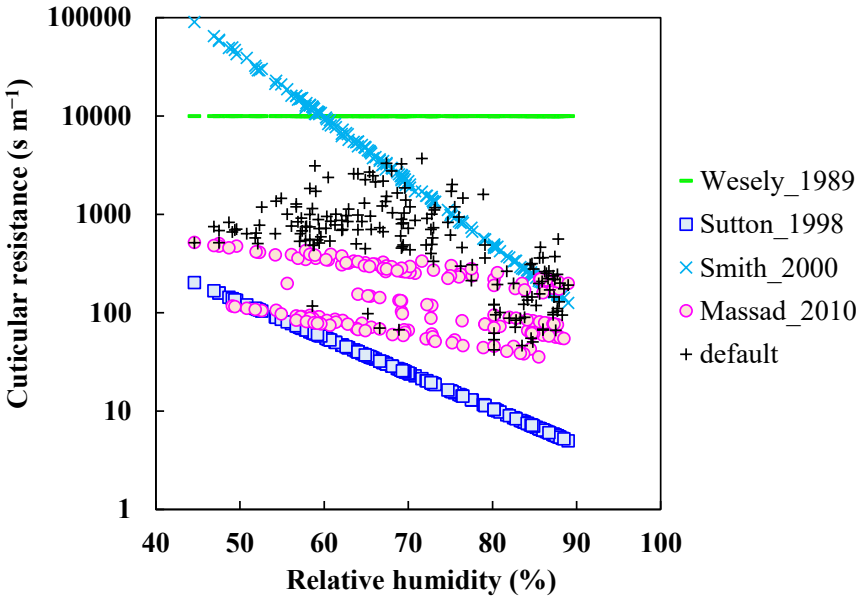

Fig. 5-4. Relationships between each cuticular resistance and relative humidity. Cuticular resistance was calculated from Zhang et al. (2003) (default), Wesely (1989), Sutton et al. (1998), Smith et al. (2000), and Massad et al. (2010), respectively.

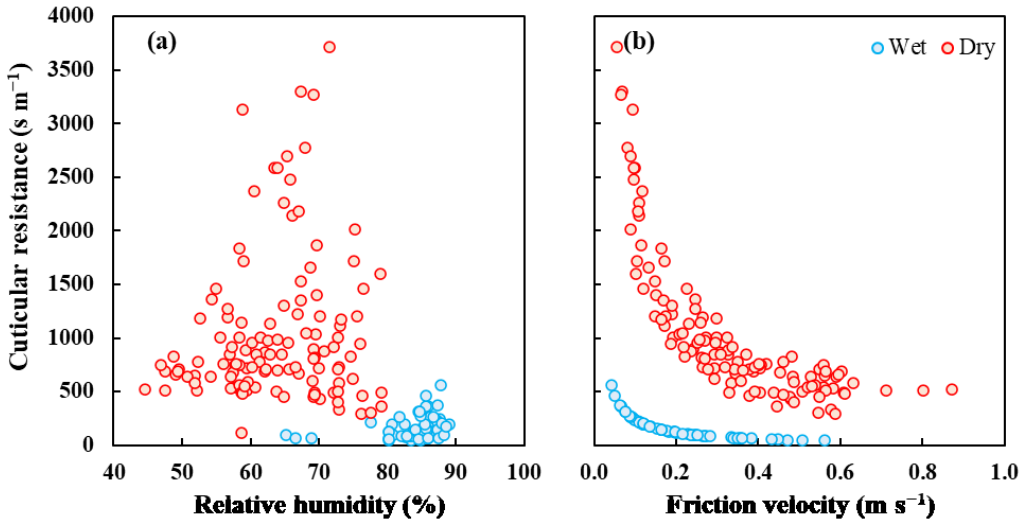

Fig. 5-5. Relationships between cuticular resistance calculated from Zhang et al. (2003) and (a) relative humidity and (b) friction velocity at wet and dry conditions.

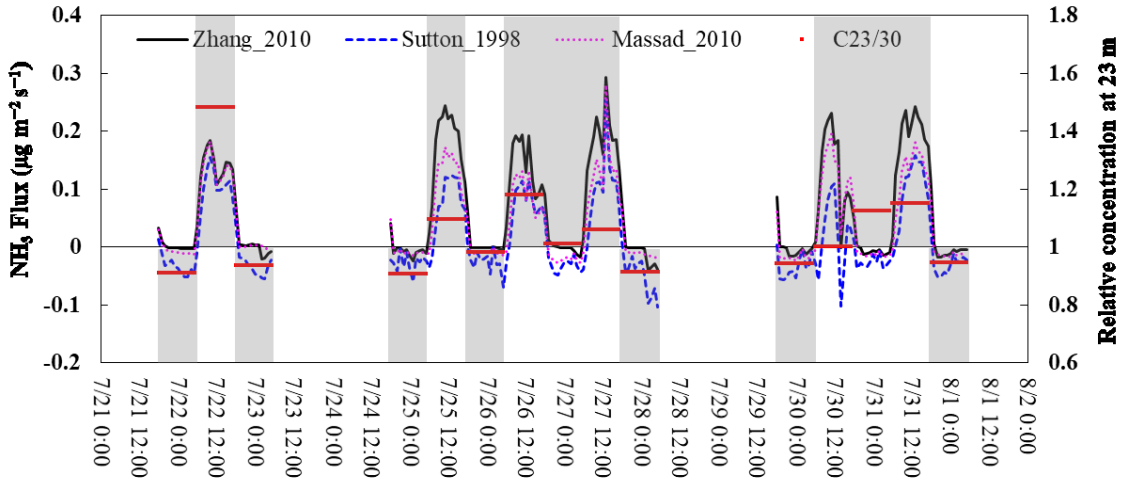

Fig. 5-6. Temporal variations in NH_3 flux inferred from the bi-directional exchange model using cuticular resistance calculated from Zhang et al. (2003), Sutton et al. (1998), and Massad et al. (2010), and measured relative concentration of NH_3 at 23 m (red line) during 15-summer. The relative concentration is the concentration ratio with respect to the concentration at 30 m. The gray layers indicate the trend of NH_3 emission or deposition based on measurements and concentration higher than 1 implies NH_3 emission.

Chapter 6 Conclusions

6.1 Conclusions

- The mechanism of the air−vegetated surface exchanges of NO_3^- and HNO_3 associated with the NH_4NO_3−NH_3−HNO_3 interactions

In order to better understand the mechanisms of the enhancement process of dry deposition of NO_3^- in $PM_{2.5}$ and the emission process of HNO_3 associated with the NH_4NO_3−NH_3−HNO_3 interactions, I conducted vertical profile measurements in a deciduous forest site (FM Tama) in suburban Tokyo, Japan. The observations were performed during the daytime and nighttime during two leafy periods (summer in 2015 and autumn in 2016) and one leafless period (winter in 2016). I also conducted long-term flux measurements using the REA system incorporating the denuder/filter-pack sampling technique and determined the V_d of NO_3^- in $PM_{2.5}$ and HNO_3 during leafy and leafless periods above the forest.

[The enhancement process of dry deposition of NO_3^-]

In the vertical profile measurements, the vertical gradients of NO_3^- concentration in the forest were clearly larger than those of SO_4^{2-} in the same $PM_{2.5}$ during both the daytime and nighttime. The differences were larger especially for the leafy periods. Moreover, the daytime decreasing rate of NO_3^- in the $PM_{2.5}$ below the canopy was sometimes larger than that of SO_2 during the leafy periods. As a result of the long-term REA measurement, the V_d of NO_3^- (median value = 0.71 cm s^{-1}) were not only significantly ($p < 0.05$) larger than those of SO_4^{2-} (median value = −0.01 cm s^{-1}), but also the same level of those of HNO_3 regardless of the leafy and leafless periods.

The large concentration gradients and V_d of NO_3^- in the $PM_{2.5}$ were caused by the equilibrium shift from NH_4NO_3 to NH_3 and HNO_3 near the deposition surfaces. In the daytime, the Temp was higher near the canopy surface during the leafy periods, and near the forest floor during the leafless period. These conditions enhanced the volatilization of NH_4NO_3 near the deposition surfaces in the daytime. Moreover, the lower concentration of HNO_3 near the surfaces caused by its fast removal enhanced the equilibrium during both the daytime and nighttime. Therefore, NO_3^- in the $PM_{2.5}$ was quickly removed in the forest and the removal was larger than those of SO_4^{2-} in the $PM_{2.5}$, even to the point of being equal to those of gaseous substance.

[The emission process of HNO_3]

In the REA flux measurements, the median value of HNO_3 V_d was 0.76 cm s^{-1}, and V_d was high in the leafy period and low in the leafless period. I also obtained many negative values of V_d indicating that some HNO_3 emission occurred. Moreover, the median value of V_d measured by the REA was much lower than that inferred from the resistance model, especially during the leafless periods. The smaller and negative V_d of HNO_3 measured by REA were possibly associated with the equilibrium shift of NH_4NO_3 to NH_3 and HNO_3 near the surface, which enhanced the deposition of NO_3^- and induced suppressed deposition and apparent emission of HNO_3. The equilibrium shift caused the suppressed deposition and apparent emission of HNO_3, particularly in the leafless period due to the high HNO_3 concentration near the surface caused by small removal of the leafless canopy.

- The mechanism of the NH_3 bi-directional exchange and the improvement of the bi-directional exchange model

To investigate the NH_3 bi-directional exchange at East Asia, I conducted vertical profile measurements in the

deciduous forest in FM Tama and flux measurements using REA in an agricultural field in FM Fuchu in west of central Tokyo, Japan. I also evaluated the applicability of the NH_3 bi-directional exchange model in this region by comparing the results of the measurements and inferred fluxes from the model.

From the vertical profile measurements, there were clear seasonal and diurnal variations in the NH_3 exchange in the forest; emission in daytime (summer and winter) and deposition in nighttime (summer, winter, autumn). Inferred NH_3 fluxes using the bi-directional exchange model showed the emission during the daytime in leafy period and agreed with the observation results. However, the model could not reproduce the deposition at nighttime. I improved this discrepancy using some suitable R_{cut}.

In the flux measurements, the NH_3 flux was between −0.197 and 0.055 μg m^{-2} s^{-1} and mostly showed deposition throughout the observation periods, except two cases showed emission. The NH_3 V_d had a visible tendency, which was smaller in summer and larger in winter. Contrary to the measured fluxes, the inferred fluxes using default inputs showed only NH_3 emission. This was probably due to the inappropriate default values of emission potential for crops LUC presented in the literature and input parameters for R_{st}. The inferred fluxes showed deposition after I revised emission potential and R_{st} of the model based on on-site soil and foliage information. However, the inferred fluxes were still smaller than the measured fluxes, suggesting that some unknown processes could enhance NH_3 deposition in the agricultural field.

6.2 Towards the assessment of nitrogen deposition in East Asia including Japan

Each process clarified in this study mentioned above is of great benefit to the East Asia including Japan, where the effects of Nr deposition are of particular concern. However, there are still uncertainties in the Nr exchange process, and many problems remain for accurate assessment of the effects of Nr deposition. Since the NH_4NO_3−NH_3−HNO_3 interactions during dry deposition are not treated in current models for estimating Nr deposition, future studies focused on the quantification of these processes are required to improve the model accuracy. This is one of the key factors that cause large uncertainties in the V_d of these nitrogen compounds. As reviewed in Table 1-1, few observational and model studies targeting these Nr have been conducted in East Asia, except for my group (Yamazaki et al., 2015; Honjo et al., 2016; Sakamoto et al., 2018; Nakahara et al., 2019). In order to achieve the ultimate goal of incorporating these processes into chemical transport models, it is required to accumulate long-term, intensive, and highly accurate observation data at various vegetation in this region.

As my results show, many challenges remain especially for NH_3. The bi-directional exchange of NH_3 is different for each vegetation and also has a temporal variation. Furthermore, the NH_3 sources and sinks are also diverse. Regarding research on NH_3 bi-directional exchange, East Asia is far behind Europe and the United States, and it is necessary to pay particular attention to it in the future. Specifically, it is necessary not only to develop flux observations at various sites, but also actively conduct soil and foliage analysis to determine emission potentials. Further observations should also focus on the chemical reaction of NH_3 with acidic substances near the surface. By developing a unique East Asian model based on these results, the understanding for Nr deposition in the region will be further advanced.

References

Andersen, H.V., Hovmand, M.F., Jensen, N.O. (1993) Measurements of ammonia flux to a spruce stand in Denmark. Atmospheric Environment 27, 189-202, https://doi.org/10.1016/0960-1686(93)90350-8

Andersen, H.V., Hovmand, M.F., Hummelshøj, P., Jensen, N.O. (1999) Measurements of ammonia concentrations, fluxes and dry deposition velocities to a spruce forest 1991–1995. Atmospheric Environment 33, 1367-1383, https://doi.org/10.1016/S1352-2310(98)00363-X

Baldocchi, D.D., Hicks, B.B., Camara, P. (1987) A canopy stomatal resistance model for gaseous deposition to vegetated surfaces. Atmospheric Environment 21, 91-101, https://doi.org/10.1016/0004-6981(87)90274-5

Ban, S., Matsuda, K., Sato, K., Ohizumi, T. (2016) Long-term assessment of nitrogen deposition at remote EANET sites in Japan. Atmospheric Environment 146, 70-78, https://doi.org/10.1016/j.atmosenv.2016.04.015

Bash, J.O., Cooter, E.J., Dennis, R.L., Walker, J.T., Pleim, J.E. (2013) Evaluation of a regional air-quality model with bidirectional NH3 exchange coupled to an agroecosystem model. Biogeosciences 10, 1635-1645, https://doi.org/10.5194/bg-10-1635-2013

Bleeker, A., Hicks, W.K., Dentener, F., Galloway, J., Erisman, J.W. (2011) N deposition as a threat to the World's protected areas under the Convention on Biological Diversity. Environmental Pollution, 159, 2280-2288, https://doi.org/10.1016/j.envpol.2010.10.036

Brost, R.A., Delany, A.C., Huebert, B.J. (1988) Numerical modeling of concentrations and fluxes of HNO_3, NH_3, and NH_4NO_3 near the surface. Journal of Geophysical Research 93, 7137-7152, https://doi.org/10.1029/JD093iD06p07137

Businger, J.A., Oncley, S.P. (1990) Flux measurement with conditional sampling. Journal of Atmospheric and Oceanic Technology 7, 349-352, https://doi.org/10.1175/1520-0426(1990)007%3C0349:FMWCS%3E2.0.CO;2

Duyzer, J. (1994) Dry deposition of ammonia and ammonium aerosols over heathland. Journal of Geophysical Research 99, 18757-18763, https://doi.org/10.1029/94JD01210

EANET (Acid Deposition Monitoring Network in East Asia) (2000) Guidelines for Acid Deposition Monitoring in East Asia. pp. 12-19. https://www.eanet.asia/wp-content/uploads/2019/04/monitorguide.pdf

EANET (Acid Deposition Monitoring Network in East Asia) (2010) Technical Manual for Dry Deposition Flux Estimation in East Asia, pp. 23-26, https://www.eanet.asia/wp-content/uploads/2019/04/techdry.pdf

Endo, T., Yagoh, H., Sato, K., Matsuda, K., Hayashi, K., Noguchi, I., Sawada, K. (2011) Regional characteristics of dry deposition of sulfur and nitrogen compounds at EANET sites in Japan from 2003 to 2008. Atmospheric Environment 45, 1259-1267

Erisman, J.W., Draaijers, G.P.J. (1995) Atmospheric deposition in relation to acidification and eutrophication. Studies in Environmental Research, vol. 63. Elsevier, The Netherlands, pp.55-75, pp.85-97, https://doi.org/10.1016/S0166-1116(06)80335-3

Erisman, J.W., Wyers, G.P. (1993) Continuous measurements of surface exchange of SO_2 and NH_3; Implications for their possible interaction in the deposition process. Atmospheric Environment 27, 1937-1949, https://doi.org/10.1016/0960-1686(93)90266-2

Erisman, J.W., Beier, C., Draaijers, G., Lindberg, S. (1994) Review of deposition monitoring methods. Tellus B: Chemical and Physical Meteorology 46, 79-93, https://doi.org/10.3402/tellusb.v46i2.15754

Erisman, J.W., Galloway, J.N., Seitzinger, S., Bleeker, A., Dise, N.B., Petrescu, A.M.R., Leach, A.M., de Vries, W. (2013) Consequences of human modification of the global nitrogen cycle. Philosophical Transactions of the Royal Society B 368, 20130116, https://doi.org/10.1098/rstb.2013.0116

Farmer, D. K., Wooldridge, P. J., Cohen, R. C. (2006) Application of thermal-dissociation laser induced fluorescence (TD-LIF) to measurement of HNO3, Σalkyl nitrates, Σperoxy nitrates, and NO2 fluxes using eddy covariance. Atmospheric Chemistry and Physics 6, 3471–3486, https://doi.org/10.5194/acp-6-3471-2006

Farquhar, G.D., Firth, P.M., Wetselaar, R., Weir, B. (1980) On the Gaseous Exchange of Ammonia between Leaves and the Environment: Determination of the Ammonia Compensation Point. Plant Physiology 66, 710–714, https://doi.org/10.1104/pp.66.4.710

Flechard, C.R., Fowler, D. (1998) Atmospheric ammonia at a moorland site. II: Long-term surface-atmosphere micrometeorological flux measurements. Quarterly Journal of the Royal Meteorological Society 124, 759-791, https://doi.org/10.1002/qj.49712454706

Flechard, C.R., Nemitz, E. Smith, R.I., Fowler, D., Vermeulen, A.T., Bleeker, A., Erisman, J.W., Simpson, D., Zhang, L., Tang, Y.S., Sutton, M.A. (2011) Dry deposition of reactive nitrogen to European ecosystems: a comparison of inferential models across the NitroEurope network. Atmospheric Chemistry and Physics 11, 2703-2728, https://doi.org/10.5194/acp-11-2703-2011

Flechard, C.R., Massad, R.-S., Loubet, B., Personne, E., Simpson, D., Bash, J.O., Cooter, E.J., Nemitz, E., Sutton, M.A. (2013) Advances in understanding, models and parameterizations of biosphere-atmosphere ammonia exchange. Biogeosciences 10, 5183-5225, https://doi.org/10.5194/bg-10-5183-2013

Fowler, D., Pilegaard, K., Sutton, M.A., Ambus, P., Raivonen, M., Duyzer, J., Simpson, D., Fagerli, H., Fuzzi, S., Schjoerring, J.K., Granier, C., Neftel, A., Isaksen, I.S.A., Laj, P., Maione, M., Monks, P.S., Burkhardt, J., Daemmgen, U., Neirynck, J., Personne, E., Wichink-Kruit, R., Butterbach-Bahl, K., Flechard, C., Tuovinen, J.P., Coyle, M., Gerosa, G., Loubet, B., Altimir, N., Gruenhage, L., Ammann, C., Cieslik, S., Paoletti, E., Mikkelsen, T.N., Ro-Poulsen, H., Cellier, P., Cape, J.N., Horváth, L., Loreto, F., Niinemets, Ü., Palmer, P.I., Rinne, J., Misztal, P., Nemitz, E., Nilsson, D., Pryor, S., Gallagher, M.W., Vesala, T., Skiba, U., Brüggemann, N., Zechmeister-Boltenstern, S., Williams, J., O'Dowd, C., Facchini, M.C., de Leeuw, G., Flossman, A., Chaumerliac, N., Erisman, J.W. (2009) Atmospheric composition change: Ecosystems–Atmosphere interactions. Atmospheric Environment 43, 5193-5267, https://doi.org/10.1016/j.atmosenv.2009.07.068

Fowler, D., Coyle, M., Skiba, U., Sutton, M.A., Cape, J.N., Reis, S., Sheppard, L.J., Jenkins, A., Grizzetti, B., Galloway, J.N., Vitousek, P., Leach, A., Bouwman, A.F., Butterbach-Bahl, K., Dentener, F., Stevenson, D., Amann, M., Voss, M. (2013) The global nitrogen cycle in the twenty-first century. Philosophical Transactions of the Royal Society B 368, 20130164, https://doi.org/10.1098/rstb.2013.0164

Fowler, D., Brimblecombe, P., Burrows, J., Heal, M.R., Grennfelt, P., Stevenson, D.S., Jowett, A., Nemitz, E., Coyle, M., Lui, X., Chang, Y., Fuller, G.W., Sutton, M.A., Klimont, Z., Unsworth, M.H., Vieno, M. (2020) A chronology of global air quality. Philosophical Transactions of the Royal Society A 378, 20190314, https://doi.org/10.1098/rsta.2019.0314

Fueki, N., Sawamoto, T., Higashida, S., Nakatsu, S. (2006) Factors affecting nitrification in arable soils in Hokkaido, Japan. Influence of applied nitrogen concentration, form of nitrogen source, soil pH and soil organic matter. Japanese Society of Pedology 50, 81–90, https://doi.org/10.18920/pedologist.50.2_81

Gallagher, M.W., Beswick, K.M., Duyzer, J., Westrate, H., Choularton, T.W., Hummelshøj, P. (1997) Measurements of aerosol fluxes to speulder forest using a micrometeorological technique. Atmospheric Environment 31, 359-373, https://doi.org/10.1016/S1352-2310(96)00057-X

Galloway, J.N. (1998) The global nitrogen cycle: changes and consequences. Environmental Pollution 102, 15-24, https://doi.org/10.1016/S0269-7491(98)80010-9

Galloway, J.N., Cowling, E.B. (2002) Reactive Nitrogen and The World: 200 Years of Change. AMBIO: A Journal of the Human Environment 31, 64-71, https://doi.org/10.1579/0044-7447-31.2.64

Galloway, J.N., Aber, J.D., Erisman, J.W., Seitzinger, S.P., Howarth, R.W., Cowling, E.B., Cosby, B.J. (2003) The Nitrogen Cascade. BioScience 53, 341–356, https://doi.org/10.1641/0006-3568(2003)053[0341:TNC]2.0.CO;2

Galloway, J.N., Leach, A.M., Bleeker, A., Erisman, J.W. (2013) A chronology of human understanding of the nitrogen cycle. Philosophical Transactions of the Royal Society B 368, 20130120, http://doi.org/10.1098/rstb.2013.0120

Gruber, N., Galloway, J.N. (2008) An Earth-system perspective of the global nitrogen cycle. Nature 451, 293–296, https://doi.org/10.1038/nature06592

Hansen, K., Pryor, S.C., Boegh, E., Hornsby, K.E., Sørensen, L.L. (2015) Background concentrations and fluxes of atmospheric ammonia over a deciduous forest. Agricultural and Forest Meteorology 214–215, 380-392, https://doi.org/10.1016/j.agrformet.2015.09.004

Harrison, R.M., Rapsomanikis, S., Turnbull, A. (1989) Land-surface exchange in a chemically-reactive system; surface fluxes of HNO3, HCl and NH3. Atmospheric Environment 23, 1795-1800, https://doi.org/10.1016/0004-6981(89)90062-0

Hayashi, K., Komada, M., Miyata, A. (2007) Atmospheric Deposition of Reactive Nitrogen on Turf Grassland in Central Japan: Comparison of the Contribution of Wet and Dry Deposition. Water, Air, & Soil Pollution: Focus 7, 119–129, https://doi.org/10.1007/978-1-4020-5885-1_14

Hayashi, K., Hayakawa, A., Akiyama, H., Yagi, K. (2009) Measurement of ammonia volatilization loss using a dynamic chamber technique: A case study of surface-incorporated manure and ammonium sulfate at an upland field of light-colored Andosol. Soil Science and Plant Nutrition 55, 571-581, https://doi.org/10.1111/j.1747-0765.2009.00392.x

Hayashi, K., Ono, K., Tokida, T., Takimoto, T., Mano, M., Miyata, A., Matsuda, K. (2012) Atmosphere-rice paddy exchanges of inorganic particles and relevant gases during a week in winter and a week in summer. Journal of Agricultural Meteorology 68, 55-68, https://doi.org/10.2480/agrmet.68.1.8

Hayashi, K., Ono, K., Matsuda, K., Tokida, T., Hasegawa, T. (2017) Characteristics of atmosphere-rice paddy exchange of gaseous and particulate reactive nitrogen in terms of nitrogen input to a single-cropping rice paddy area in central Japan. Asian Journal of Atmospheric Environment 11, 202-216, https://doi.org/10.5572/ajae.2017.11.3.202

Hicks, B.B., Baldocchi, D.D., Meyers, T.P., Hosker Jr., R.P., Matt, D.R. (1987) A preliminary multiple resistance routine for deriving dry deposition velocities from measured quantities. Water, Air, & Soil Pollution 36, 311-330, https://doi.org/10.1007/BF00229675

Hole, L.R., Brunner, S.H., Hanssen, J.E., Zhang, L. (2008) Low cost measurements of nitrogen and sulphur dry deposition velocities at a semi-alpine site: Gradient measurements and a comparison with deposition model estimates. Environmental Pollution 154, https://doi.org/10.1016/j.envpol.2007.06.061

Honjo, T., Takahashi, A., Matsuda, K. (2016) Deposition velocity of sulfate and nitrate in $PM_{2.5}$ above a forest in suburban Tokyo using relaxed eddy accumulation. Journal of Japan Society for Atmospheric Environment 51, 257-265 (in Japanese), https://doi.org/10.11298/taiki.51.257

Horváth, l., Asztalos, M., Führer, E., Mészáros, R., Weidinger, T. (2005) Measurement of ammonia exchange over grassland in the Hungarian Great Plain. Agricultural and Forest Meteorology 130, 282-298, https://doi.org/10.1016/j.agrformet.2005.04.005

Huebert, B.J., Robert, C.H. (1985) The dry deposition of nitric acid to grass. Journal of Geophysical Research 90, 2085-2090, https://doi.org/10.1029/JD090iD01p02085

Huebert, B.J., Luke, W.T., Delany, A.C., Brost, R.A. (1988) Measurements of concentrations and dry surface fluxes of atmospheric nitrates in the presence of ammonia. Journal of Geophysical Research 93, 7127-7136, https://doi.org/10.1029/JD093iD06p07127

Kamii, Y., Chikamori, K., Maruyama, T. (1996) Estimation of diffuse solar radiation from hourly global radiation. Transactions of the Japanese Society of Irrigation, Drainage and Reclamation Engineering 183, 41-46 (in Japanese), https://doi.org/10.11408/jsidre1965.1996.395

Katata, G., Hayashi, K., Ono, K., Nagai, H., Miyata, A., Mano, M. (2013) Coupling atmospheric ammonia exchange process over a rice paddy field with a multi-layer atmosphere-soil-vegetation model. Agricultural and Forest Meteorology 180, 1-21, https://doi.org/10.1016/j.agrformet.2013.05.001

Katata, G., Matsuda, K., Sorimachi, A., Kajino, M., Takagi, K. (2020) Effects of aerosol dynamics and gas–particle conversion on dry deposition of inorganic reactive nitrogen in a temperate forest. Atmospheric Chemistry and Physics 20, 4933–4949, https://doi.org/10.5194/acp-20-4933-2020

Khoomsab, K., Khummongkol, P. (2013) The Relaxed Eddy Accumulation for Estimating Aerosols Dry Deposition above Tropical Forest. Journal of Atmospheric Pollution 1, 1-4, DOI: 10.12691/jap-1-1-1

Kruit, R.J.R.W., van Pul, W.A.J., Otjes, R.P., Hofschreuder, P., Jacobs, A.F.G., Holtslag, A.A.M. (2007) Ammonia fluxes and derived canopy compensation points over non-fertilized agricultural grassland in The Netherlands using the new gradient ammonia—high accuracy—monitor (GRAHAM). Atmospheric Environment 41, 1275-1287, https://doi.org/10.1016/j.atmosenv.2006.09.039

Kurokawa, J., Ohara, T. (2020) Long-term historical trends in air pollutant emissions in Asia: Regional Emission inventory in ASia (REAS) version 3. Atmospheric Chemistry and Physics 20, 12761-12793, https://doi.org/10.5194/acp-20-12761-2020

Massad, R.-S., Nemitz, E., Sutton, M.A. (2010) Review and parameterisation of bi-directional ammonia exchange between vegetation and the atmosphere. Atmospheric ChemisAtmospheric Chemistry and Physics 10, 10359-10386, https://doi.org/10.5194/acp-10-10359-2010

Matsuda, K., Watanabe, I., Mizukami, K., Ban, S., Takahashi, A. (2015) Dry deposition of $PM_{2.5}$ sulfate above a hilly forest using relaxed eddy accumulation. Atmospheric Environment 107, 255-261, https://doi.org/10.1016/j.atmosenv.2015.02.050

Mattsson, M., Herrmann, B., David, M., Loubet, B., Riedo, M., Theobald, M.R., Sutton, M.A., Bruhn, D., Neftel, A., Schjoerring, J.K. (2009) Temporal variability in bioassays of the stomatal ammonia compensation point in relation to plant and soil nitrogen parameters in intensively managed grassland. Biogeosciences 6, 171-179, https://doi.org/10.5194/bg-6-171-2009

Meyers, T.P., Luke, W.T., Meisinger, J.J. (2006) Fluxes of ammonia and sulfate over maize using relaxed eddy accumulation. Agricultural and Forest Meteorology 136, 203-213, https://doi.org/10.1016/j.agrformet.2004.10.005

Milford, C., Hargreaves, K.J., Sutton, M.A., Loubet, B., Cellier, P. (2001a) Fluxes of NH_3 and CO_2 over upland moorland in the vicinity of agricultural land. Journal of Geophysical Research 106, 24169-24181, https://doi.org/10.1029/2001JD900082

Milford, C., Theobald, M.R., Nemitz, E., Sutton, M.A. (2001b) Dynamics of Ammonia Exchange in Response to Cutting and Fertilising in an Intensively-Managed Grassland. Water, Air and Soil Pollution: Focus 1, 167–176, https://doi.org/10.1023/A:1013142802662

Milne, R., Beverland, I.J., Hargreaves, K., Moncrieff, J.B. (1999) Variation of the β coefficient in the relaxed eddy accumulation method. Boundary-Layer Meteorology 93, 211-225, https://doi.org/10.1023/A:1002061514948

Morioka, T., Sorimachi, A., Sase, H., Matsuda, K. (2020) Ammonia exchange flux above a forest in suburban Tokyo using relaxed eddy accumulation, Proceedings of 61th JSAE annual meeting, 227.

MÜller, H., Kramm, G., Meixner, F., Dollard, G.J., Fowler, D., Possanzini, M. (1993) Determination of HNO_3 dry deposition by modified Bowen ratio and aerodynamic profile techniques, Tellus B: Chemical and Physical Meteorology 45, 346-367, https://doi.org/10.3402/tellusb.v45i4.15735

Myles, L., Meyers, T.P., Robinson, l. (2007) Relaxed eddy accumulation measurements of ammonia, nitric acid, sulfur dioxide and particulate sulfate dry deposition near Tampa, FL, USA. Environmental Research Letters 2, 034004, https://doi.org/10.1088/1748-9326/2/3/034004

Myles, L., Kochendorfer, J., Heuer, M.W., Meyers, T.P. (2011) Measurement of trace gas fluxes over an unfertilized agricultural field using the flux-gradient technique. Journal of Environmental Quality 40, 1359-1365, https://doi.org/10.2134/jeq2009.0386

Nakahara, A., Takagi, K., Sorimachi, A., Katata, G., Matsuda, K. (2019) Enhancement of dry deposition of PM2.5 nitrate in a cool-temperate forest. Atmospheric Environment 212, 136–141, https://doi.org/10.1016/j.atmosenv.2019.05.053

Neftel, F., Blatter, A., Hesterberg, R., Staffelbach, T. (1996) Measurements of concentration gradients of HNO_2 and HNO_3 over a semi-natural ecosystem. Atmospheric Environment 30, 3017-3025, https://doi.org/10.1016/1352-2310(96)00011-8

Neirynck, J., Kowalski, A.S., Carrara, A., Ceulemans, R. (2005) Driving forces for ammonia fluxes over mixed forest subjected to high deposition loads. Atmospheric Environment 39, 5013-5024, https://doi.org/10.1016/j.atmosenv.2005.05.027

Nelson, A.J., Koloutsou-Vakakis, S., Rood, M.J., Myles, L., Lehmann, C., Bernacchi, C., CBalasubramanian, S., Joo, E. Heuer, M., Vieira-Filho, M., Lin, J. (2017) Season-long ammonia flux measurements above fertilized corn in central Illinois, USA, using relaxed eddy accumulation. Agricultural and Forest Meteorology 239, 202-212, https://doi.org/10.1016/j.agrformet.2017.03.010

Nelson, A.J., Lichiheb, N., Koloutsou-Vakakis, S., Rood, M.J., Heuer, M., Myles, L., Joo, E., Miller, J., Bernacchi, C. (2019) Ammonia flux measurements above a corn canopy using relaxed eddy accumulation and a flux gradient system. Agricultural and Forest Meteorology 264, 104-113, https://doi.org/10.1016/j.agrformet.2018.10.003

Nemitz, E. (2015) Surface/atmosphere Exchange of Atmospheric Acids and Aerosols, Including the Effect and Model Treatment of Chemical Interactions. Review and Integration of Biosphere-Atmosphere Modelling of Reactive Trace Gases and Volatile Aerosols. Springer, The Netherlands, pp. 115–149, https://doi.org/10.1007/978-94-017-7285-3_5

Nemitz, E., Sutton, M.A., Wyers, G.P., Otjes, R.P., Schjoerring, J.K., Gallagher, M.W., Parrington, J., Fowler, D., Choularton, T.W. (2000) Surface/atmosphere exchange and chemical interaction of gases and aerosols over oilseed rape. Agricultural and Forest Meteorology 105, 427-445, https://doi.org/10.1016/S0168-1923(00)00207-0

Nemitz, E., Milford, C., Sutton, M.A. (2001) A two-layer canopy compensation point model for describing bi-directional biosphere-atmosphere exchange of ammonia. Quarterly Journal of the Royal Meteorological Society 127, 815-833, https://doi.org/10.1002/qj.49712757306

Nemitz, E., Sutton, M.A., Wyers, G.P., Jongejan, P. A. C. (2004a) Gas-particle interactions above a Dutch heathland: I. Surface exchange fluxes of NH_3, SO_2, HNO_3 and HCl. Atmospheric Chemistry and Physics 4, 989–1005, https://doi.org/10.5194/acp-4-989-2004

Nemitz, E., Sutton, M.A., Wyers, G.P., Otjes, R.P., Mennen, M.G., van Putten, E.M., Gallagher, M.W. (2004b) Gas-particle interactions above a Dutch heathland: Ⅱ. Concentrations and surface exchange fluxes of atmospheric particles. Atmospheric Chemistry and Physics 4, 1007-1024, https://doi.org/10.5194/acp-4-1007-2004

Ohyama, T., Tewari, K., Ishikawa, S., Tanaka, K., Kamiyama, S., Ono, Y., Hatano, S., Ohtake, N., Sueyoshi, K., Hasegawa, H., Sato, T., Tanabata, S., Nagumo, Y., Fujita, Y., Takahashi, Y. (2017). Role of Nitrogen on Growth and Seed Yield of Soybean and a New Fertilization Technique to Promote Nitrogen Fixation and Seed Yield. Soybean - The Basis of Yield, Biomass and Productivity. IntechOpen, London, https://doi.org/10.5772/66743

Personne, E., Tardy, F., Génermont, S., Decuq, C., Gueudet, J.C., Mascher, N., Durand, B., Masson, S., Lauransot, M., Fléchard, C., Burkhardt, J., Loubet, B. (2015) Investigating sources and sinks for ammonia exchanges between the atmosphere and a wheat canopy following slurry application with trailing hose. Agricultural and Forest Meteorology 207, 11-23, https://doi.org/10.1016/j.agrformet.2015.03.002

Petroff, A., Mailliat, A., Amielh, M., Anselmet, F. (2008) Aerosol dry deposition on vegetative canopies. Part I: Review of present knowledge. Atmospheric Environment 42, 3625-3653, https://doi.org/10.1016/j.atmosenv.2007.09.043

Phillips, S.B., Pal Arya, S., Aneja, V.P. (2004) Ammonia flux and dry deposition velocity from near-surface concentration gradient measurements over a grass surface in North Carolina. Atmospheric Environment 38, 3469-3480, https://doi.org/10.1016/j.atmosenv.2004.02.054

Pryor, S.C., Klemm, O. (2004) Experimentally derived estimates of nitric acid dry deposition velocity and viscous sub-layer resistance at a conifer forest. Atmospheric Environment 38, 2769-2777, https://doi.org/10.1016/j.atmosenv.2004.02.038

Pryor, S.C., Barthelmie, R.J., Jensen, B., Jensen, N.O., Sørensen, L.L. (2002) HNO_3 fluxes to a deciduous forest derived using gradient and REA methods. Atmospheric Environment 36, 5993-5999, https://doi.org/10.1016/S1352-2310(02)00765-3

Pryor, S.C., Gallagher, M., Sievering, H., Larsen, S.E., Barthelmie, R.J., Birsan, F., Nemitz, E., Rinne, J., Kulmala, M., Grönholm, T., Taipale, R., Vesala, T. (2008) A review of measurement and modelling results of particle atmosphere–surface exchange. Tellus B: Chemical and Physical Meteorology 60, 42-75, https://doi.org/10.1111/j.1600-0889.2007.00298.x

Rattray, G., Sievering, H. (2001) Dry deposition of ammonia, nitric acid, ammonium, and nitrate to alpine tundra at Niwot Ridge, Colorado. Atmospheric Environment 35, 1105-1109, https://doi.org/10.1016/S1352-2310(00)00276-4

Sakamoto, T., Nakahara, A., Takahashi, A., Sorimachi, A., Katata, G., Matsuda, K. (2018) Deposition velocity of $PM_{2.5}$ nitrate and gaseous nitric acid above a forest in suburban Tokyo using relaxed eddy accumulation with denuder sampling technique. Journal of Japan Society for Atmospheric Environment 53, 136–143 (in Japanese), https://doi.org/10.11298/taiki.53.136

Saylor, R.D., Baker, B.D., Lee, P., Tong, D., Pan, L., Hicks, B.B. (2019) The particle dry deposition component of total deposition from air quality models: right, wrong or uncertain?. Tellus B: Chemical and Physical Meteorolog 71, 1550324, https://doi.org/10.1080/16000889.2018.1550324

Schwede, D., Zhang, L., Vet, R., Lear, G. (2011) An intercomparison of the deposition models used in the CASTNET and CAPMoN networks. Atmospheric Environment 45, 1337-1346, https://doi.org/10.1016/j.atmosenv.2010.11.050

Seinfeld, J.H., Pandis, S.N. (2006). Atmospheric Chemistry and Physics: From Air Pollution to Climate Change, second edition. Wiley-Interscience, USA, pp. 900-931.

Shimadera, H., Hayami, H., Chatani, S., Morino, Y., Mori, Y., Morikawa, T., Yamaji, K., Ohara, T. (2014) Sensitivity analyses of factors influencing CMAQ performance for fine particulate nitrate. Journal of the Air & Waste Management Association 64, 374-387, https://doi.org/10.1080/10962247.2013.778919

Sievering, H., Enders, G., Kins, L., Kramm, G., Ruoss, K., Roider, G., Zelger, M., Anderson, L., Dlugi, R. (1994) Nitric acid, particulate nitrate and ammonium profiles at the bayerischer wald: evidence for large deposition rates of total nitrate. Atmospheric Environment 28, 311-315, https://doi.org/10.1016/1352-2310(94)90106-6

Sievering, H., Kelly, T., McConville, G., Seibold, C., Turnipseed, A. (2001) Nitric acid dry deposition to conifer forests:: Niwot Ridge spruce–fir–pine study. Atmospheric Environment 35, 3851-3859, https://doi.org/10.1016/S1352-2310(01)00156-X

Sintermann, J., Spirig, C., Jordan, A., Kuhn, U., Ammann, C., Neftel, A. (2011) Eddy covariance flux measurements of ammonia by high temperature chemical ionisation mass spectrometry. Atmospheric Measurement Techniques 4, 599–616, https://doi.org/10.5194/amt-4-599-2011

Smith, R.I., Fowler, D., Sutton, M.A., Flechard, C., Coyle, M. (2000) Regional estimation of pollutant gas dry deposition in the UK: model description, sensitivity analyses and outputs. Atmospheric Environment 34, 3757-3777, https://doi.org/10.1016/S1352-2310(99)00517-8

Spindler, G., Teichmann, U., Sutton, M.A. (2001) Ammonia dry deposition over grassland-micrometeorological flux-gradient measurements and bidirectional flux calculations using an inferential model. Quarterly Journal of the Royal Meteorological Society 127, 795-814, https://doi.org/10.1002/qj.49712757305

Sutton M.A., Schjørring J.K., Wyers G.P. (19959 Plant—atmosphere exchange of ammonia. Philosophical Transactions of the Royal Society A 351, 261–278, http://doi.org/10.1098/rsta.1995.0033

Sutton, M.A., Burkhardt, J.K., Guerin, D., Nemitz, E., Fowler, D. (1998) Development of resistance models to describe measurements of bi-directional ammonia surface-atmosphere exchange. Atmospheric Environment 32, 473-480, https://doi.org/10.1016/S1352-2310(97)00164-7

Sutton, M.A., Nemitz, E., Milford, C., Fowler, D., Moreno, J., José, R.S., Wyers, G.P., Otjes, R.P., Harrison, R., Husted, S., Schjoerring, J.K. (2000) Micrometeorological measurements of net ammonia fluxes over oilseed rape during two vegetation periods. Agricultural and Forest Meteorology 105, 351-369, https://doi.org/10.1016/S0168-1923(00)00203-3

Sutton, M.A, Oenema, O., Erisman, J.W., Leip, A., van Grinsven, H., Winiwarter, W. (2011) Too much of a good thing. Nature 472, 159–161, https://doi.org/10.1038/472159a

Sutton, M.A., van Dijk, N., Levy, P.E., Jones, M.R., Leith, I.D., Sheppard, L.J., Leeson, S., Sim Tang, Y., Stephenss, A., Braban, C.F., Dragosits, U., Howard, C.M., Vieno, M., Fowler, D., Corbett, P., Naikoo, M.I., Munzi, S., Ellis, C.J., Chatterjee, S., Steadman, C.E., Móring, A., Wolseley, P.A. (2020) Alkaline air: changing perspective on nitrogen and air pollution in an ammonia-rich world. Philosophical Transactions of the Royal Society A 378, 20190315, https://doi.org/10.1098/rsta.2019.0315

Takahashi, A., Wakamatsu, T. (2004) Estimation of deposition velocity of particles to a forest using the concentration gradient method. Journal of Japan Society for Atmospheric Environment 39, 53-61 (in Japanese), https://doi.org/10.11298/taiki1995.39.53

Twigg, M.M., House, E., Thomas, R., Whitehead, J., Phillips, G.J., Famulari, D., Fowler, D., Gallagher, M.W., Cape, J.N., Sutton, M.A., Nemitz, E. (2011) Surface/atmosphere exchange and chemical interactions of reactive nitrogen compounds above a manured grassland. Agricultural and Forest Meteorology 151, 1488-1503, https://doi.org/10.1016/j.agrformet.2011.06.005

Van Oss, R., Duyzer, J., Wyers, P. (1998) The influence of gas-to-particle conversion on measurements of ammonia exchange over forest. Atmospheric Environment 32, 465-471, https://doi.org/10.1016/S1352-2310(97)00280-X

Vet, R., Artz, R.S., Carou, S., Shaw, M., Ro, C., Aas, W., Baker, A., Bowersox, V.C., Dentener, F., Galy-Lacaux, C., Hou, A., Pienaar, J.J., Gillett, R., Forti, M.C., Gromov, S., Hara, H., Khodzher, T., Mahowald, N.M., Nickovic, S., Rao, P.S.P., Reid, N.W. (2014) A global assessment of precipitation chemistry and deposition of sulfur, nitrogen, sea salt, base cations, organic acids, acidity and pH, and phosphorus. Atmospheric Environment 93, 3-100, https://doi.org/10.1016/j.atmosenv.2013.10.060

Walker, J.T., Robarge, W.P., Wu, Y., Meyers, T.P. (2006) Measurement of bi-directional ammonia fluxes over soybean using the modified Bowen-ratio technique. Agricultural and Forest Meteorology 138, 54-68, https://doi.org/10.1016/j.agrformet.2006.03.011

Walker, J.T., Jones, M.R., Bash, J.O., Myles, L., Meyers, T.P., Schwede, D., Herrick, J., Nemitz, E., Robarge, W. (2013) Processes of ammonia air-surface exchange in a fertilized Zea mays canopy. Biogeosciences 10, 981-998, https://doi.org/10.5194/bg-10-981-2013

Walker, J.T., Beachley, G., Amos, H.M., Baron, J.S., Bash, J., Baumgardner, R., Bell, M.D., Benedict, K.B., Chen, X., Clow, D.W., Cole, A., Coughlin, J.G., Cruz, K., Daly, R.W., Decina, S.M., Elliott, E.M., Fenn, M.E., Ganzeveld, L., Gebhart, K., Isil, S.S., Kerschner, B.M., Larson, R.S., Lavery, T., Lear, G.G., Macy, T., Mast, M.A., Mishoe, K., Morris, K.H., Padgett, P.E., Pouyat, R.V., Puchalski, M., Pye, H.O.T., Rea, A.W., Rhodes, M.F., Rogers, C.M., Saylor, R., Scheffe, R., Schichtel, B.A., Schwede, D.B., Sexstone, G.A., Sive, B.C., Sosa Echeverría, R., Templer, P.H., Thompson, T., Tong, D., Wetherbee, G.A., Whitlow, T.H., Wu, Z., Yu, Z., Zhang, L. (2019). Toward the improvement of total nitrogen deposition budgets in the United States. Science of The Total Environment 691, 1328-1352, https://doi.org/10.1016/j.scitotenv.2019.07.058

Walker, J.T., Beachley, G., Zhang, L., Benedict, K.B., Sive, B.C., Schwede, D.B. (2020) A review of measurements of air-surface exchange of reactive nitrogen in natural ecosystems across North America. Science of The Total Environment 698, 133975, https://doi.org/10.1016/j.scitotenv.2019.133975

Wentworth, G. R., Murphy, J. G., Benedict, K. B., Bangs, E. J., Collett Jr., J. L. (2016) The role of dew as a night-time reservoir and morning source for atmospheric ammonia. Atmospheric Chemistry and Physics 16, 7435–7449, https://doi.org/10.5194/acp-16-7435-2016

Wesely, M.L. (1989) Parameterization of surface resistances to gaseous dry deposition in regional-scale numerical models. Atmospheric Environment 23, 1293-1304, https://doi.org/10.1016/0004-6981(89)90153-4

Wesely, M.L., Hicks, B.B. (2000) A review of the current status of knowledge on dry deposition. Atmospheric Environment 34, 2261-2282, https://doi.org/10.1016/S1352-2310(99)00467-7

Wolff, V., Trebs, I., Foken, T., Meixner, F. X. (2010a) Exchange of reactive nitrogen compounds: concentrations and fluxes of total ammonium and total nitrate above a spruce canopy. Biogeosciences 7, 1729–1744, https://doi.org/10.5194/bg-7-1729-2010

Wolff, V., Trebs, I., Ammann, C., Meixner, F. X. (2010b) Aerodynamic gradient measurements of the NH3-HNO3-NH4NO3 triad using a wet chemical instrument: an analysis of precision requirements and flux errors. Atmospheric Measurement Techniques 3, 187–208, https://doi.org/10.5194/amt-3-187-2010

Wright, L.P., Zhang, L., Cheng, I., Aherne, J., Wentworth, G.R. (2018) Impacts and Effects Indicators of Atmospheric Deposition of Major Pollutants to Various Ecosystems - A Review. Aerosol and Air Quality Research 18, 1953–1992, http://dx.doi.org/10.4209/aaqr.2018.03.0107

Wyers, G.P., Duyzer, J.H. (1997) Micrometeorological measurement of the dry deposition flux of sulphate and nitrate aerosols to coniferous forest. Atmospheric Environment 31, 333-343, https://doi.org/10.1016/S1352-2310(96)00188-4

Wyers, G.P., Erisman, J.W. (1998) Ammonia exchange over coniferous forest. Atmospheric Environment 32, 441-451, https://doi.org/10.1016/S1352-2310(97)00275-6

Yamaga, S., Ban, S., Xu, M., Sakurai, T., Itahashi, S., Matsuda, K. (2021) Trends of sulfur and nitrogen deposition from 2003 to 2017 in Japanese remote areas. Environmental Pollution 289, 117842, https://doi.org/10.1016/j.envpol.2021.117842

Yamashita, N., Ohta, S., Sase, H., Luangjame, J., Visaratana, T., Kievuttinon, B., Garivait, H., Kanzaki, M. (2010) Seasonal and spatial variation of nitrogen dynamics in the litter and surface soil layers on a tropical dry evergreen forest slope. Forest Ecology and Management 259, 1502-1512, https://doi.org/10.1016/j.foreco.2010.01.026

Yamazaki, T., Takahashi, A., Matsuda, K. (2015) Differences of dry deposition between sulfate and nitrate in PM2.5 to a forest in suburban Tokyo by vertical profile observations. Journal of Japan Society for Atmospheric Environment 50, 167-175 (in Japanese), https://doi.org/10.11298/taiki.50.167

Yamulki, S., Harrison, R.M., Goulding, K.W.T. (1996) Ammonia surface-exchange above an agricultural field in Southeast England. Atmospheric Environment 30, 109-118, https://doi.org/10.1016/1352-2310(95)00233-O

Zhang, L., Moran, M.D., Makar, P.A., Brook, J.R., Gong, S. (2002) Modelling gaseous dry deposition in AURAMS: a unified regional air-quality modelling system. Atmospheric Environment 36, 537-560, https://doi.org/10.1016/S1352-2310(01)00447-2

Zhang, L., Brook, J.R., Vet, R. (2003) A revised parameterization for gaseous dry deposition in air-quality models. Atmospheric Chemistry and Physics 3, 2067-2082, https://doi.org/10.5194/acp-3-2067-2003

Zhang, L., Wright, L.P., Asman, W.A.H. (2010) Bi-directional air-surface exchange of atmospheric ammonia: A review of measurements and a development of a big-leaf model for applications in regional-scale air-quality models. Journal of Geophysical Research 115, D20310. https://doi.org/10.1029/2009JD013589

Zhao, X., Zheng, S, Arima, S. (2014) Influence of nitrogen enrichment during reproductive growth stage on leaf nitrogen accumulation and seed yield in soybean. Plant Production Science 17, 209-217, https://doi.org/10.1626/pps.17.209

Zhou, X., Zhang, N., TerAvest, M., Tang, D., Hou, J., Bertman, S., Alaghmand, M.,
Shepson, P. B., Carroll, M. A., Griffith, S., Dusanter, S., Stevens, P. S. (2011) Nitric acid photolysis on forest canopy surface as a source for tropospheric nitrous acid. Nature Geoscience 4, 440-443, https://doi.org/10.1038/ngeo1164

Supplementary

- Papers that make up the dissertation

[1] Xu, M., Matsuda, K. (2020) Dry Deposition of $PM_{2.5}$ Nitrate in a Forest according to Vertical Profile Measurements. Asian Journal of Atmospheric Environment 14, 367-377, https://doi.org/10.5572/ajae.2020.14.4.367

[2] Xu, M., Kasahara, K., Sorimachi, A., Matsuda, K. (2021) Nitric acid dry deposition associated with equilibrium shift of ammonium nitrate above a forest by long-term measurement using relaxed eddy accumulation. Atmospheric Environment 256, 118454, https://doi.org/10.1016/j.atmosenv.2021.118454

[3] Xu, M., Umehara, M., Sase, H., Matsuda, K. (2022) Ammonia fluxes over an agricultural field in growing and fallow periods using relaxed eddy accumulation. Atmospheric Environment 284, 119195, https://doi.org/10.1016/j.atmosenv.2022.119195

Acknowledgment

I express my great gratitude to Prof. Kazuhide Matsuda (the Tokyo University of Agriculture and Technology), who is my supervisor, for his kind support and perfect guidance to carry out this study and complete my dissertation. During my six years research life, I was able to experience a lot of activities unique to the Matsuda laboratory, such as participation in academic conferences and various observations both in Japan and overseas. These experiences given by Prof. Matsuda are treasures in my life and will support my research life in the future.

I also gratefully acknowledge the support and advices of Dr. Akira Takahashi (Central Research Institute of Electric Power Industry) and Prof. Atsuyuki Sorimachi (Toyo University), who are visiting professors at the Tokyo University of Agriculture and Technology. I would like to thank Dr. Genki Katata (Ibaraki University), Prof. Tatsuya Sakurai (Meisei University), and Dr. Hiroyuki Sase (ACAP) for the experiences of joint research and useful discussions.

I sincerely acknowledge the numerous support of Mr. Takaaki Honjo, Mr. Taiichi Sakamoto, Mr. Akiyoshi Nakahara, Mr. Keita Suzuki, Mr. Kenta Kasahara, Mr. Ryota Inoue, Ms. Miku Umehara, Mr. Ryota Matsumoto and other members of Matsuda Laboratory (Tokyo University of Agriculture and Technology) for the observations. I also express my gratitude to Prof. Takashi Motobayashi and other members of FM Fuchu (Tokyo University of Agriculture and Technology) for the support to measurements in the agricultural field, and to Mr. Genki Niwano (Niigata University) and Mr. Masayuki Morohashi (ACAP) for the foliar analysis.

Finally, I would also like to thank my family for their emotional and financial support.